Identifying the Ultrastructural Adaptations that Drive the Mechanical Load-Induced Growth of Skeletal Muscle

By

Kent W. Jorgenson

A dissertation submitted in partial fulfillment of

the requirements for the degree of

Doctor of Philosophy

(Molecular and Cellular Pharmacology)

at the

UNIVERSITY OF WISCONSIN-MADISON

2024

Date of final oral examination: 08/29/2024

The dissertation is approved by the following members of the Final Oral Committee:

Troy A. Hornberger, Professor, Comparative Biosciences (PI)

Kevin W. Eliceiri, Professor, Medical Physics and Biomedical Engineering

Junsu Kang, Professor, Cell and Regenerative Biology

Dudley Lamming, Professor, Endocrinology, Diabetes and Metabolism

Abstract

The preservation of skeletal muscle mass is crucial for maintaining overall health and well-being. Mechanical loading, particularly through resistance exercise, plays a key role in regulating skeletal muscle mass. While extensive research has shed light on the macroscopic and microscopic changes associated with increased mechanical load, the specific ultrastructural adaptations driving muscle growth remain poorly understood. In particular, it is still unclear whether the radial growth of muscle fibers in response to mechanical load is driven by myofibril hypertrophy, myofibrillogenesis, or both. To address this gap, we developed a novel technique called fluorescence microscopy with image deconvolution (FIM-ID) to visualize myofibrils with enhanced resolution and contrast using standard fluorescence microscopy. This innovative method enables automated measurement of myofibril size and number, offering a more efficient and cost-effective approach for analyzing muscle structure. Application of FIM-ID in both mouse and human models of increased mechanical loading revealed that the radial growth of muscle fibers is primarily driven by myofibrillogenesis.

Acknowledgments

First and foremost, I would like to express my heartfelt gratitude to you, Troy, for welcoming me as a graduate student in your lab. Your belief in my potential, especially during a challenging time in my academic journey, means the world to me. Despite my limited background in skeletal muscle physiology, you gave me the opportunity to grow and learn. While I may not have been the easiest student to mentor, I'd like to believe our experience has been mutually enriching, and the discipline you've instilled in me will be invaluable as I pursue my career in industry. Your guidance pushed me to explore new experimental techniques, broaden my knowledge, and refine my skills. The hands-on training you provided reflects your passion for the research in the Hornberger lab, and I am excited to see the lab's future growth and discoveries.

I also want to thank all the members of my thesis committee—Dr. Troy Hornberger, Dr. Kevin Eliceiri, Dr. Dudley Lamming, and Dr. Junsu Kang. Your valuable feedback and recommendations have been instrumental in shaping my project, and your dedication to mentoring graduate students like myself is truly inspiring.

I am deeply grateful to both past and present members of the Hornberger lab. While it's impossible to thank everyone individually, I would like to acknowledge a few people in particular. Dr. Nathaniel Steinert, thank you for helping me acclimate to the lab and for teaching me essential surgical and wet lab techniques. Dr. Kuan-Hung Lin, I have always valued your sharp critiques, which have pushed my research forward. Dr. Jamie Hibbert, your support, not only for my research but also for my well-being, has been a source of strength, and your holistic mentorship will make you a phenomenal professor. Furthermore, to all the undergraduate students, your dedication has been crucial to the lab's success. Thank you for your hard work.

Lastly, I owe who I am today to the unwavering support of my friends and family. Mom, Elizabeth Jorgenson, your encouragement and dedication to fostering my curiosity have been foundational to my success. Dad, William Jorgenson, your lessons on the importance of hard work and love for nature have deeply shaped my character. And to my brother, Dale, thank you for always being there, tolerating my antics, and being my greatest friend and role model.

This work is a testament to my collective support throughout my academic path. I am truly grateful to each and every one of you.

Table of Contents

Chapter One: Identifying the Structural Adaptations that Drive the Mechanical Load-Induced Growth of Skeletal Muscle: A Scoping Review

Kent W. Jorgenson[1], Stuart M. Phillips[2], and Troy A. Hornberger[1*]

[1]School of Veterinary Medicine and the Department of Comparative Biosciences, University of Wisconsin –Madison, WI, USA, [2]Department of Kinesiology, McMaster University, Hamilton, ON, L8S 4K1, Canada

*Corresponding author (Lead Contact): Troy A. Hornberger

2015 Linden Drive

Madison WI, 53706

Phone: (608) 890-2174

Email: troy.hornberger@wisc.edu

This chapter was published in The Journal *Cells* in July 2020 and modified slightly to comply with the format of this dissertation.

Abstract

The maintenance of skeletal muscle mass plays a critical role in health and quality of life. One of the most potent regulators of skeletal muscle mass is mechanical loading, and numerous studies have led to a reasonably clear understanding of the macroscopic and microscopic changes that occur when the mechanical environment is altered. For instance, an increase in mechanical loading induces a growth response that is mediated, at least in part, by an increase in the cross-sectional area of the myofibers (i.e., myofiber hypertrophy). However, very little is known about the ultrastructural adaptations that drive this response. Even the most basic questions, such as whether mechanical load-induced myofiber hypertrophy is mediated by an increase in the size of the pre-existing myofibrils and/or an increase in the number myofibrils, have not been resolved. In this review, we thoroughly summarize what is currently known about the macroscopic, microscopic and ultrastructural changes that drive mechanical load-induced growth and highlight the critical gaps in knowledge that need to be filled.

Keywords

Fascicle; Myofiber; Myofibril; Sarcomere; Hypertrophy; Hyperplasia; Splitting; Radial Growth; Longitudinal Growth; Exercise

1. Introduction

Skeletal muscle comprises approximately 40% of body mass and plays a critical role in posture, breathing, motion, and metabolic regulation [1]. As we age, the occurrence of age-related diseases, such as the loss of muscle mass (i.e., sarcopenia), are expected to become more prevalent [2]. For instance, between the ages of 25–80 years, the average individual will lose approximately 25% of their muscle mass [3, 4]. This age-associated loss of muscle mass leads to an increased risk of fall-related injury, institutionalization, loss of independence, and disease [5-7]. Indeed, in the United States alone, the healthcare costs for muscle wasting related illnesses were estimated to be $18.5 billion in 2000 [8]. Based on this figure, reducing the rate of muscle wasting related diseases by even 10% could save a striking $1.1 billion in annual healthcare costs. The number of people over the age of 60 is expected to double by 2050, and thus, the costs associated with sarcopenia will only continue to increase [9]. Accordingly, the development of therapies that can restore, maintain, and/or increase muscle mass will be of great clinical and fiscal significance. However, to develop such therapies, we will first need to establish a comprehensive understanding of the mechanisms that regulate the size of this vital tissue.

Mechanical load-induced signals are one of the most widely recognized regulators of skeletal muscle mass. Indeed, historical evidence suggests that the growth-promoting effects of mechanical loading has been recognized since at least the 7th century BC [10]. During the last century, a variety of human and animal models have been used to further establish this point. For instance, in humans, resistance exercise is the most commonly used model of mechanical load-induced growth and it typically induces a 5–20% increase in skeletal muscle volume/mass within 8–16 weeks [11-17]. Similar changes in muscle mass have also been observed in animal models that are intended to mimic human resistance exercise [18-20]. Furthermore, animal models that use

extreme forms of mechanical loading, such as synergist ablation, can promote a doubling of muscle mass within as little as 2 weeks [21-23]. Collectively, these models have provided extensive insight into the macroscopic and microscopic changes that contribute to the mechanical load-induced growth response, but surprisingly, the ultrastructural changes that drive these changes remain poorly understood. In this review, we will thoroughly summarize what is currently known about the structural adaptations that drive mechanical load-induced growth and highlight the critical gaps in knowledge that need to be filled.

2. Overview of Skeletal Muscle Structure

Before considering the structural changes that drive mechanical load-induced growth, we want to ensure that the reader appreciates the basic structural design of skeletal muscle. One of the easiest ways to appreciate this design is to consider skeletal muscle as a hierarchy of contractile machinery that is visible at the macroscopic level (viewable without magnification), followed by the microscopic level (viewable with standard microscopy), and finally the ultrastructural level (viewable with high resolution microscopy). Below we will provide a brief overview of the primary components that are found at each of these levels. For excellent illustrations and more comprehensive discussions on this topic, the reader is referred to the following reviews [24-26].

At the macroscopic level, it can be noted that skeletal muscles are connected to bones via tendinous attachments and enact their contractile function by providing movement and articulation of the skeletal system. Moreover, as illustrated in Figure 1-1, skeletal muscles are surrounded by an outer layer of connective tissue called the epimysium, and underneath the epimysium are bundles of myofibers (i.e., fascicles) that are surrounded by another layer of connective tissue called the perimysium [24]. In most skeletal muscles, the fascicles, and their associated myofibers,

are not directly aligned with the longitudinal axis of the muscle, but instead are offset at an angle called the pennation angle (Figure 1-2) [27].

At the microscopic level, a cross-section of skeletal muscle will reveal the presence of individual myofibers (Figure 1-1A-B). The myofibers are multinucleated cells that are encased by a layer of connective tissue called the endomysium, and they are surrounded by interstitial cells such as fibroblasts, immune cells, pericytes and fibro-adipogenic progenitors (Figure 1-1A–C) [28, 29]. Furthermore, another important class of cells, called satellite cells, resides between the endomysium and the plasma membrane of the myofibers (i.e., the sarcolemma) [30]. The endomysium is physically coupled to the sarcolemma, and everything the resides underneath the sarcolemma is typically referred to as the sarcoplasm.

The gelatinous sarcoplasm contains the primary ultrastructural elements of the myofiber, and as illustrated in Figure 1-1, an examination at the ultrastructural level reveals that ≈80% of the sarcoplasm is filled with an in-parallel array of rod-like structures called myofibrils [31-35]. The myofibrils are composed of a long in-series array of force-generating elements called sarcomeres and are surrounded by a mitochondrial reticulum and a membranous structure called the sarcoplasmic reticulum [36, 37]. The sarcomeres within the myofibrils enact their function through the active sliding of thick and thin myofilaments, and in a longitudinal view, it can be seen that the sarcomeres consist of regions called the Z-disc, the I-band which contains the thin (actin) myofilaments, and the A-band which contains the thick (myosin) myofilaments [38, 39]. It should also be noted that within a given species, the optimal/resting length of sarcomeres (2.0–2.5 μm) is highly conserved, and alterations in this length can profoundly influence force production [40-42].

When considering the structure of skeletal muscle, it is also essential to recognize that all myofibers are not created equal. For instance, some types of myofibers are heavily reliant on

oxidative metabolism, exhibit a slow contractile speed and are resistant to fatigue. In contrast, other types of myofibers rely on anaerobic glycolytic metabolism, exhibit a fast contractile speed and rapidly fatigue when stimulated to contract [39]. Different fiber types are typically grouped according to the predominant isoform of the myosin heavy chain that they express, and these isoforms include Type I (slow oxidative), Type IIA (fast oxidative), and Type IIB (fast glycolytic) fibers [43, 44]. It is also important to point out that humans do not express the Type IIB myosin isoform, but instead express a very similar (yet slightly slower) Type IIX myosin isoform [45]. However, since this differentiation was only solidified in 1990′s [46-48], some older studies with human subjects used the Type IIB classification, while other studies have grouped Type IIB and Type IIX fibers together as a similar fiber type [49]. This use of IIB and IIX myosin labeling has led to some confusion when comparing earlier muscle growth studies to current studies, so it is important to keep this distinction in mind when relating fiber type-specific adaptations across the current body of literature.

3. Mechanical Load-Induced Growth of Skeletal Muscle at the Macroscopic Level

3.1. Whole Muscle

At the whole muscle level, mechanical load-induced growth can be mediated by an increase in the length and/or an increase in the cross-sectional area (CSA) of the muscle. Growth resulting from an increase in length is referred to as longitudinal growth, and it can occur in response to a variety of different perturbations. For instance, during development, the length of muscles can more than double from birth to the termination of bone growth [50-52]. Longitudinal growth can also be induced in adults by placing muscles in a chronically stretched state [53]. As a case in point, it has been shown that immobilizing a rat lower hindlimb in a fully dorsiflexed position can

lead to a >20% increase in the length of the soleus muscle [54]. Likewise, limb-lengthening procedures can lead to a >20% increase in muscle length [55, 56]. Indeed, even some of the more extreme models of mechanical load-induced growth can lead to an increase in muscle length [23, 57]. For example, surgical removal of the gastrocnemius and soleus muscles (i.e., synergist ablation) is a commonly used rodent model for stimulating mechanical load-induced growth, and it has been reported that this can lead to a 13% increase length of the plantaris muscle [57, 58]. Thus, it is clear that both adolescent and adult skeletal muscles can undergo longitudinal growth.

Although skeletal muscle is capable of undergoing longitudinal growth, most models of mechanical loading do not lead to notable alterations in whole muscle length [18, 59]. Instead, mechanical load-induced growth is usually driven by an increase in the CSA of the muscle (also known as radial growth). For example, in humans, 8-16 weeks of resistance exercise will generally produce a 5–30% increase in whole muscle CSA but no change in muscle length [16, 59-66]. Interestingly, the magnitude of increase in CSA is often greater than the increase that is observed for muscle volume/mass. An excellent example of this paradox was reported by Roman et al. (1993), whom reported that 12 weeks of resistance exercise led to a 14% increase in the volume of the elbow flexors, but the CSA at the mid-belly increased by 23% [60]. Importantly, however, the magnitude of the increase is CSA got progressively smaller towards the proximal and distal ends of the muscle, which explained why the muscle volume only increased by 14%. Simply put, the study by Roman et al. (1993) demonstrated that the radial growth response was not evenly distributed along the length of the muscle. Indeed, regional differences in the magnitude of radial growth have been reported in several animal and human-based studies, and in our opinion, this phenomenon represents an often overlooked aspect of the mechanical load-induced growth response [13, 59, 64, 67-72].

3.2. Muscle Fascicles

Previous studies have shown that the initial mechanical load-induced increase in whole muscle CSA can be attributed, at least in part, to edema. However, the long-term changes are primarily caused by an expansion of the contractile elements [63, 73, 74]. For instance, using a rat model of resistance exercise, we have shown that 8 weeks of training resulted in a 24% increase in the CSA of the flexor hallucis longus muscle, and this was matched by a proportionate increase in total myofibrillar protein content and peak tetanic force production [18]. Thus, if the mechanical load-induced increase in whole muscle CSA was driven by an expansion of the contractile elements, then the increase should be reflective of the changes that occurred at the preceding level within the hierarchy of the contractile machinery (i.e., myofilaments → myofibrils → myofibers → fascicles → whole muscle).

Based on the aforementioned point, mechanical load-induced changes in whole muscle CSA should be driven by changes that happen at the level of the muscle fascicles, and there are effectively two predominant ways in which this is thought to occur: 1) longitudinal growth of the fascicles or 2) radial growth of the fascicles. It is also possible that mechanical loading could lead to an increase in the number of fascicles per muscle, but we are not aware of any studies that have attempted to answer this technically difficult question.

Upon first consideration, it can be challenging to appreciate how both longitudinal and radial growth of fascicles can lead to an increase in whole muscle CSA. Thus, to visualize these points, we have taken advantage of a geometric model that can be used to predict changes in the architectural properties of skeletal muscle [75, 76]. Specifically, as shown in Figure 1-3, we used this model to illustrate how changes in either fascicle length (Lf), or fascicle diameter (Df), could produce a 30% increase in whole muscle CSA (the upper end of what is typically observed in

humans after 8-16 weeks of resistance exercise). For simplicity, our model considers a hypothetical muscle that is composed of 50 fascicles aligned in parallel. Moreover, in the control (starting) state, the fascicle length to muscle length (Lm) ratio is 0.25, and the fascicles are offset at a pennation angle of 16° (similar to the properties of the vastus lateralis muscle in humans [77]). Based on these parameters, if the 30% increase in CSA was purely due to longitudinal growth of the fascicles, then fascicle length would have to increase by 11%, and the pennation angle would remain unaltered (Figure 1-3B). On the other hand, if the 30% increase in CSA was due exclusively to an increase in radial growth of the fascicles, then the fascicle diameter would have to increase by 14%, and this would result in a concomitant 15% increase in pennation angle (from 16°→18.4°) (Figure 1-3C). It is also worth noting that in the example of pure longitudinal growth, the number of fascicles visible in a cross-section of the mid-belly of the muscle would also increase by 30% and could easily lead one to mistakenly conclude that the increase in whole muscle cross-sectional area was driven by new fascicle formation.

Having illustrated how radial and longitudinal growth of fascicles can lead to an increase in whole muscle CSA, we will now consider the studies that have tested whether these types of adaptations occur. Specifically, we will first consider the studies that have examined whether mechanical load-induced alterations in whole muscle CSA are associated with changes in fascicle length, and fortunately, this has been a subject of extensive investigation [13, 59, 62, 65, 78-85]. For instance, Ema et al. (2016) recently compiled data from 38 different studies that addressed this topic and found that a significant positive relationship existed between the exercise-induced increases in muscle size and fascicle length [86]. Nonetheless, some of the studies that reported an increase in muscle size did not observe an increase in fascicle length [59, 83-85], and there are even examples in which small but significant declines in fascicle length have been reported [78].

However, when Ema et al. (2016) compared the magnitude of change across all studies which showed a significant alteration in fascicle length versus those which did not, the average values from these studies still showed a 12.4% versus 7.7% increase in fascicle length, respectively [86]. Thus, there is a high level of support for the notion that mechanical load-induced alterations in whole muscle CSA can be driven, at least in part, by an increase in fascicle length.

As mentioned above, the radial growth of fascicles could also lead to an increase in whole muscle CSA. Importantly, as detailed by the work of Maxwell et al. (1974), and as illustrated in Figure 1-3C, a direct relationship exists between fascicle diameter and the pennation angle of the fascicles. Specifically, if the length of the muscle, the length of the fascicles, and the number of fascicles is held constant, then an increase in fascicle diameter will lead to an increase in the pennation angle. Hence, it is not surprising that most studies reporting a significant resistance exercise-induced increase in muscle size, but no change in fascicle length, instead find a significant increase in the pennation angle [59, 83-85]. Indeed, just as with changes in fascicle length, Ema et al. (2016) determined that a significant positive relationship exists between the resistance exercise-induced increase in muscle size and pennation angle. On average, the studies that reported a significant change in pennation angle showed a 13.5% increase, while those that did not detect a significant change still found an average increase of 7.7% [86]. Accordingly, just as with changes in fascicle length, there is a high level of support for the notion that mechanical load-induced alterations in whole muscle CSA can be driven by an increase in fascicle diameter / pennation angle. Indeed, a collective view of the literature suggests that mechanical loading can lead to both longitudinal and radial growth of fascicles, and the exact contribution of these components is probably determined by a variety of different factors, such as the type of mechanical loads that are

placed on the muscle (e.g., concentric vs. eccentric contractions) and the architectural properties of the muscle that is being considered (e.g., fusiform, unipennate, bipennate, etc.) [86-89].

4. Mechanical Load-Induced Growth of Skeletal Muscle at the Microscopic Level

As previously noted, mechanical load-induced alterations at each level of the skeletal muscle structure should be reflective of the changes that occurred at the preceding level within the hierarchy of the contractile machinery. Thus, having established that mechanical loading can lead to both longitudinal and/or radial growth of the fascicles, we will now consider how these changes can be mediated by alterations at the level of the myofibers.

4.1. Longitudinal Growth of Fascicles

Fascicles are composed of bundles of myofibers, and the myofibers can either run the entire length of the fascicle, or only part of the length of the fascicle and exhibit an intrafascicular termination [90-92]. For fascicles that are composed of myofibers that run the entire length of the fascicle, longitudinal growth of the fascicle would be exclusively dependent on the longitudinal growth of the individual myofibers. Alternatively, longitudinal growth of the fascicles with myofibers that exhibit intrafascicular terminations could result from longitudinal growth of the myofibers and/or the addition of new myofibers in-series. Although we are not aware of any studies that have addressed whether mechanical loading can lead to the formation of new myofibers in-series, a consistent body of literature has shown that myofibers are capable of undergoing longitudinal growth [57, 72, 93-95]. For instance, Alway et al. (1989) subjected the anterior latissimus dorsi (ALD) muscle of quails to chronic mechanical loading by securing a weight (10% of body mass) to one of the wings. In response to this perturbation, the mass of the ALD increased by 182%, which was associated with a 24% increase in the average length of the myofibers [72].

Similarly, Roy et al. (1982) demonstrated that in rats, chronic mechanical loading of the plantaris via synergist ablation resulted in doubling of its mass and a concomitant 19% increase in the myofiber to muscle length ratio [94]. Based on these, and related studies, it is clear that extreme models of mechanical loading can induce longitudinal growth of the myofibers.

Although a compelling body of evidence indicates that extreme models of mechanical loading can promote longitudinal growth of myofibers, only a handful of studies have directly addressed this topic within the confines of more physiologically relevant models. For instance, it has been shown that the eccentric contractions induced by downhill walking [96], and downhill running [97], can lead to an increase in the number of sarcomeres per myofiber; however, neither of these studies reported measurements of myofiber length. Indeed, we could only find one study that reported measurements of myofiber length within the context of a physiologically relevant model of mechanical load-induced growth [18]. In this case, rats were subjected to 8 weeks of resistance exercise which led to a 24% increase in whole muscle CSA, but myofiber length was not altered. Importantly; however, this study did not indicate whether the increase in muscle CSA was mediated by longitudinal vs. radial growth of the fascicles, and hence, it is difficult to extrapolate any meaningful insights from the data.

Given the paucity of data on this topic, we believe that it is worthwhile to mention unpublished results that we recently obtained from mice that had their plantaris muscles subjected to 16 days of myotenectomy (a much milder form of synergist ablation [98]). Specifically, we determined that myotenectomy led to 72% increase in the mass of the plantaris along with an 8% increase in length of the myofibers ($p < 0.01$). Likewise, Goh et al. (2019) recently described a high intensity interval training (HIIT) for mice that leads to a 17% increase in the mass of the extensor digitorum longus muscle [99], and this was associated with a 9% increase in the length of the myofibers (*p*

< 0.05, personal communication from Dr Doug Millay). Thus, it appears that even physiologically relevant models of mechanical load-induced growth can induce longitudinal growth of myofibers; however, additional studies on this topic will need to be published before a clear consensus can be reached.

4.2. Radial Growth of Fascicles

As illustrated in Figure 1-4, radial growth of fascicles could result from an increase in the CSA of the existing myofibers (i.e., myofiber hypertrophy, Figure 1-4A) and/or an increase in the number of myofibers per cross-section (from myofiber splitting and/or hyperplasia, Figure 1-4B). These concepts have been widely studied within the context of mechanical load-induced growth, and in the following sections we will summarize the body of literature that exists on these topics. Before moving into these sections, we also want to point out that the radial growth of fascicles could result from the longitudinal growth of myofibers with intrafascicular terminations (Figure 1-4C) [91]. However, as mentioned above, very few studies have examined whether physiologically relevant models of mechanical loading can induce longitudinal growth of myofibers. Accordingly, this mechanism will not be subjected to further discussion.

4.2.1. Myofiber Hypertrophy

Radial growth of myofibers leads to an increase in the CSA, and such a change is typically referred to as myofiber hypertrophy. Myofiber hypertrophy is, by far, the longest-standing and most widely acknowledged contributor to the mechanical load-induced growth of skeletal muscle. Indeed, the ability of mechanical loads to induce myofiber hypertrophy has been recognized since the late 1800′s [100]. As summarized by Huan et al. [101], most of the early research on this topic used animals such as dogs [100], cats [102], mice [103], rats [104], hamsters [34], and birds [105].

Some of these animal-based studies employed rather extreme forms of chronic mechanical loading (e.g., synergist ablation, wing-weighting, etc.), whereas others used interventions that were intended to mimic human resistance exercise. A notable example was described by Goldspink (1964) in which young mice were trained to pull on a weighted cord so that they could gain access to their food, and it was determined that 25 days of this training resulted in a ≈30% increase in the CSA of myofibers within the biceps brachii [103]. Another classic example involves the model described by Gonyea and Ericson (1976) [102]. In this model, cats were operantly conditioned to move a weighted bar with their paw in exchange for a food reward, and it was found that the CSA of the myofibers within the flexor carpi radialis increased by 21–32% after 41 weeks of this type of training [102]. The magnitude of change in myofiber CSA observed in the above examples is similar to the 10–35% that is typically observed in humans after 8-16 weeks of resistance exercise [16, 17, 43, 60, 66, 101, 106-108]. However, this magnitude of change pales in comparison to what has been observed with some of the more extreme models of mechanical loading. For instance, Antonio and Gonyea (1993) observed an astonishing 142% increase in CSA of the myofibers of the ALD muscle after just 16 days of wing-weighting [109]. Simply stated, an extremely high level of evidence supports the notion that mechanical loading can induce myofiber hypertrophy and the capacity for this type of growth appear to be quite large.

4.2.2. Myofiber Splitting

As recently reviewed by Murach et al. (2019), split myofibers are characterized by the presence of “branching,” “fragmentation,” or “splitting” along the length of the myofiber [110]. Split myofibers can be found in healthy muscles, and an increased frequency of split myofibers is commonly observed in muscular dystrophy and various neurogenic myopathies [111, 112]. An increased frequency of split myofibers has also been observed in muscles subjected to mechanical

loading. For instance, the most extraordinary example of this was published by Antonio and Gonyea (1994) who reported that the frequency of split myofibers in the quail ALD muscle increased from 0.25% to 5.25% after 28 days of wing-weighting [113]. Tamaki et al. (1996) also found that the frequency of split myofibers in the rat plantaris muscle increased from 0.6% to 1.8% after 6 weeks of synergist ablation [114]. An increase in the occurrence of split myofibers (1.4% of all myofibers) has also been observed in powerlifters that used anabolic steroids [115]. Based on these reports, it would appear mechanical loading can result in an increased prevalence of split myofibers. However, it is important to point out that many of the studies that are frequently cited as providing support for this concept never actually quantified the number of split myofibers [116-118]. Moreover, there are multiple examples in which the number of split myofibers was quantified, and it was concluded that mechanical loading did not alter the frequency of their appearance [119-122]. Even the study by Antonio and Gonyea (1994) found that 16 days of wing-weighting resulted in an 88% increase in the mass of the ALD muscle, yet the frequency of split myofibers at this time point was still only 0.28% [113]. One potential explanation for this observation is that splitting along the entire length of the myofiber rapidly runs to completion, and thus, only a small fraction of the myofibers that split are effectively detected. However, if this were the case, then the total number of myofibers per muscle should increase. To test this, Antonio and Gonyea (1994) directly counted all of the fibers in the ALD muscles and found that the total number did not change after 16 days of wing-weighting [113]. Thus, it is our conviction that although mechanical loading may be capable of inducing myofiber splitting, the frequency of this event is low and thus does not typically make a major contribution to the overall growth process.

4.2.3. Hyperplasia

Hyperplasia refers to the generation of new myofibers, and as illustrated in Figure 1-4B, hyperplasia could lead to the radial growth of muscle fascicles. Indeed, numerous studies have shown that the number of myofibers per muscle rapidly increases during the early stages of developmental growth [123-125]. Although it is well accepted that hyperplasia occurs during developmental growth, whether hyperplasia can occur in adult skeletal muscles remains a subject of debate.

Part of the debate over whether hyperplasia occurs in adult skeletal muscle results from the types of measurements that have been used to address this question [126, 127]. Specifically, two primary methods have been employed: 1) counting the number of myofibers per cross-section of the muscle, and 2) digestion of the muscle's connective tissue followed by a direct count of all myofibers present in the muscle. The direct counting method is ideal, but this approach requires the manual dissociation and counting of thousands of myofibers. Accordingly, most studies that describe measurements of hyperplasia are based on counts of the myofibers per cross-section. With this point in mind, it is imperative to recognize that the number of myofibers that appear in a cross-section can be highly influenced by changes in the architectural properties of the muscle (e.g., fiber length and/or pennation angle) [75, 76, 91, 127]. Such effects have been thoroughly described by Maxwell et al. (1974), and can be appreciated by considering the illustrations presented in Figures 1-3 and 1-4 [75]. For instance, Figure 1-3B shows how an 11% increase in fascicle length would lead to a 30% in the number of fascicles per cross-section, and the same principles would hold at the level of the myofibers. Furthermore, as illustrated in Figure 1-4C, longitudinal growth of myofibers with intrafascicular terminations could also lead to an increase in the number of myofibers per cross-section. Hence, extreme caution needs to be exercised when interpreting the

results from studies that rely on myofiber per cross-section counts to make conclusions about hyperplasia.

Unfortunately, the majority of studies that have examined whether mechanical loading induces hyperplasia have relied on counts of the myofibers per cross-section [22, 34, 109, 116-118, 128-130]; however, there are a handful of studies that have reported direct myofiber counts. For instance, investigators with ties to Dr Gonyea reported that 7–30 days of wing-weighting resulted in a 60–294% increase in muscle mass and a 30–50% increase in the number of myofibers per muscle [72, 93, 113, 131]. In stark contrast, investigators with links to Dr Gollnick reported that 6-65 days of wing-weighting resulted in a 22–225% increase in muscle mass but no change in the number of myofibers per muscle [120]. The Gollnick group also reported that other extreme forms of mechanical loading such as synergist ablation does not alter the number of myofibers per muscle [119, 121]. The conflicting conclusions from these groups has existed for over 25 years, and surprisingly, the controversy has still not been resolved [126, 127, 132, 133]. Thus, in our opinion, the notion that extreme forms of mechanical loading can induce hyperplasia remains controversial.

Due to a minimal number of studies, a similar controversy exists with regards to whether more physiologically relevant models of mechanical loading can induce hyperplasia. Indeed, we are only aware of two studies that have directly addressed whether a resistance exercise-like stimulus can alter the number of myofibers per muscle. The first of these studies was performed by Gonyea et al. (1986) whom painstakingly counted the number of myofibers in the flexor carpi radialis of cats that had been subjected to 60–129 weeks of weight training, and the results indicated that the training stimulus led to a 9% increase in the number of myofibers per muscle (39,759 vs. 36,550 myofibers per muscle) [122]. Likewise, Tamaki et al. (1992) subjected rats to weight-lifting

exercise and found that the number of myofibers in the plantaris muscle increased by 14% after 12 weeks of training; however, in this case, the absolute mass of the plantaris was not significantly altered by the training, and thus, the basis for the increase in fiber number is difficult to interpret [134]. Mixed and cautious interpretations can also be drawn from studies that have used myofiber per cross-section counts as a readout for hyperplasia, with some studies showing an increase in the number of myofibers per section [110, 116, 128], while other have reported no change [34, 100, 110]. Accordingly, a firm conclusion with regards to whether physiologically relevant forms of mechanical loading can induce hyperplasia remains elusive.

5. Mechanical Load-Induced Growth of Skeletal Muscle at the Ultrastructural Level

5.1. Longitudinal Growth of Myofibers

As summarized in the previous section, a compelling body of literature has shown that extreme models of mechanical loading can promote the longitudinal growth of myofibers. Furthermore, several lines of evidence suggest that longitudinal growth of myofibers can also be induced by physiologically relevant forms of mechanical loading. Since myofibers are composed of an in-series connection of sarcomeres, it follows that an increase in myofiber length would be mediated by an increase in the length of the sarcomeres and/or the serial addition of new sarcomeres. When considering these options, it is essential to bear in mind that the optimal length of sarcomeres (≈2.5 μm) is highly conserved, and most muscles operate within a narrow range of the sarcomeres optimal length (94 ± 13%) [42]. Hence, it can be inferred that a mechanical load-induced increase in myofiber length would most likely be driven by the serial addition of new sarcomeres, as this would allow for the optimal length of the sarcomeres to be maintained in the elongated myofiber.

In support of the above rationale, Williams and Goldspink (1971) demonstrated that the increase in myofiber length that occurs during development is highly correlated with the serial addition of new sarcomeres [51], and a similar relationship is observed during the myofiber lengthening that occurs in response to increased mechanical loading. For instance, Williams and Goldpink (1973) demonstrated that the number of sarcomeres along the length of mouse soleus myofibers increases by 23% after ≈ 7 days of tenotomy (a milder form of the synergist ablation model) [135]. Likewise, Aoki et al. (2009) have shown that the number of sarcomeres along the length of rat soleus myofibers increases by 27% after just 4 days of chronic stretch [54]. Collectively, these, and many other studies [51, 54, 95-97, 135-140], have not only indicated that mechanical loading could lead to the serial addition of new sarcomeres but also suggest that this type of growth can occur in a very rapid manner.

If mechanical loading leads to the serial addition of new sarcomeres, then it raises the question of where along the length of the myofibers the new sarcomeres are added. According to Goldspink (1983) "The point or points at which the sarcomeres are added has been rather uncertain until recently. With radioactively labeled amino acids and radioactively labeled adenosine the site of longitudinal growth was shown to be at the ends of the myofibrils" [141]. Although this is a fundamentally important conclusion, its validity remains highly contestable.

The first study that Goldspink cited as providing support for his conclusion was published by Griffin et al. (1971) and used ^{3}H-adenosine as a means for labeling where newly synthesized actin was deposited during the postnatal growth of myofibers [142]. Specifically, young mice were injected ^{3}H-adenosine, and then single myofibers were imaged with autoradiography. Based on the results, Griffin et al. concluded that the ^{3}H-adenosine was primarily deposited at the ends of

the myofibers. Importantly, however, this conclusion was not supported by quantitative data, and the images included in the manuscript were far from persuasive [142].

The second study that Goldspink cited as support for his conclusion used ^{3}H-adenosine in an effort to identify where new sarcomeres were added in adult soleus muscles that were recovering from being immobilized in a shortened position [135]. The study began with a clear demonstration that serial sarcomere addition occurred during the recovery period. After establishing this point, the muscles were cut into 5 separate regions along the longitudinal axis and then analyzed for ^{3}H-adenosine. As shown in Figure 1-5, the outcomes revealed that the amount of ^{3}H-adenosine in the two most distal regions of the muscle was significantly elevated in muscles that were undergoing recovery. Importantly, however, whether the enhanced ^{3}H-adenosine deposition was due to formation of new sarcomeres at the ends of the myofibrils was not directly tested. Indeed, it could be argued that the results from this study simply reflect the type of regional differences in the mechanical load-induced growth that we described in Section 3.1.

In contrast to the notion that new sarcomeres are added at the ends of the myofibrils, others have provided evidence which suggests that new sarcomeres can be inserted throughout the length of the myofibrils [118, 143-150]. For instance, when studying the developmental growth of single myofibers that possess two separate motor endplates, Bennett et al. (1985) discovered that the distance between the motor endplates increased in a manner that was directly proportional to the increase in myofiber length [146]. Similar evidence was obtained by Mackay and Harrop (1969) whom inserted wire markers at various points along the length of the sternomastoid and anterior gracilis muscles of 4 week old rats and then tracked their position with x-ray images during the subsequent 8 weeks of developmental growth [145]. In this case, a proportionate increase in the distance between wires occurred as the muscles grew in length, and this led the authors to conclude

that the myofibers “must be adding new material at points all along their length as they grow”. Indeed, Jahromi and Charlton (1979) obtained support for this concept when they found evidence of a longitudinal growth process that appears to involve the transverse splitting of sarcomeres that are embedded within the midst of the myofibrils (Figure 1-6A) [143].

As described by Jahromi and Charlton (1979), the transverse splitting of sarcomeres appears to occur through an ordered sequence of events which include: 1) splitting of the thick filaments at the H-zone, 2) elongation of the two halves of the thick filaments along with the formation of new thin filaments in the previous H-zone, and 3) formation of a new Z-disc in the center of the newly formed thin filaments [143]. Although this process was originally described in crab skeletal muscles, there is evidence to suggest that the same process takes place in vertebrates. For instance, as shown in Figure 1-6B, Vaughan and Goldspink (1979) observed a similar phenomenon in soleus muscles of mice that had been subjected synergist ablation; however, in this instance, it was thought that the splitting was reflective of damage to the sarcomeres [118]. In fact, focal disruptions of the sarcomere, such as lesions, Z-disc streaming, and Z-disc smearing have long been viewed as markers of damage [151-155]. However, as detailed in a series of publications by Yu et al., these regions might simply be areas of remodeling that result in new sarcomere formation [147-149]. For instance, when examining soleus muscles from humans that had engaged in a bout of intense eccentric contractions, Yu et al. detected a 5-fold increase in the appearance of regions with “supernumerary sarcomeres” (Figure 1-6C-D) [147]. Such regions are remarkably similar to the “sphenode” regions that were described by Heidenhain over 100 years ago, which are characterized by the presence of additional sarcomeres that are out of register with the surrounding sarcomeres [156]. Interestingly, these regions appear to include areas that resemble H-zone transverse sarcomere splitting, as well as another potential type of transverse sarcomere splitting

that occurs at the Z-disc (Figure 1-6F) [150]. Thus, when considering the studies that have been highlighted in this section, it is fair to conclude that mechanical loading can lead to the longitudinal growth of myofibers and this process is primarily driven by the serial addition of new sarcomeres. However, exactly how and where new sarcomeres get added along the length of the myofibrils remains to be resolved.

5.2. Radial Growth of Myofibers

In Section 4.2.1. we reviewed the evidence which indicates that the radial growth of myofibers (i.e., myofiber hypertrophy) is one of, if not the, primary contributor to the growth that occurs in response to increased mechanical loading. We will now examine what is known about the ultrastructural adaptations that drive this process. However, before going deeper into this topic, it is important to consider the concept of specific tension, which is defined as the maximal isometric force produced per CSA. At the myofiber level, the underlying premise for this concept is that the maximal isometric force is directly dependent on the number of the force-generating elements that act in parallel with the line of force production, and that the number of these elements is directly dependent on the CSA of the myofiber [157, 158]. This thesis becomes particularly important when formulating hypotheses about the mechanisms that potentially contribute to the radial growth of the myofibers. For instance, if the CSA of a myofiber increases and specific tension remains constant, then it can be inferred that the radial growth was due to a proportionate addition of both force-generating elements (e.g., myofilaments / sarcomeres / myofibrils) and non-force-generating elements (e.g., mitochondria, sarcoplasmic reticulum, intracellular fluid, connective tissue, etc.). Alternatively, if the CSA of a myofiber increases and specific tension decreases, then it can be inferred that the radial growth was due to a disproportionately greater increase in the amount of

non-force-generating elements. Thus, through measurements of specific tension, one can obtain fundamental insight into the mechanisms that drive the radial growth of the myofibers.

As summarized in a recent meta-analysis by Dankel et al. (2019), at least 15 different studies have assessed whether the specific tension of individual myofibers is impacted by resistance exercise. Importantly, the overwhelming majority of these studies have concluded that specific tension is either not significantly altered, or slightly increases in hypertrophied myofibers [159-167]. Similar observations have also been made in myofibers that were isolated from muscles that have adapted to extreme forms of mechanical loading, such as synergist ablation [168]. Thus, it would appear that the radial growth of myofibers is driven by a proportional increase in the force-generating and non-force-generating elements. However, despite this evidence, some have argued that a disproportionate increase in the non-force-generating elements can make a substantive contribution to radial growth. This type of radial growth has generically been referred to as sarcoplasmic hypertrophy, and in the following sections we will address in greater detail whether radial myofiber growth is driven by sarcoplasmic hypertrophy and/or the expansion of the force-generating elements that act in parallel with the line of force production.

5.2.1. Sarcoplasmic Hypertrophy

Anecdotal observations suggest that although bodybuilders have bigger muscles than powerlifters, they are not as strong. Such observations have led many to contend that myofiber hypertrophy in bodybuilders is due to a disproportionately larger increase in non-force-generating elements (i.e., sarcoplasmic hypertrophy). It has also been hypothesized that these non-force-generating elements could include osmotically active metabolites (e.g., creatine and glycogen) that would draw water into the myofiber, and/or organelles such as the sarcoplasmic reticulum and mitochondria [101, 169, 170]. However, the relevance of these hypotheses is dependent on whether

sarcoplasmic hypertrophy makes a substantive contribution to the mechanical load-induced growth of myofibers. Thus, in this section, we will critically evaluate the evidence that surrounds this concept.

Several studies have been commonly cited as providing support for the existence of sarcoplasmic hypertrophy [31, 35, 163, 171-174]. For instance, D'Antona et al. (2006) measured specific tension in single myofibers from recreationally active subjects, and from subjects that had engaged in bodybuilding for at least 2 years. With regards to providing support for sarcoplasmic hypertrophy, the often-cited outcome is that specific tension was lower in the Type I fibers of bodybuilders [163]. However, it is important to point out that the same study also observed an increase in specific tension of the Type IIA and IIX myofibers from the same bodybuilders [163]. The work of Meijer et al. (2015) is another frequently cited study that measured specific tension in single myofibers. In this case, specific tension was measured in myofibers from control subjects, bodybuilders, and powerlifters. Importantly, it was concluded that specific tension was lower in the myofibers obtained from bodybuilders [172]. At first glance it would appear that this study provides clear support for the notion that bodybuilders experience sarcoplasmic hypertrophy; however, 9 of the 12 bodybuilders in the study admitted to recent use of anabolic steroids [172]. This is noteworthy because the use of anabolic steroids has been associated with alterations in protein composition and the morphological properties of myofibers [175, 176]. Indeed, MacDougall et al. (1982) reported a 9.8% decrease in the proportion of the myofiber CSA that is occupied by the myofibrils in elite bodybuilders and powerlifters (6 of 7 of whom admitted to the use of anabolic steroids), whereas only a 1.6% difference was observed after 6 months of resistance exercise in subjects that denied the use of anabolic steroids [31]. In addition to the aforementioned concerns, it also bears mentioning that the studies by D'Antona et al. and Meijer et al. were both

cross-sectional in nature. This is important because it is well known that cross-sectional studies cannot be used to infer cause and effect relationships [177-179]. Thus, caution needs to be used when considering whether the outcomes of D'Antona et al. and Meijer et al. provide support for the presence of sarcoplasmic hypertrophy.

Other studies that have been cited as providing support for the existence of sarcoplasmic hypertrophy include the work of Penman (1969) who subjected participants to 8 weeks of an exercise intervention that included either progressive resistance exercise, isometric contractions, or stair running [171]. The frequently cited outcome from this study is that exercise led to a decrease in the "myosin concentration" (defined as number of myofibrils in a 5 μm^2 area) [171]. However, this study only included 2 subjects per group, there was a substantial amount of variance in the data, and no statistical analyses were performed.

Another commonly cited study involves the work of Toth et al. (2012) whom subjected older subjects (≈73 years of age) to 18 weeks of resistance exercise and observed a significant decrease in the proportion of the myofiber CSA that was occupied by the myofibrils [35]. Importantly, however, the resistance exercise program employed in this study did not lead to a significant increase in myofiber CSA. Thus, if anything, the observed decrease in the proportion of the CSA that was occupied by the myofibrils would suggest that the resistance exercise program led to the selective loss of the myofibrils rather than a disproportionately large increase in non-force-generating elements (i.e., sarcoplasmic hypertrophy).

More recently, Haun et al. (2019) concluded that the myofiber hypertrophy that occurs after 6 weeks of high-volume resistance training can be largely attributed to sarcoplasmic hypertrophy [173]. Specifically, the key piece of evidence in this study was the observed trend for a decrease in the concentrations of myosin and actin after the 6 weeks of training ($P = 0.052$ and $P = 0.055$,

respectively) [173]. Although these results are interesting, it should be noted that 15 subjects were analyzed in this study, and they only represented a subset of the 31 subjects that participated in the original training intervention [180]. More importantly, the 15 subjects that were examined only included the subjects who showed an “increase” in myofiber CSA (responders by the authors’ definition) [173]. This is important because when all 31 subjects from the original training intervention were considered, it was determined that the 6 weeks of training did not induce myofiber hypertrophy [180]. Accordingly, the results of Haun et al. (2019) cannot be viewed as being representative of the whole population, and are therefore, difficult to interpret within the context of whether sarcoplasmic hypertrophy normally makes a substantive contribution to the mechanical load-induced growth of myofibers.

In summary, we remind the reader that as summarized by Dankel et al. (2019), a large number of longitudinal studies have shown that specific tension is preserved in myofibers that have experienced radial growth as a result of increased mechanical loading [159-168]. This consistent body of evidence strongly suggests that the radial growth of myofibers is not driven by sarcoplasmic hypertrophy, but rather is due to a proportionate increase in the force-generating and non-force-generating elements that act in parallel with the line of force production.

5.2.2. Expansion of the Force-Generating Elements

In myofibers from vertebrates, the force-generating myofilaments are contained within the sarcomere and organized into a hexagonal array of thick and thin myofilaments [181]. The overall geometry and spacing between the myofilaments is highly conserved, and thus, any changes in the number of force-generating myofilaments that are aligned in parallel would likely be matched by a proportionate alteration in the CSA that is occupied by the sarcomeres / myofibrils [182, 183]. Given that specific tension is preserved in myofibers that have experienced radial growth as a

result of increased mechanical loading, and that specific tension is dependent on the number of in parallel force-generating elements, it would follow that the radial growth is mediated by a propionate increase in the CSA that is occupied by the sarcomeres / myofibrils. Indeed, a handful of studies have directly tested this thesis, and all of them reported that induction of myofiber hypertrophy was associated with minimal changes (≤ 4%) in the relative proportion of the CSA that was occupied by the myofibrils [31-34, 184]. For instance, MacDougall et al. (1982) reported that 6 months of resistance exercise in humans led to a 22–25% increase in the CSA of myofibers along with almost no change in the proportion of the CSA that was occupied by the myofibrils (84.2% vs. 82.6% in the pre- and post-trained states, respectively) [31]. Put differently, the data from MacDougall et al. indicated that the total area occupied by the myofibrils increased by ≈23%, but whether this was due to radial growth of the pre-existing myofibrils (myofibril hypertrophy) and/or an increase the number of myofibrils (myofibril hyperplasia) was not determined (Figure 1-7A) [31]. In fact, we are not aware of any studies that have systematically addressed whether mechanical load-induced myofiber hypertrophy is mediated by myofibril hypertrophy and/or myofibril hyperplasia. In our opinion, it is easy to envision how the induction of myofibril hypertrophy and/or myofibril hyperplasia could serve as the foundational events by which mechanical loading drives the radial growth of myofibers, thus the lack of knowledge on this topic is quite surprising.

Even though the concepts of myofibril hypertrophy and myofibril hyperplasia have not been thoroughly examined within the confines of mechanical load-induced skeletal muscle growth, there is still much that can be learned from related fields of study (e.g., developmental growth of skeletal muscle, mechanical load-induced growth of the heart, etc.). For instance, seminal work by Goldspink (1970) used mice of various ages to establish that a positive linear relationship exists

between myofibril diameter and myofiber CSA, and a similar relationship was also found to exist between myofibril number and myofiber CSA (Figure 1-7B-C) [185]. Collectively, the results of this study provided some of the first evidence that both myofibril hypertrophy and myofibril hyperplasia could contribute to the radial growth of myofibers. Moreover, these observations provided the basis for Dr Goldspink's intriguing model of radial growth which involves a process he called myofibril splitting [141, 185-187]. Specifically, Dr Goldspink proposed that the increase in myofibril number that occurs during the radial growth of myofibers could be explained by the longitudinal splitting of pre-existing myofibrils. In support of his hypothesis, he published numerous longitudinal images of single myofibrils that appeared to split into two smaller daughter myofibrils (Figure 1-8A) [185-187]. Moreover, he demonstrated that the splits usually occurred in the middle of Z-disc, and were typically found in myofibrils that are twice as large as myofibrils that did not contain splits [185].

In addition to his observations on longitudinal splitting, Dr Goldspink also noted that the thin myofilaments in sarcomeres do not run directly perpendicular to the Z-disc, but instead are offset at a slightly oblique angle (≈6–10°) [186]. This was an important observation because it suggested that the thin myofilaments could exert outward radial forces on the Z-disc when the sarcomeres contract. Indeed, this became a key part of his myofibril splitting model in which it was proposed that myofibrils initially undergo hypertrophy and, as their diameter increases, the outward radial forces that they exert on the Z-disc also increases. The outward radial forces place a strain on the center of the Z-disc, and when these forces reach a critical threshold, it causes the Z-disc to break (Figure 1-8B). The break begins at the center of the Z-disc and forms a split which then propagates through the remainder of the myofibril and ultimately forms two smaller daughter myofibrils.

Dr Goldspink's model of myofibril splitting was developed over 40 years ago, and it has frequently served as the textbook explanation of how myofibril number could increase during the radial growth of myofibers [188-191]. However, despite being widely accepted, the validity of the model has not been rigorously tested. For instance, we are not aware of any direct evidence that a single myofibril can split into daughter myofibrils. Furthermore, we are not aware of any studies that have established whether the outward radial forces generated by the obliquely aligned myofilaments would be physically capable of "breaking" the Z-disc. In addition to limited evidence, there are also parts of myofibril splitting model that seem to be incomplete. For instance, as shown in Figure 1-8B, it has been shown that the diameter of the myofibrils is directly related to the size of the myofibers, and from our point of view, Dr Goldspink's model is not capable of explaining this relationship [185]. Nevertheless, the general concepts of the myofibril splitting model are well reasoned and, as such, it will serve as framework for remainder of our discussions on myofibril hypertrophy and myofibril hyperplasia.

5.2.3. Myofibril Hypertrophy

If we assume that the basic concepts of the myofibril splitting model are correct, and that they can be applied to the radial growth of myofibers that occurs in response to increased mechanical loading, then the first part of the overall growth process would involve myofibril hypertrophy. This initial hypertrophic response would continue until the myofibrils reached the critical size that induces splitting. The splitting would result in the formation of daughter myofibrils that would then undergo hypertrophy until they split, and the cycle would repeat until the radial growth of the myofiber commenced. We will now examine the limited body of literature that surrounds this thesis.

To the best of our knowledge, only one study has addressed whether mechanical load-induced myofiber hypertrophy is associated with myofibril hypertrophy [184]. This study was performed by Ashmore and Summers (1981) and was focused on defining the changes that occur in the patigialis muscle of young chickens after 1–7 days of wing-weighting [184]. Importantly, the same group had previously demonstrated their model of wing-weighting leads to an ≈55% in myofiber CSA after 7 days [136], and not surprisingly, their 1981 publication revealed that the increase in myofiber CSA was matched by a proportionate increase in the CSA that was occupied by the myofibrils [184]. In this study, they also found that the average CSA of the individual myofibrils increased by 36% after 7 days, and this was associated with a 2.6-fold increase in the proportion of myofibrils that presented with signs of splitting [136]. When taken together these results are very noteworthy because they provide critical support for the notion that mechanical loading can induce myofibril hypertrophy, and that this effect is associated with an increase in myofibril splitting.

The results of Ashmore and Summers (1981) provided support for the notion that mechanical loading can induce myofibril hypertrophy, and therefore raise questions about the processes that drive this response [184]. When considering these processes it is important to remember that the force-generating myofilaments within the myofibrils are organized into a hexagonal array and the spacing between the myofilaments is highly conserved [181-183]. Thus, it can be predicted that an increase in the CSA of the myofibril would be met by a proportionate increase in the number of force-generating myofilaments per CSA. If this is correct, then one is left with the question of where the new myofilaments get deposited.

As illustrated in Figure 1-9, some possible locations of new myofilament deposition include but are not limited to: A) the periphery of the pre-existing myofibril, B) the center of the pre-

existing myofibril, or C) throughout the pre-existing myofibril. All these options seem plausible, but options B and C would likely require extensive remodeling of the pre-existing myofilament lattice, whereas option A presumably would not. Thus, from a resources/energetic standpoint, the deposition of new myofilaments at the periphery of the pre-existing myofibril would appear to be the most cost-effective and least disruptive option.

The work of Morkin (1970) is often cited as providing support for the notion that new myofilaments are added to the periphery of myofibrils [192]. Specifically, in this study, rat diaphragm muscles were incubated with ^{3}H-leucine to label newly synthesized proteins, and then electron microscope autoradiography was used to identify the location of the newly synthesized proteins [192]. As shown in Figure 1-10A, the location of the newly synthesized proteins was indicated by the presence of relatively large (≈300 nm) electron dense grains. The quantitative results from this study are shown in Figure 1-10B with the bars indicating how frequently the center of the grains appeared at various distances from the periphery of the myofibril, and the green highlighted curve illustrating the theoretical distribution of the grains that would be expected if the myofibrils were labeled exclusively at the periphery. At first glance, the close match between the theoretical and observed values appears to provide compelling support for the conclusion that new myofilaments are added to the periphery of the myofibrils [192]. However, this evidence becomes less persuasive when one considers that ribosomes are typically localized in the intermyofibrillar space and many of these ribosomes appear in polysomal configurations which is indicative of active protein synthesis (Figure 1-10C) [193, 194]. This point leads us to question how well the data from Morkin (1970) would fit with a different hypothesis. In this case, the hypothesis was that the ribosomes in the intermyofibrillar space are actively engaged in the synthesis of new proteins. In Figure 1-10D–E, we have illustrated how well the data from Morkin (1970) fit with

the theoretical distribution of the grains that would be expected if the myofibrils were labeled exclusively at the periphery, and compared that with the theoretical distribution of the grains that would be expected if newly synthesized proteins were located exclusively within the intermyofibrillar space. The key point from this illustration is that the data appears to be consistent with both theoretical distributions, and this is because the resolution provided by autoradiography simply does not allow for a clear distinction between the two possibilities.

The limitations of the resolution that can be obtained with electron microscope autoradiography have been thoroughly described by Caro (1962) and Salpeter et al. (1969) [195, 196]. Importantly, both of these studies demonstrate that under typical conditions, 50% of the grains will develop within ≈130 nm of the source and 95% of the grains will develop within ≈300 nm [195, 196] (Figure 1-10F). This level of resolution would be outstanding if the goal was to identify the location of newly synthesized proteins within a myofiber (typical diameter of 25,000 nm), but it is far from ideal when the goal is to identify the location of newly synthesized proteins within a myofibril (typical diameter 850 nm). To effectively accomplish this goal, technologies that offer a much higher level of resolution are needed, and fortunately, such technologies are now available. For instance, it is now possible to identify the location of newly synthesized proteins with immunological and click-chemistry-based technologies [197, 198]. This is noteworthy because, as illustrated in Figure 1-10F, a typical immunoelectron microscopy-based approach will result in 100% of the signal appearing within 20 nm of the source, and the use of more advanced approaches (e.g., 1 nm gold conjugated Fab antibody fragments, or click-chemistry-based linkers) can allow for a resolution of less than 7 nm [199-202]. Thus, although we still do not know whether mechanical load-induced hypertrophy of myofibers is driven by myofibril hypertrophy, or where

new myofilaments get added during the process of myofibril hypertrophy, the technologies that are needed to answer these fundamental questions are now within our reach.

5.2.4. Myofibril Hyperplasia

As mentioned in the previous section, the study by Ashmore and Summers (1981) provided support for the notion that the mechanical load-induced radial growth of myofibers is associated with myofibril hypertrophy, but unfortunately, the study did not address the concept of myofibril hyperplasia [184]. In fact, we are not aware of any studies that have directly addressed this concept, and the only study we could find that even came remotely close was performed by Holmes and Rasch (1958) [203]. Specifically, this study involved 7 weeks of training rats with progressively more intense running and concluded that the number of myofibrils per myofiber in the sartorius muscle was not significantly altered by the training regime [203]. However, it was also determined that the training regime did not lead to a significant increase in mass of the sartorius muscle and, thus, it is difficult to extrapolate any meaningful insights from the data.

Although we are not aware of any studies in skeletal muscle that have directly addressed whether mechanical load-induced myofiber hypertrophy is associated with myofibril hyperplasia, there are a few studies that have addressed this topic in the heart. For instance, Toffolo and Ianuzzo (1994) used aortic constriction to subject rat hearts to mechanical overload and found that after 30 days, the cardiomyocyte area had increased by ≈50% and this was associated with an ≈70% increase in the number of myofibrils per cardiomyocyte [204]. An increase in the number of myofibrils per cardiomyocyte has also been observed in hypertrophied human hearts that were examined postmortem [205]. Furthermore, Anversa et al. (1980) examined heart papillary muscles after 8 days of mechanical overload and observed a 55% increase in the CSA of the cardiomyocytes that was occupied by the myofibrils, but no change in the CSA of the individual myofibrils, thus

implying an increase in myofibril number [206]. Taken together, these studies consistently suggest that an increase in mechanical loading can lead to an increase in myofibril number in the heart, but whether the same effect occurs in skeletal muscles remains to be determined

5.2.5. The Radial Growth of Myofibers—Closing Remarks

As we have discussed, a substantial body of evidence indicates that the mechanical load-induced radial growth of myofibers is mediated by a proportional increase in the force-generating and non-force-generating elements. The force-generating elements are contained within the myofibrils, and the myofibrils account for ≈80% of the myofiber CSA. Thus, it can be argued that the bulk of the radial growth is driven by an expansion of the myofibrils. However, whether this expansion is due to hypertrophy of the individual myofibrils and/or myofibril hyperplasia remains to be established. Based on our collective view of the literature, we propose that both processes are involved, and can be explained by a model that we have defined as the "myofibril expansion cycle". Specifically, as illustrated in Figure 1-11, the myofibril expansion cycle begins with the deposition of new myofilaments around the periphery of the pre-existing myofibrils, and results in myofibril hypertrophy. Once the myofibrils reach a critical size, they split and subsequently form two smaller daughter myofibrils. The daughter myofibrils are then able to enter another round of the cycle, and the cycle repeats until the radial growth of the myofiber has commenced. Clearly, our model is based on an integration of hypotheses that were proposed more than 40 years ago, and as emphasized throughout this section, the validity of these hypotheses have not been rigorously tested. Fortunately, the technologies that are needed to test these hypotheses are now available. Thus, we hope that this section will help to inspire new investigations into this seemingly forgotten, yet critically important aspect of skeletal muscle biology.

6. Take Home Messages

Mechanical loads are one of the most potent regulators of muscle mass and the maintenance of muscle mass plays a critical role in health and quality of life. In Table 1-1 we have summarized the major structural adaptations that have been implicated in the mechanical load-induced growth of skeletal muscle. Based on our review, we have also considered whether each of these adaptations makes a substantive contribution to the overall growth process, as well as the level of evidence that is available to support that conclusion. The table also lists some of the major gaps in knowledge that we identified during our review of the literature. Importantly, this is not meant to be an exhaustive summary, and exclusion from the table does not indicate that a given adaptation or gap in knowledge is unimportant (e.g., satellite cell fusion, are satellite cells necessary for mechanical load-induced growth, etc.).

As documented in this review, several of the adaptations that we consider as having weak supporting evidence have been engrained in the literature as "textbook" mechanisms (e.g., the longitudinal growth of myofibers is driven by the addition of new sarcomeres at the ends of myofibers, new myofibrils are formed via myofibril splitting, etc.). We hope that after reading this review, the reader appreciates how little we actually know about the structural adaptations that drive skeletal muscle growth, and the number of extremely fundamental gaps in knowledge that remain to be filled.

Author Contributions: K.W.J., S.M.P. and T.A.H.; all contributed to the writing of this manuscript and have read and agreed to the published version of the manuscript.

Funding: The research reported in this publication was supported by the National Institute of Arthritis and Musculoskeletal and Skin Diseases of the National Institutes of Health under Award

Number AR074932 to SMP and TAH. The content is solely the responsibility of the authors and does not necessarily represent the official views of the National Institutes of Health.

Conflicts of Interest: The authors declare no conflict of interest.

Figure 1-1

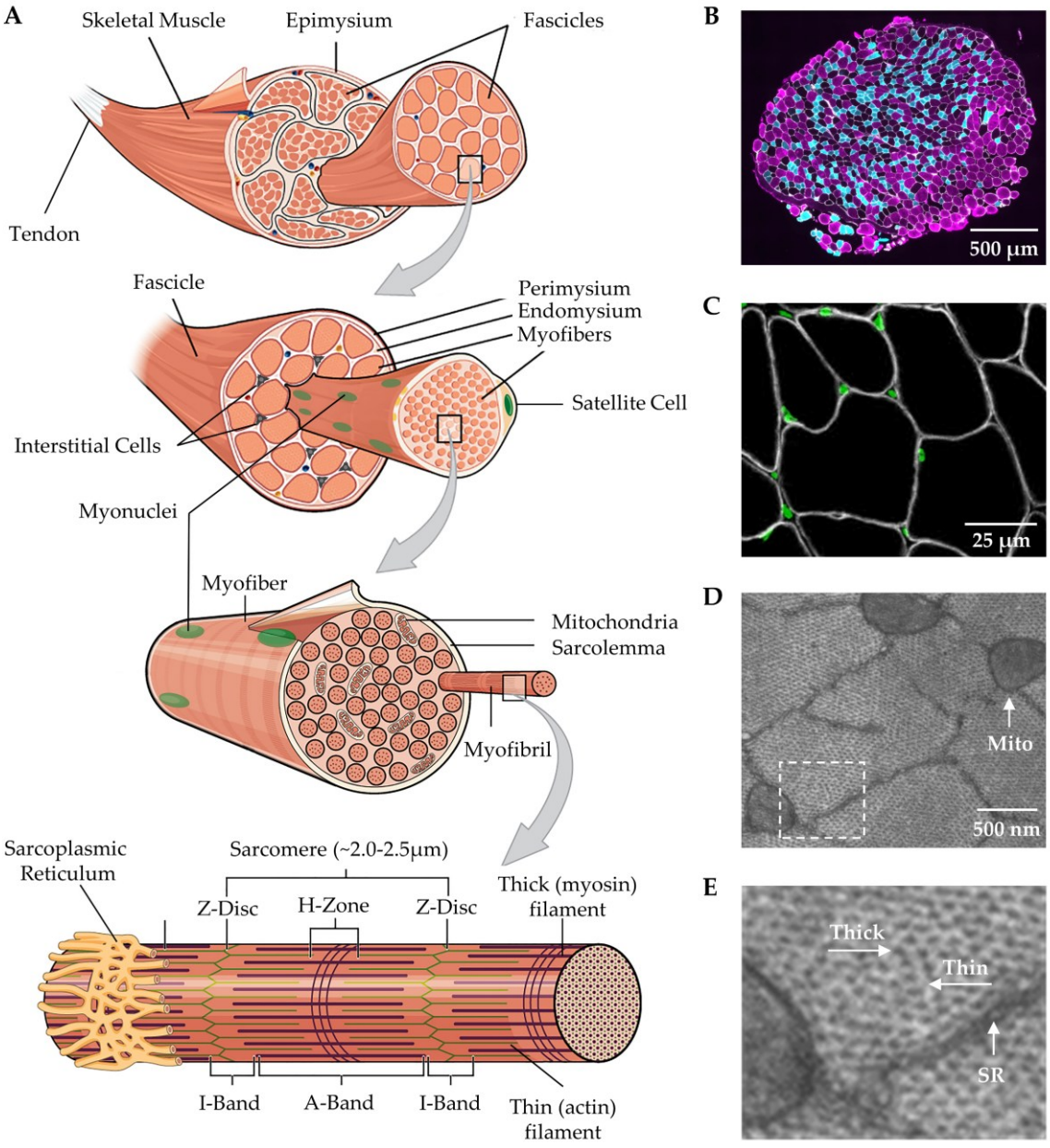

Figure 1-1. (**A**) Illustration of skeletal muscle structure copied with permission under the Creative Commons Attribution 4.0 International license and adapted for this review, available online: https://openstax.org/books/anatomy-and-physiology/pages/10-2-skeletal-muscle (accessed on 6/1/2020) [207]. (**B**) Cross-section of a mouse plantaris muscle that was subjected to immunohistochemistry for the identification of Type IIA (cyan), and Type IIB (magenta) myofibers as well as laminin to identify the endomysium (white). (**C**) Cross-section of a mouse plantaris muscle that was subjected to immunohistochemistry for the identification of dystrophin to identify the inner boundary of the sarcolemma (white) and nuclei (green). (**D**) Cross-section of a mouse plantaris muscle that was subjected to electron microscopy to highlight the sarcoplasmic reticulum (SR) that surrounds individual myofibrils as well as the mitochondria (Mito) that run between the myofibrils. (**E**) Higher magnification of the boxed region in D reveals the presence of the thick and thin myofilaments.

Figure 1-2

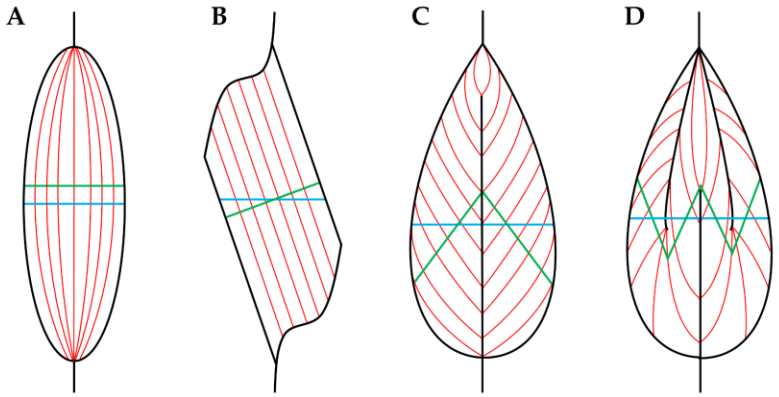

Figure 1-2. Various pennation angle arrangements of the fascicles / myofibers in skeletal muscle: (**A**) fusiform, (**B**) unipennate, (**C**) bipennante, (**D**) multipennate. Blue lines indicate the plane for the anatomical cross-sectional area (CSA) (i.e., the CSA that runs perpendicular to the longitudinal axis of the muscle), and green lines indicate the plane for physiological CSA (i.e., the CSA that runs perpendicular to the longitudinal axis of the fascicles / myofibers). Adapted under the Creative Commons Attribution-Share Alike 3.0 Unported license from original work by Uwe Gille (Available online: https://creativecommons.org/licenses/by-sa/3.0/deed.en (accessed on 6/1/2020).

Figure 1-3

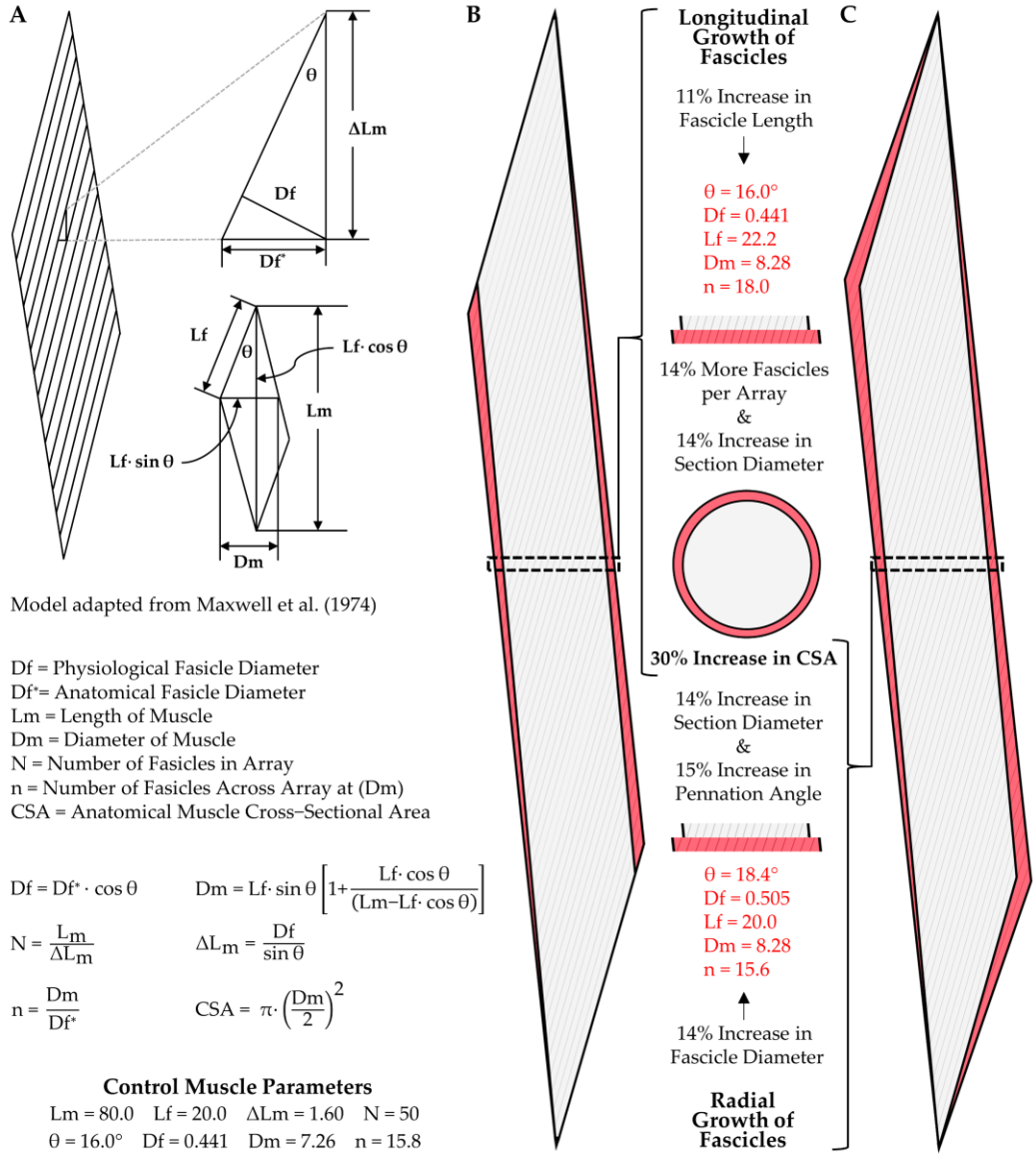

Figure 1-3. Illustration of how the longitudinal and radial growth of fascicles can lead to changes in muscle cross-sectional area (CSA). (**A**) Key elements of a geometric model that can be used to predict the architectural properties of skeletal muscle [75]. (**B**) Illustration of how an 11% increase in fascicle length would result in 30% increase in CSA, as well as a 30% increase in the number of fascicles per cross-section. (**C**) Illustration of how a 14% in fascicle diameter would lead to a 15% increase in the pennation angle and a 30% increase in the CSA, but essentially no change in the number of fascicles per cross-section.

Figure 1-4

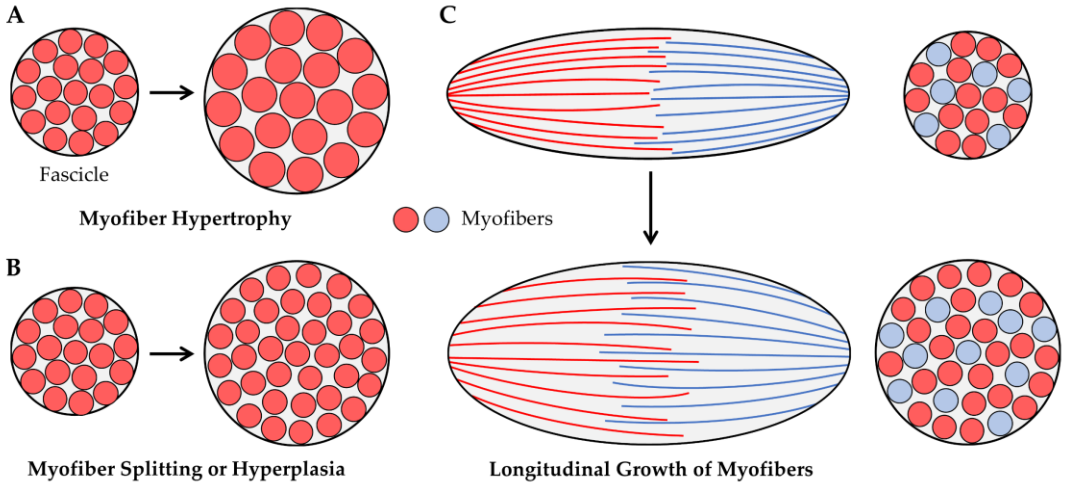

Figure 1-4. Illustration of how the radial growth of muscles fascicles could result from (**A**) myofiber hypertrophy, (**B**) myofiber splitting or hyperplasia, or (**C**) longitudinal growth of myofibers that exhibit intrafascicular terminations, such as those observed in the long sartorius and gracilis muscles of humans [91].

Figure 1-5

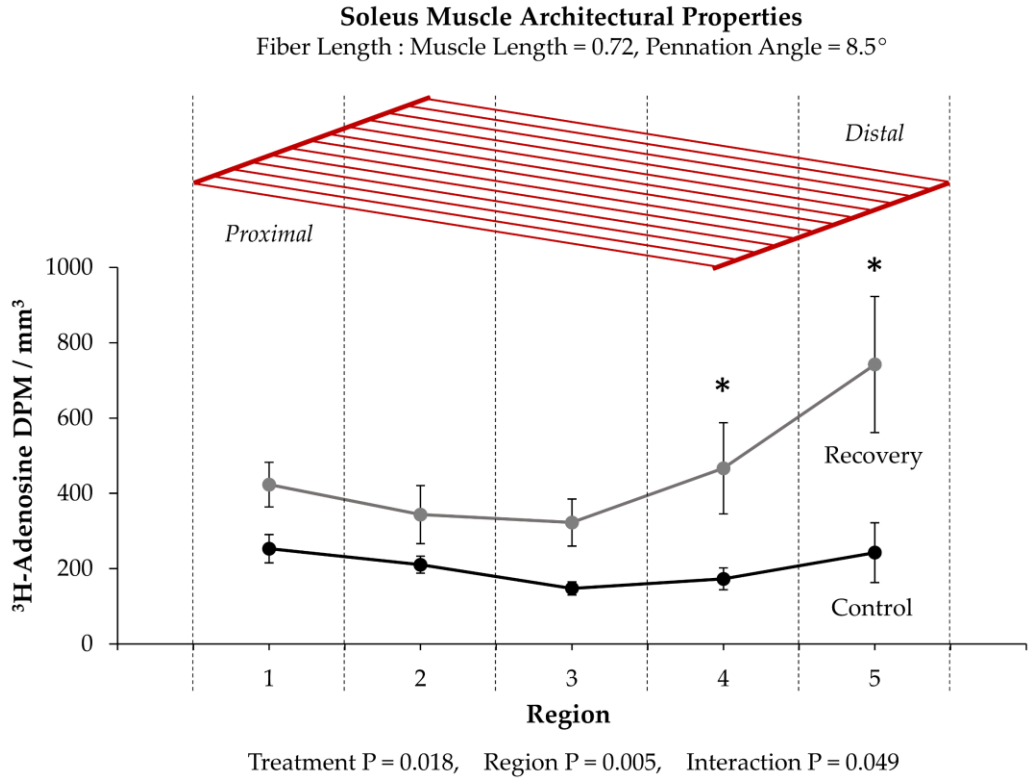

Figure 1-5. (Top) Schematic illustration of the soleus muscle and its basic architectural properties [208]. (Bottom) Summary of the data provided by Williams and Goldspink (1973) [135]. Values are presented as the means ± SEM and were analyzed with 2-way repeated measures ANOVA. *p*-values for the main effects (i.e., Treatment and Region) and interaction are provided. * Significantly different from the region-matched control condition.

Figure 1-6

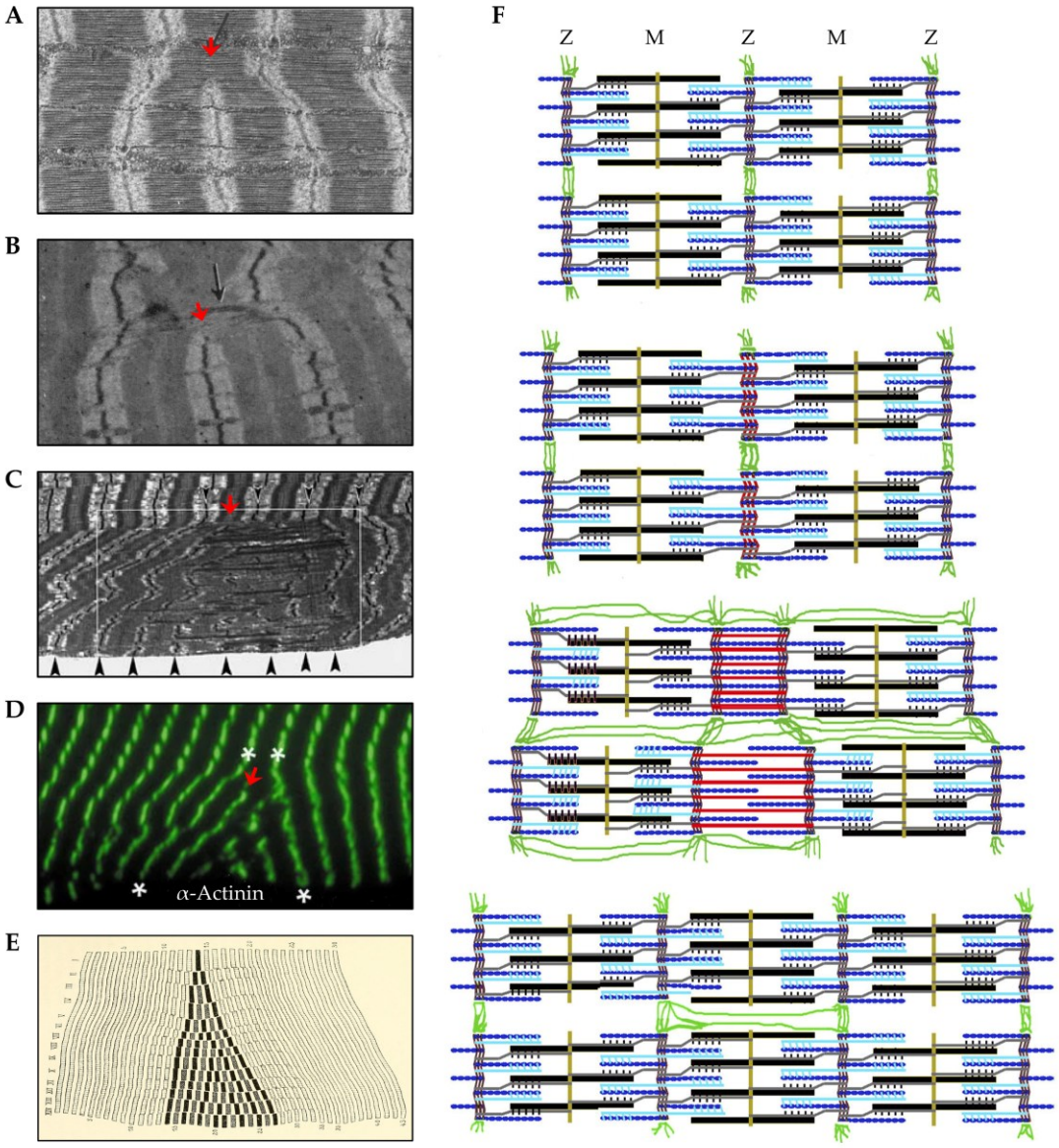

Figure 1-6. (**A**) Electron micrograph (EM) image that shows a group of myofibrils along with sarcomeres embedded within these myofibrils that possess a transverse split (red arrow) at the H-zone. The image was copied with permission under a Creative Commons License Attribution–Noncommercial–Share Alike 4.0 Unported license, and is available online at https://www.ncbi.nlm.nih.gov/pmc/articles/PMC2110374/ (accessed on 6/20/2020) [143]. (**B**) EM image of myofibrils from a muscle that was subjected to synergist ablation and appears to possess a transverse split at the H-zone (copied with permission from [118]). (**C**–**D**) EM image (**C**) and immunohistochemical image (**D**) of regions with "supernumerary sarcomeres" that are found in human skeletal muscles several days after being subjected to a bout of eccentric contractions (copied with permission from [147, 148]). (**E**) Depiction of a "sphenode" region as detailed by Heidenhain (1919) [156]. (**F**) Illustration describing a mechanism for the in-series addition of new sarcomeres via transverse splitting at the Z-disc (copied with permission from [150]).

Figure 1-7

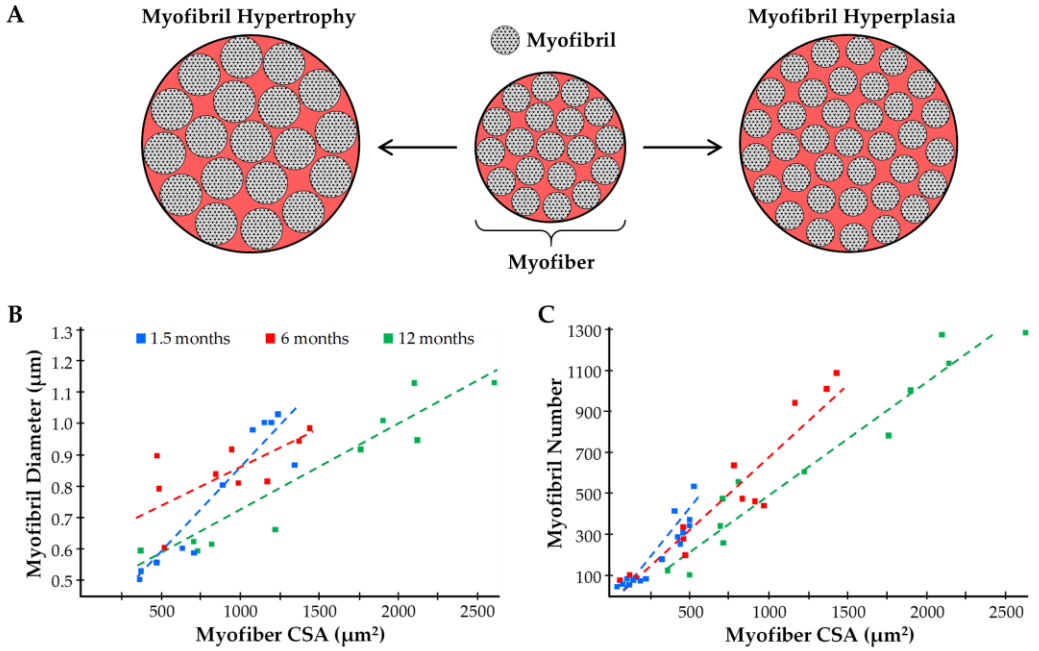

Figure 1-7. (**A**) Illustration of how an increase in the CSA of the pre-existing myofibrils (myofibril hypertrophy) and an increase in the number of myofibrils (myofibril hyperplasia) can contribute to the radial growth of myofibers. (**B**–**C**) Summary of the data from Goldspink (1970) which highlights the relationship that exists between myofiber CSA and myofibril diameter (**B**), as well as myofiber CSA and myofibril number (**C**), in mice of various ages [185].

Figure 1-8

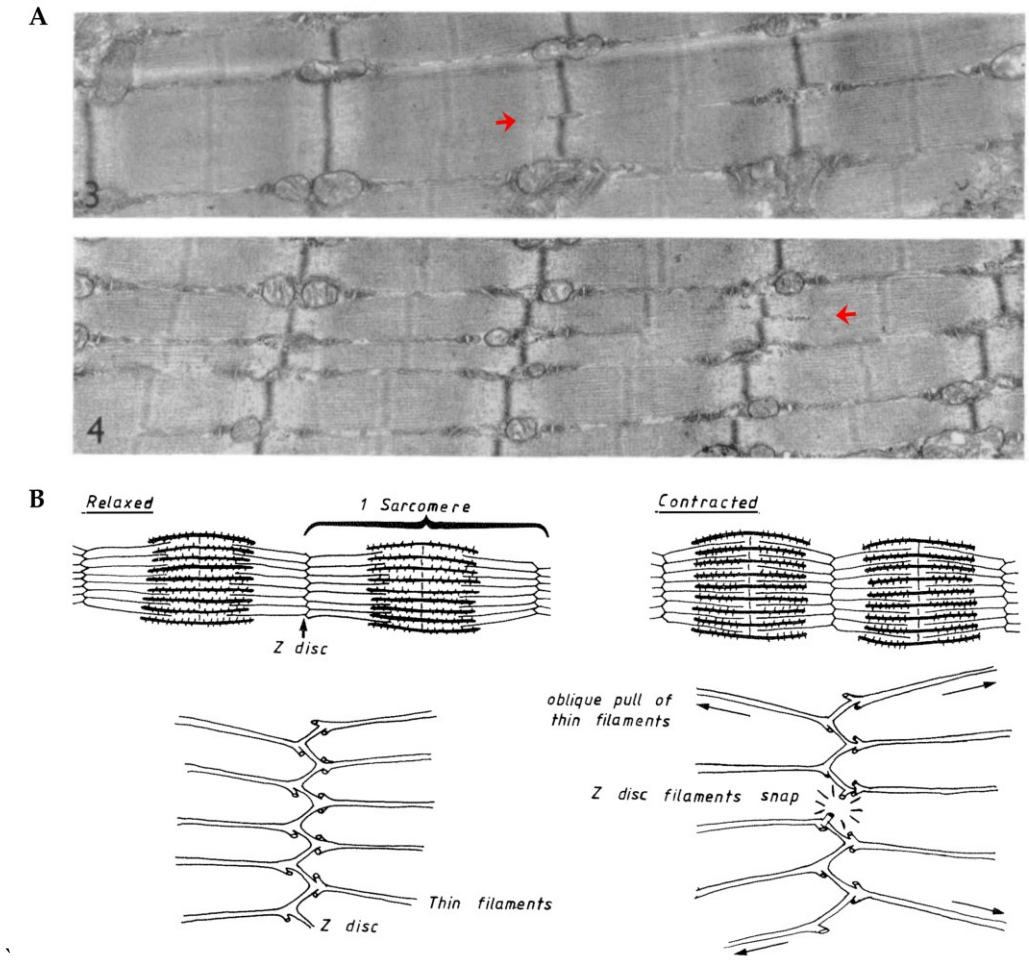

Figure 1-8. (**A**) Electron micrographs of longitudinal sections from mouse skeletal muscle. Red arrows highlight myofibrils that appear to split into two smaller daughter myofibrils (copied with permission from [186]). (**B**) Illustration from Goldspink (1983) which describes how the oblique angle of the thin myofilaments could exert outward radial forces on the Z-disc when the sarcomeres contract (copied with permission from [141]).

Figure 1-9

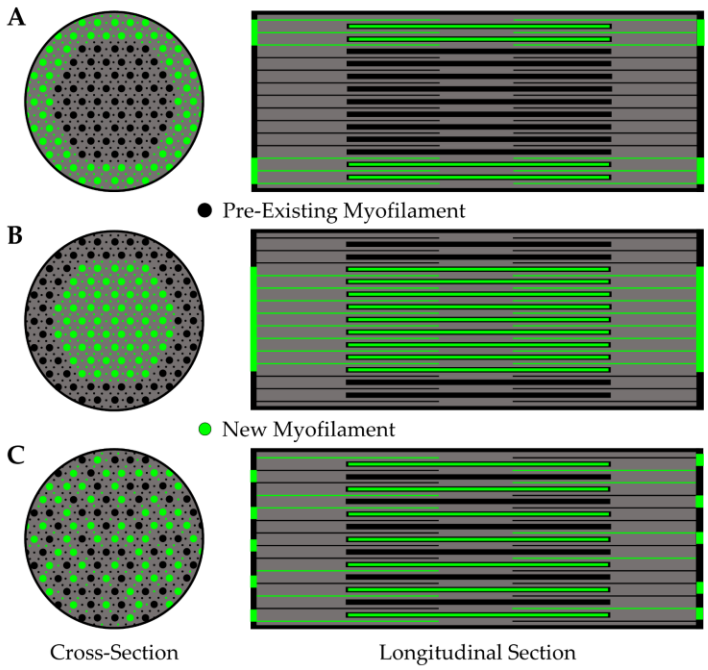

Figure 1-9. Illustration of where new myofilaments might be added during myofibril hypertrophy. The described possibilities include: (**A**) the periphery of the pre-existing myofibril, (**B**) the center of the pre-existing myofibril, or (**C**) throughout the pre-existing myofibril.

Figure 1-10

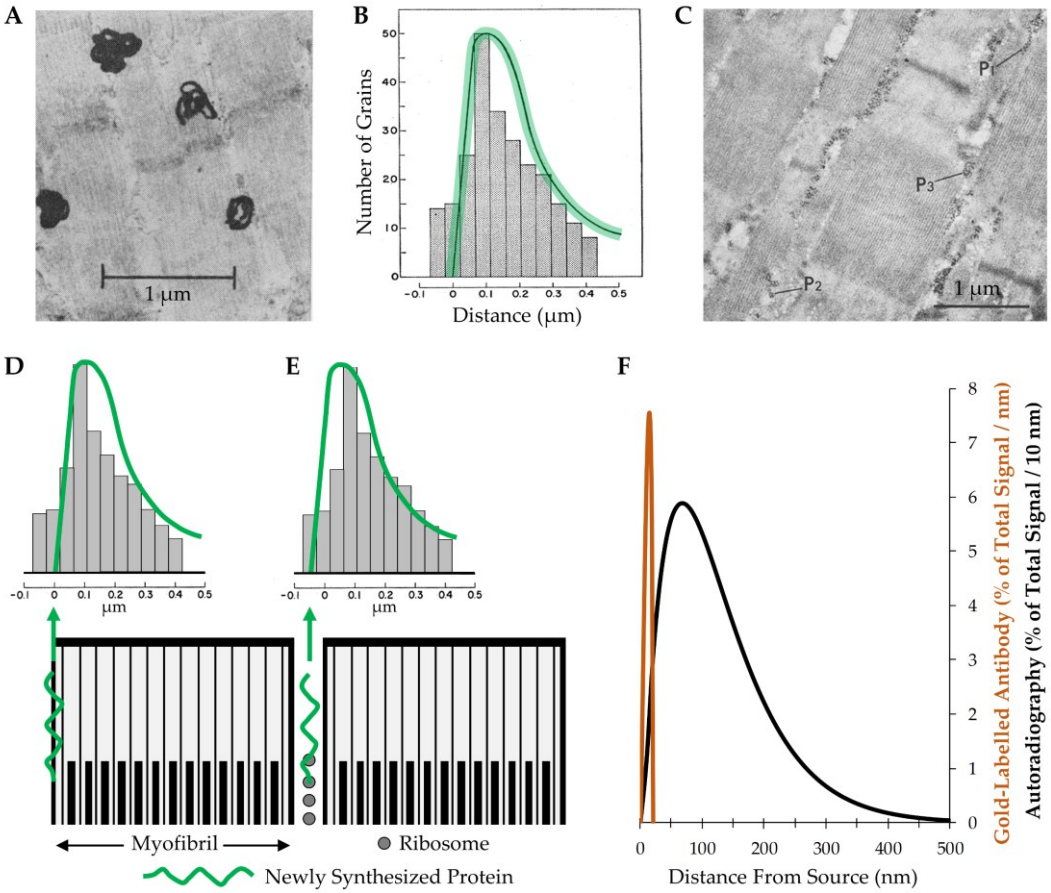

Figure 1-10. (**A**) Electron microscope autoradiograph from Morkin (1970) which shows the large electron dense grains that were used to identify the location of newly synthesized proteins in the rat diaphragm. (**B**) Bars represent the frequency distribution of the grains relative to the periphery of the myofibril, and the green shaded curve illustrates the theoretical distribution that would be expected if the newly synthesized proteins were located exclusively at the periphery of the myofibril. The images in both A and B were copied with permission from [192]. (**C**) Electron micrograph of the levator ani muscle from an adult rat which reveals the presence of ribosomes in the intermyofibrillar space. Please note that many of the ribosomes appear in different polysomal configurations (P1, P2 and P3) (copied with permission from [193]). (**D**–**E**) Illustration of how well the data from Morkin 1970 fit with the theoretical distribution that would be expected if the newly synthesized proteins were located exclusively at the periphery of the myofibril (**D**) versus being located exclusively within the intermyofibrillar space (**E**). (**F**) A graph illustrating the theoretical radial distribution of the signal obtained with electron microscope autoradiography versus with immunoelectron microscopy that employed a primary antibody (15 nm diameter) conjugated to a 10 nm gold-particle [196, 202, 209].

Figure 1-11

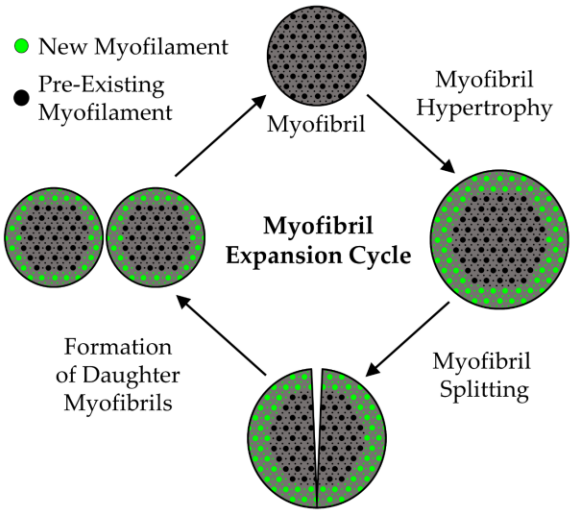

Figure 1-11. Illustration of the proposed "Myofibril Expansion Cycle".

Table 1-1

Table 1-1. The Structural Adaptations that Drive the Mechanical Load-Induced Growth of Skeletal Muscle

Adaptation	Evidence	Gaps in Knowledge
Longitudinal Growth of Fascicles	High	Does mechanical loading alter the number of fascicles? Can mechanical loading lead to the addition of new myofibers in-series?
Radial Growth of Fascicles	High	To what extent does myofiber hyperplasia, myofiber splitting, and the lengthening of myofibers with intrafascicular terminations contribute to the radial growth of fascicles?
Myofiber Splitting	Low	Do physiologically relevant models of mechanical loading induce myofiber splitting?
Myofiber Hyperplasia	Low & Controversial	To what extent, if any, does myofiber hyperplasia contribute to the radial growth of fascicles?
Longitudinal Growth of Myofibers	Mixed - Model Dependent	Do physiologically relevant forms of mechanical loading induce the longitudinal growth of myofibers? Where, and how, are new sarcomeres added during the longitudinal growth of myofibers?
Radial Growth of Myofibers	Extremely High	Is mechanical load-induced myofiber hypertrophy driven by myofibril hypertrophy and/or myofibril hyperplasia?
Sarcoplasmic Hypertrophy	Low & Controversial	Are there specific conditions during which sarcoplasmic hypertrophy might make substantive contribution to the mechanical load-induced growth of myofibers?
Myofibril Hypertrophy	Low	Does mechanical loading lead to myofibril hypertrophy? Where are new myofilaments deposited during myofibril hypertrophy?
Myofibril Hyperplasia	Very Low	Does mechanical loading lead to myofibril hyperplasia? Are new myofibrils generated via the process of myofibril splitting?

Chapter Two: A Novel Imaging Method (FIM-ID) Reveals that Myofibrillogenesis Plays a Major Role in the Mechanically Induced Growth of Skeletal Muscle

Kent W. Jorgenson[1], Jamie E. Hibbert[1], Ramy K. A. Sayed[1,2], Anthony N. Lange[1], Joshua S. Godwin[3], Paulo H. C. Mesquita[3], Bradley A. Ruple[3], Mason C. McIntosh[3], Andreas N. Kavazis[3], Michael D. Roberts[3], Troy A. Hornberger[1*]

[1]School of Veterinary Medicine and the Department of Comparative Biosciences, University of Wisconsin-Madison, Madison, WI, USA. [2]Department of Anatomy and Embryology, Faculty of Veterinary Medicine, Sohag University, Sohag, Egypt. [3]School of Kinesiology, Auburn University, Auburn, AL, USA.

*Corresponding author (Lead Contact): Troy A. Hornberger

2015 Linden Drive

Madison WI, 53706

Phone: (608) 890-2174

Email: troy.hornberger@wisc.edu

This chapter was published in The Journal *eLife* in March 2024 and modified slightly to comply with the format of this dissertation.

Abstract

An increase in mechanical loading, such as that which occurs during resistance exercise, induces radial growth of muscle fibers (i.e., an increase in cross-sectional area). Muscle fibers are largely composed of myofibrils, but whether radial growth is mediated by an increase in the size of the myofibrils (i.e., myofibril hypertrophy) and/or the number of myofibrils (i.e., myofibrillogenesis) is not known. Electron microscopy (EM) can provide images with the level of resolution that is needed to address this question, but the acquisition and subsequent analysis of EM images is a time- and cost-intensive process. To overcome this, we developed a novel method for visualizing myofibrils with a standard fluorescence microscope (FIM-ID). Images from FIM-ID have a high degree of resolution and contrast, and these properties enabled us to develop pipelines for automated measurements of myofibril size and number. After extensively validating the automated measurements, we used both mouse and human models of increased mechanical loading to discover that the radial growth of muscle fibers is largely mediated by myofibrillogenesis. Collectively, the outcomes of this study offer insight into a fundamentally important topic in the field of muscle growth and provide future investigators with a time- and cost-effective means to study it.

Introduction

Comprising ~45% of the body's mass, skeletal muscles are not only the motors that drive locomotion, but they also play a critical role in respiration, whole-body metabolism, and maintaining a high quality of life [1, 210-212]. Indeed, both sedentary and active adults will lose 30-40% of their muscle mass by the age of 80, and this loss in muscle mass is associated with disability, loss of independence, an increased risk of morbidity and mortality, as well as an estimated $40 billion in annual hospitalization costs in the United States alone [212-216]. Thus, the development of therapies that can restore, maintain, and/or increase muscle mass is of great clinical and fiscal significance. However, to develop such therapies, we will first need to define the basic mechanisms that regulate skeletal muscle mass.

Skeletal muscle mass can be regulated by a variety of different stimuli with one of the most widely recognized being mechanical signals [217-220]. For instance, a plethora of studies have shown that an increase in mechanical loading, such as that which occurs during resistance exercise, can induce radial growth of the muscle fibers [51, 86, 101, 106, 221]. Surprisingly, however, the ultrastructural adaptations that drive this response have not been well defined [101, 221, 222]. Indeed, a number of seemingly simple and fundamental important questions have not been answered. For instance, during radial growth, the cross-sectional area (CSA) of the muscle fiber increases, but whether this is mediated by an increase in the CSA of the individual myofibrils (i.e., myofibril hypertrophy) and/or the number of myofibrils (i.e., myofibrillogenesis) has not been resolved [184, 221-223].

A longstanding model in the field proposes that the radial growth of muscle fibers can be explained by a process called "myofibril splitting" [185-187, 224]. The myofibril splitting model was developed by Goldspink in the 1970s and contends that, during radial growth, myofibrils initially undergo hypertrophy. Then, as the CSA of the myofibrils increases, the outward radial

force that they exert on the Z-disc increases. The outward radial forces place a strain on the center of the Z-disc, and when the forces reach a critical threshold the Z-disc will break. It is proposed that the break will begin at the center of the Z-disc and form a longitudinal split that will then propagate through the remainder of the myofibril and, in turn, result in the formation of two smaller daughter myofibrils. It is also proposed that the daughter myofibrils can undergo a cycle of further hypertrophy and splitting, and this cycle will continue until the radial growth of the muscle fiber ceases.

In support of his model, Goldspink published numerous images of single myofibrils that appeared to split into two smaller daughter myofibrils, as well as quantitative data which demonstrated that longitudinal splits usually occur in myofibrils that are significantly larger than myofibrils that do not contain splits [185-187]. Indeed, the model seemed so convincing that, when discussing how an increase in mechanical loading leads to the growth of muscle fibers, Goldspink concluded *"The number of myofibrils increases ([34]), and this is almost certainly due to the longitudinal splitting of existing myofibrils rather than de novo assembly"* [224]. This statement has been highlighted because, for decades, the myofibril splitting model has served as the textbook explanation of how muscle fibers undergo radial growth [188-190]. However, after performing an exhaustive review of the literature, it was clear that this model has not been rigorously tested [221]. In fact, in many instances, the potential implications of the model are based on erroneous claims. For instance, in Goldspink's aforementioned conclusion, neither reference [34], nor any other study that we are aware of, has ever shown that an increase in mechanical loading leads to an increase in the number of myofibrils per fiber. Thus, one is left to wonder why this widely cited model of growth has not been rigorously tested.

When considering currently available technologies, electron microscopy (EM) would be viewed as the gold standard method for testing the myofibril splitting model; however, EM has several drawbacks/limitations. For instance, electron microscopes are highly specialized instruments, and their use requires immense training and potentially cost-prohibitive user fees. Furthermore, the extensive fixation and processing required for EM often yields samples that are not readily amenable to immunolabeling [225], and EM images typically do not have a high degree of contrast between the area that is occupied by the myofibrils and the intermyofibrillar components that surround the myofibrils (e.g., the sarcoplasmic reticulum, see Figure 2-4A). The latter point is particularly important because it serves as a barrier to the development of programs that can perform automated measurements of features such as myofibril CSA and myofibril number. Thus, with EM, such measurements would need to be manually derived.

To gain insight into the effort that manual measurements of myofibril CSA would require, we collected pilot data from EM images of mouse skeletal muscles. We then used Cochran's formula to determine how many myofibrils per fiber would have to be measured to estimate the mean myofibril CSA with a 5% margin of error at a 95% level of confidence [226]. The outcomes revealed that >180 myofibrils per fiber would have to be manually traced. Bear in mind that estimating the average myofibril CSA for the entire sample would require measurements from multiple fibers. For instance, if just 20 fibers per sample were analyzed, it would require the manual tracing of >3600 myofibrils. Taking this a step further, it would mean that a two-group comparison with 7 samples per group would require the manual tracing of >50,000 myofibrils. In our hands, it took 1 hr to measure ~125 myofibrils, and thus the simple two-group comparison described above would require ~400 hours of manual tracing. With numbers like this, it was easy to appreciate why the basic elements of Goldspink's model have not been rigorously tested. Thus,

the first goal of this study was to develop a time- and cost-effective method for visualizing myofibrils with a level of resolution and contrast that would support automated measurements of myofibril size and myofibril number. With this method in hand, we then set out to answer the fundamentally important question of whether the radial growth of muscle fibers that occurs in response to an increase in mechanical loading is mediated by myofibril hypertrophy and/or myofibrillogenesis.

Results

Optimization of the fixation, cryoprotection, and sectioning conditions for Fluorescence Imaging of Myofibrils with Image Deconvolution (FIM-ID).

As explained in the introduction, one of the primary goals of this study was to develop a time- and cost-effective method for visualizing myofibrils with a level of resolution and contrast that would support automated measurements of myofibril size. To accomplish this, we took advantage of the fact that myofibrils are largely surrounded by a sarcoplasmic reticulum (SR) that is highly enriched with an enzyme called the sarco(endo)plasmic reticulum calcium-ATPase (SERCA) [227-229]. There are two major isoforms of SERCA (SERCA1 which is found in Type II fibers, and SERCA2 which is found in Type I fibers), and monoclonal antibodies for each isoform have been in existence for many years [229-233]. Importantly, these antibodies have been shown to possess excellent reactivity in both flash-frozen and aldehyde-fixed tissues [234-236]. Thus, we reasoned that these antibodies could be used to illuminate the periphery of the myofibrils in muscles that had been subjected to a variety of different preservation conditions.

To test our hypothesis, we first performed immunohistochemistry (IHC) for SERCA1 on cross-sections of mouse plantaris muscles that had been flash-frozen in optimal cutting temperature compound (OCT). As shown in Figure 2-1A, small patches within the fibers revealed

seemingly intact myofibrils, but the overall integrity of the myofibrils was very poor. This was not surprising because it is known that flash-frozen muscles can suffer from freezing artifacts that present as holes within the fibers [237-239]. Thus, to determine if the integrity of the myofibrils was being distorted by freezing artifacts, we co-stained the cross-sections with phalloidin, and the results confirmed that regions of poor myofibril integrity were directly associated with the presence of freezing artifacts (Figure 2-1B). As such, it was concluded that the development of a time- and cost-effective method for visualizing intact myofibrils would require the use of a procedure that eliminates freezing artifacts.

In 1973, Tokuyasu described a fixation and cryoprotection procedure that could preserve the ultrastructure of skeletal muscle at a level that was equivalent to that obtained with the conventional resin-embedding procedures of EM [240]. Importantly, unlike resin-embedded tissues, it was shown that tissues preserved with the Tokuyasu method retain a high level of immunoreactivity and are therefore amenable to immunolabelling [202]. Indeed, in 1982, the Tokuyasu method was used to define the ultrastructural localization of SERCA [227]. The key components of the Tokuyasu method involve an aldehyde-based fixative and sucrose which not only serves as a cryoprotectant but it also controls the consistency of the tissue to allow for ultrathin (< 0.2 μm) sectioning. Specifically, Tokuyasu demonstrated that with a proper combination of the sucrose and sectioning temperature, one could obtain ultrathin sections of various tissues [240]. However, the traditional Tokuyasu method requires sectioning temperatures that range from -50 to -110º C, and such sectioning temperatures are dependent on the use of a cryo-ultramicrotome which is a rare and expensive instrument. Hence, although it appeared that the traditional Tokuyasu method would enable us to obtain immunoreactive sections that were devoid of freeze artifacts, the need for a cryo-ultramicrotome defeated our goal of developing a cost-effective method.

Nevertheless, we were inspired by the Tokuyasu method, and we predicted that the right combination of sucrose and sectioning temperature would enable us to obtain adequately cryoprotected and immunoreactive semi-thin sections with a regular cryostat.

To examine the validity of our prediction we performed a lengthy series of trial-and-error experiments, and through these experiments, we discovered that SERCA immunoreactive cross-sections that were devoid of freeze artifacts could be obtained from muscles that had been extensively fixed with 4% paraformaldehyde and subsequently cryoprotected with 30 - 45% sucrose (Figure 2-1C-D). Qualitatively, we concluded that the best integrity of the myofibrils was found in samples that had been cryoprotected with 45% sucrose and we also discovered that by lowering the sectioning temperature to -30º C we could eliminate sectioning artifacts that were readily present on the surface of samples that had been sectioned at warmer temperatures (Figure 2-2). Thus, whenever possible, all future studies were performed on tissues that had been fixed with 4% paraformaldehyde, cryoprotected with 45% sucrose, and sectioned at -30º C.

As shown in Figure 2-1C, immunolabelling of SERCA1 on muscles that had been subjected to the optimized fixation/cryoprotection/sectioning procedure led to a moderately well-contrasted illumination of the periphery of the myofibrils on a standard widefield fluorescence microscope. We chose to use a widefield fluorescence microscope for image acquisition because the per frame capture time on a widefield fluorescence microscope is extremely short when compared with alternatives such as a confocal fluorescence microscope. For instance, our image acquisition parameters required <1 sec per frame on a Leica Widefield Thunder Microscope compared with >3 min per frame on a Leica confocal SP8 microscope. In other words, the use of widefield microscopy aligned with our goal of developing a time-effective method. However, it is known that the resolution and contrast in widefield images can be negatively impacted by the

acquisition of light that resides outside of the focal plane. Fortunately, major advancements in deconvolution algorithms have made it possible to reassign the out-of-focus light to its appropriate location [241]. Moreover, it has been shown that deconvoluted widefield images can actually have better resolution and contrast than confocal images [242]. Thus, to improve the resolution and contrast of the widefield images we employed Leica's 'Computational Clearing' algorithm for image deconvolution [243]. As shown in Figure 2-1E-F, the application of the deconvolution algorithm led to a dramatic increase in the resolution and contrast. Thus, by applying our optimized fixation, cryoprotection, and sectioning conditions, along with widefield fluorescence microscopy and image deconvolution, we fulfilled our goal of developing a time- and cost-effective method for visualizing intact myofibrils with a high degree of resolution and contrast, and we refer to the collective method as FIM-ID (Figure 2-1 – Figure Supplement 1).

Validation of an automated pipeline for measuring myofibril size with FIM-ID

Having established the conditions for FIM-ID, we next sought to determine whether the images from FIM-ID would be amenable to automated measurements of myofibril size. To accomplish this, we first developed an automated pipeline in the open-source CellProfiler image analysis software[244] that could distinguish the periphery of the myofibrils (i.e., the SERCA signal) from the background within a single muscle fiber, and then all objects that were >90% enclosed by the signal from SERCA were identified (Figure 2-3A-C). Approximately one-half of these objects appeared to be unseparated clusters of myofibrils and/or obliquely sectioned single myofibrils. Thus, additional filtering steps were added so that subsequent measurements of size were only performed on cross-sections of single circular/oval myofibrils that had a maximal aspect ratio of approximately 2.5:1 (Figure 2-3D).

To test the accuracy of the automated measurements, eight randomly selected regions of interest (ROI) from a single fiber were subjected to measurements of myofibril CSA. The same ROIs were given to six independent investigators, and these investigators were asked to identify and manually trace the periphery of all single circular/oval myofibrils that had an aspect ratio of <2.5:1 and were >90% enclosed by the SERCA signal (Figure 2-3E). The manual measurements of myofibril CSA were derived from the investigator's traces and compared with the automated measurements. As illustrated in Figure 2-3F, the comparisons revealed that there was a very high degree of agreement between the automated and manually obtained measurements of myofibril CSA. Indeed, a highly significant correlation ($R = 0.9589$, $P = 0.0002$) was observed when the automated measurements of myofibril CSA from each ROI were compared with the mean of the manual measurements. Thus, the results from these studies established that our automated program could accurately measure the size of myofibrils as identified with FIM-ID.

Further refinement and validation of the automated measurements with FIM-ID.

EM has been extensively used to assess the ultrastructural characteristics of skeletal muscle and numerous EM-based studies have reported measurements of myofibril size [171, 184, 185, 223]. Hence, to further test the validity of our method, we directly compared our automated FIM-ID measurements of myofibril CSA with manual EM-based measurements. Specifically, we performed an experiment with four mice in which one plantaris muscle from each mouse was subjected to FIM-ID, and the other was processed for EM-based imaging. With FIM-ID it was determined that all fibers in the plantaris muscles were SERCA1 positive, but during the EM imaging it became apparent that these SERCA1 positive fibers consisted of two clearly discernable fiber types. One type was generally large in CSA and possessed very few intermyofibrillar

mitochondria, and we referred to these fibers as glycolytic (Gly) (Figure 2-4A). The other type was generally small in CSA and highly enriched with intermyofibrillar mitochondria, and we referred to these fibers as oxidative (Ox) (Figure 2-4A). The classification of the two fiber types was important because previous studies have shown that the morphological arrangement of myofibrils in different fiber types can be quite distinct. For instance, previous studies have shown that myofibrils in fibers that are rich in mitochondria typically have a "felderstruktur" appearance (i.e., field structure) whereas myofibrils in fibers that lack extensive mitochondria present with a "fibrillenstruktur" appearance (i.e., fibril structure) [245-248]. Accordingly, our experimental design was modified so that FIM-ID and EM-based measurements of myofibril CSA could be directly compared in the Ox and Gly fiber types.

To begin our comparisons, the average CSA of the myofibrils in the EM images of randomly selected Ox and Gly fibers was manually assessed as detailed in the methods. For the FIM-ID workflow, an additional step was needed to classify randomly selected fibers as being Ox or Gly, and this was done by taking advantage of previous studies which have shown that mitochondria are enriched with NADH and FAD+, which are endogenous fluorophores that can be excited with blue light [249-252]. Specifically, as shown in Figure 2-4B, excitation of the FIM-ID samples with blue light yielded a weak autofluorescent decoration of the periphery of the myofibrils in all fibers, along with a prominent punctate signal in a subset of the fibers. The strongly autofluorescent fibers were generally small in CSA and closer examination of the autofluorescent signal revealed that the puncta were positioned at points in which there was a gap in the SERCA signal (Figure 2-4 – Figure Supplement 1). It has been reported that intermyofibrillar mitochondria do not contain SERCA [227], and therefore, the presence of the autofluorescent signal at sites in which there were gaps in the signal for SERCA, the small CSA of the fibers, and

the pre-existing knowledge about the fluorescence properties of NADH and FAD+, all suggested that the autofluorescence was coming from the mitochondria. Accordingly, the strongly autofluorescent fibers were classified as being equivalent to the Ox fibers identified with EM, and the non-autofluorescent fibers were classified as Gly fibers.

Our work with the autofluorescence signal not only provided us with a means for classifying the Ox vs. Gly fibers, but it also helped us realize that any myofibrils that are heavily surrounded by intermyofibrillar mitochondria would not meet the morphological criteria for automated measurements of CSA (i.e., the myofibrils would not present as objects that were >90% enclosed by the signal for SERCA). Thus, to address this, the automated measurements were performed on images in which the signal for autofluorescence and SERCA had been merged. With this approach, a more comprehensive decoration of the periphery of the myofibrils was obtained, and therefore, all of the remaining automated measurements on mouse skeletal muscle were conducted on merged images.

Having established the finer details of our workflow, we were finally able to compare automated measurements of myofibril CSA obtained with FIM-ID with the manual EM-based measurements. As shown in Figure 2-4C, the FIM-ID- and EM-based measurements both revealed the linear correlation between myofibril CSA and fiber CSA that has been reported in previous studies [185, 221], and there was no significant difference in the slope of this correlation when the two methods were compared. Moreover, no significant differences in mean myofibril CSA to fiber CSA ratio were found when the results from the FIM-ID and EM-based measurements were directly compared, and this point was true when the data from all analyzed fibers were considered, as well as when the results were separated according to the Ox and Gly fiber type (Figure 2-4E).

Thus, it can be concluded that the automated measurements of myofibril CSA obtained with FIM-ID were indistinguishable from the manually obtained EM-based measurements.

As described in the introduction, another goal of our study was to develop a time- and cost-effective method for measuring the number of myofibrils per fiber. With the EM images, this number was estimated for each fiber by manually obtaining measurements of the average myofibril CSA, the fiber CSA, and the percentage of the fiber CSA that was occupied by myofibrils. This was a time-intensive process, but with the latter two values, the total CSA of the fiber that was occupied by myofibrils could be calculated. The number of myofibrils per fiber was then derived by dividing the total CSA of the fiber that was occupied by myofibrils by the average myofibril CSA for that fiber. The same principles were also used to calculate the number of myofibrils per fiber with FIM-ID, but in this case, the total CSA of the fiber that was occupied by myofibrils was measured with an automated pipeline in CellProfiler. As shown in Figure 2-4D, the FIM-ID and EM-based measurements both revealed the linear correlation between myofibril number and fiber CSA that has been reported in previous studies [185, 221], and there was no significant difference in the slope of this correlation when the two methods were compared. Moreover, no significant differences in the mean number of myofibrils per fiber CSA were found when the results from the FIM-ID and EM-based measurements were directly compared, and this point was true when the data from all analyzed fibers were considered, as well as when the results were separated according to the Ox and Gly fiber type (Figure 2-4F). Hence, just like myofibril CSA, the automated measurements of the number of myofibrils per fiber with FIM-ID were indistinguishable from the manually obtained EM-based measurements.

The radial growth of muscle fibers that occurs in response to chronic mechanical overload is largely mediated by myofibrillogenesis.

Having validated the accuracy of the FIM-ID measurements, we then set out to determine whether the radial growth of muscle fibers (i.e., an increase in fiber CSA) that occurs in response to an increase in mechanical loading is mediated by myofibril hypertrophy and/or myofibrillogenesis. We first addressed this in mice by subjecting their plantaris muscles to a chronic mechanical overload (MOV) or a sham surgical procedure. After a 16-day recovery period, the plantaris muscles were collected and processed for FIM-ID (Figure 2-5B). As shown in Figure 2-5C, the outcomes revealed that MOV led to a 28% increase in fiber CSA when all fibers in the muscle were considered as a single group, and fiber type-specific analyses revealed that this was mediated by a 39% increase in the CSA of Ox fibers, and a 25% increase in the CSA of the Gly fibers. Similarly, the area per fiber that was occupied by myofibrils increased by 29% for all fibers, 39% for the Ox, and 26% for the Gly (Figure 2-5D). Moreover, the area per fiber that was occupied by the intermyofibrillar components (e.g., sarcoplasmic reticulum, mitochondria, etc.) also showed a 26% increase for all fibers, a 38% increase in the Ox fibers, and a 22% increase in the Gly fibers. When taken together, these results indicate that the MOV-induced increase in fiber CSA was mediated by a proportionate increase in the area that is occupied by the myofibrils and the area that is occupied by the intermyofibrillar components.

Next, we determined whether the increase in the area per fiber that was occupied by myofibrils was mediated by an increase in the size and/or number of myofibrils. Specifically, we first examined whether MOV altered the CSA of the myofibrils and, as shown in Figure 2-5F, the outcomes revealed that MOV increased the CSA of the individual myofibrils by 9% when all fibers were considered as a single group, and fiber type-specific analyses revealed that MOV led to a

14% increase in the Ox fibers, but no significant difference was detected in the Gly fibers (P = 0.35). We then assessed the effect that MOV had on the number of myofibrils per fiber, and as shown in Figure 2-5G, it was concluded that MOV led to a 20% increase in the number of myofibrils per fiber when all fibers were considered as a single group, and fiber type-specific analyses revealed a 22% increase in the Ox fibers and a 21% increase in the Gly fibers. Importantly, during CellProfiler processing, objects in the sham and MOV samples were filtered from analysis at a very similar rate (44% vs. 46%, respectively), and as such, the differences between the groups could not be explained by overt differences in the morphological properties of the myofibrils. Thus, the collective results of these analyses indicate that the MOV-induced increase in fiber CSA could be attributed to both myofibril hypertrophy and myofibrillogenesis, with the most robust and consistent effect occurring at the level of myofibrillogenesis.

The radial growth of muscle fibers that occurs in response to progressive resistance exercise is largely mediated by myofibrillogenesis.

To further address whether the radial growth of muscle fibers that occurs in response to an increase in mechanical loading is mediated by myofibril hypertrophy and/or myofibrillogenesis, we examined vastus lateralis muscle biopsies from humans that were collected before (Pre) and after (Post) they had performed seven weeks of progressive resistance exercise (RE) (Figure 2-6A). As detailed in the methods, the samples were processed for FIM-ID with a step that allowed for the identification of SERCA1 vs. SERCA2 positive fibers (i.e., Type II vs. Type I fibers, respectively) (Figure 2-6B). As shown in Figure 2-6C, the outcomes revealed that RE led to an 18% increase in the CSA of SERCA1 positive fibers but did not significantly alter the CSA of SERCA2 positive fibers. Similar results were also observed when the SERCA1 and SERCA2

positive fibers were examined for changes in the area per fiber that was occupied by the myofibrils, as well as the area per fiber that was occupied by the intermyofibrillar components (Figure 2-6D-E). Specifically, SERCA1 positive fibers revealed an 18% and 17% increase in these values, respectively, while no significant differences were observed in SERCA2 positive fibers.

Thus, just like MOV, the RE-induced increase in the CSA of the SERCA1 positive fibers was mediated by a proportionate increase in the area that is occupied by the myofibrils and the area that is occupied by intermyofibrillar components.

To determine whether the increase in the area per fiber that was occupied by myofibrils was mediated by myofibril hypertrophy and/or myofibrillogenesis, we first examined whether RE altered the CSA of the myofibrils. As shown in Figure 2-6F, we detected a trend for a main effect of RE on myofibril CSA, but direct Pre vs. Post comparisons in the SERCA1 and SERCA2 positive fibers were not significant ($P = 0.31$ and $P = 0.38$, respectively). On the other hand, RE induced a clear fiber type-specific increase in the number of myofibrils per fiber with SERCA1 positive fibers revealing a 12% increase ($P = 0.009$) while no significant difference was observed in SERCA2 positive fibers. It should also be noted that, during CellProfiler processing, objects in the Pre and Post samples were filtered from analysis at a very similar rate (47% vs. 47%, respectively), and thus, the differences between the Pre and Post samples could not be explained by overt differences in the morphological properties of the myofibrils. As such, it can be concluded that the effects of RE were very similar to the effects of MOV in that the RE-induced increase in fiber CSA was largely mediated by the induction of myofibrillogenesis.

Discussion

In this study, we developed FIM-ID as a means for visualizing myofibrils with a fluorescence microscope. As illustrated throughout the study, the images from FIM-ID have a high degree of resolution and contrast, and these properties enabled us to develop pipelines that can perform automated measurements of myofibril size and myofibril number. Importantly, these pipelines were developed in a free open-source program (CellProfiler), and our manuscript includes copies of the pipelines along with instructions and test images so that prospective users can easily employ them (see Supplemental Material). Moreover, the bulk of the FIM-ID workflow utilizes common lab instruments, and essentially anyone who has access to a standard cryostat and a fluorescent microscope with a motorized Z-stage can perform it. Indeed, for first-time users, we suspect that the most complicated part of the workflow will be the implementation of image deconvolution. Fortunately, deconvolution modules have become a commonly available add-on for commercial imaging platforms, and when not available, there are several open-source deconvolution algorithms that users could deploy [253-256]. As such, we are confident that a broad range of investigators will be able to take advantage of our method.

With the development of our method, we were able to gain insight into whether the radial growth of muscle fibers that occurs in response to an increase in mechanical loading is mediated by myofibril hypertrophy and/or myofibrillogenesis. This is a fundamentally important question in the field of skeletal muscle growth and therefore we addressed it with two model systems. As expected, both models induced significant radial growth of the SERCA1 positive muscle fibers. However, a significant increase in myofibril CSA (i.e., myofibril hypertrophy) was not consistently observed (Figures 2-5, 2-6), and no significant correlation between the magnitude of the radial growth of the fibers and myofibril hypertrophy was detected in any of the fiber types that we examined (Figure 2-5 – Figure Supplement 1, Figure 2-6 – Figure Supplement 1). At face value,

these results could be viewed as evidence that myofibril hypertrophy does not play a major role in the radial growth response. However, it is important to consider that the results were obtained from muscles in which the radial growth response was already well advanced. This is important because, according to Goldspink's model of myofibril splitting [185-187, 224], myofibril hypertrophy would only be detected during the early stages of the radial growth response (i.e., before the induction of myofibril splitting which would lead to a reduction in the CSA of the involved myofibrils). Thus, to further address the role of myofibril hypertrophy, future studies should obtain data from muscles that are going through various stages of the radial growth response (i.e., a time course). With the use of FIM-ID, the pursuit of such studies would be a feasible endeavor and the resulting data would not only help to resolve whether myofibril hypertrophy contributes to the radial growth response, but it would also provide insight into whether myofibril hypertrophy precedes the onset of myofibrillogenesis as predicted by the myofibril splitting model.

In contrast to the induction of myofibril hypertrophy, all the fiber types in this study that showed significant radial growth also showed a significant increase in the number of myofibrils per fiber (i.e., myofibrillogenesis) (Figures 2-5, 2-6). Moreover, each of these fiber types revealed a significant positive correlation between the magnitude of radial growth and the magnitude of myofibrillogenesis (Figure 2-5 – Figure Supplement 1, Figure 2-6 – Figure Supplement 1). These points, when coupled with the other data presented in Figures 2-5 and 2-6, indicate that radial growth of the muscle fibers was largely mediated by myofibrillogenesis. Importantly, this conclusion was upheld in two very distinct models of increased mechanical loading (i.e., chronic mechanical overload in mice and progressive resistance exercise in humans). Thus, it appears that the induction of myofibrillogenesis is a conserved component of the radial growth response.

To the best of our knowledge, this is the first study to demonstrate that an increase in mechanical loading can induce myofibrillogenesis. Moreover, the results of this study indicate that myofibrillogenesis is the major driver of the radial growth response. Given these conclusions, one is faced with the question of how an increase in mechanical loading induces myofibrillogenesis. As mentioned several times, one possibility is that the induction of myofibrillogenesis is mediated by hypertrophy and subsequent splitting of the pre-existing myofibrils (i.e., the myofibril splitting model) [185-187, 224]. However, numerous studies have also described a different type of myofibrillogenesis that involves the *de novo* formation of myofibrils [257-260]. Specifically, with *de novo* myofibrillogenesis, it is thought that new myofibrils are derived from nascent proteins and that these nascent proteins are assembled into new myofibrils via a three-step sequence of events (for more details please refer to [257, 258]). Importantly, the concepts of *de novo* myofibrillogenesis have largely been studied within the context of myogenesis (i.e., during the early stages of differentiation, embryonic development, etc.), but whether *de novo* myofibrillogenesis can be induced in adult skeletal muscle remains largely unexplored. In our opinion, the concepts of myofibril splitting and *de novo* myofibrillogenesis are very intriguing, and we consider both models to be worthy of further investigation.

In summary, the outcomes of this study have revealed that the induction of myofibrillogenesis plays a major role in the mechanically induced growth of skeletal muscle. The mechanisms via which an increase in mechanical loading induces myofibrillogenesis are not known, but the groundwork for two different models has already been established. Studies aimed at testing the validity of these models should lead to important advancements in the field, and with the advent of FIM-ID, such studies can now be performed in a time- and cost-effective manner.

Materials and Methods

Animals and Ethical Approval

Experimental procedures were performed on male C57BL/6J mice (Jackson Laboratories) that were 8–10 weeks of age. All animals were housed in a room maintained at 25° C with a 12 hr light/dark cycle and received rodent laboratory chow (Purina) and water *ad libitum*. Before all surgical procedures, mice were anesthetized with 1-5% isoflurane mixed in oxygen at a flow rate of 1.0 L/min, which was maintained throughout the surgery. Immediately following the completion of the surgery, the mice were given an intraperitoneal injection of 0.05 μg/g of buprenorphine in phosphate-buffered saline (PBS). During collection, the mice were euthanized by cervical dislocation under anesthesia before removing the hindlimbs. The Institutional Animal Care and Use Committee (IACUC) at the University of Wisconsin–Madison approved all the methods used in this study under protocol #V005375.

Chronic Mechanical Overload

Bilateral chronic mechanical overload (MOV) surgeries were performed with a modified version of our previously described procedure [98]. Specifically, the plantaris muscles were subjected to MOV by removing the distal 1/3rd of the gastrocnemius muscle while leaving the soleus and plantaris muscle intact. Mice in the control groups were subjected to a sham surgery where an incision was made on the lower leg and then closed. Following the surgeries, incisions were closed with nylon non-absorbable sutures (Oasis) and Vetbond Tissue Adhesive (3M). After 16 days of recovery, the plantaris muscles were collected and processed as described below.

Collection and Processing of Mouse Skeletal Muscles

The hindlimbs were collected by retracting the skin surrounding the entire leg and then the limb was severed at the hip joint. The foot and proximal end of the femur were secured onto a circular piece of aluminum wire mesh (Saint-Gobain ADFORS insect screen) with 90° angles between the foot-tibia and tibia-femur joints using 4-0 non-absorbable silk sutures (Fine Science Tools). The hindlimbs were then submerged in a glass beaker filled with 20 mL of 4% paraformaldehyde in 0.1 M phosphate buffer (PB) solution (25 mM sodium phosphate monobasic, 75 mM sodium phosphate dibasic, pH 7.2) for 3 hrs at room temperature on a tabletop rocker set to 50 RPM. Extensor digitorum longus and plantaris muscles were then extracted from the hindlimb and submerged in a 1.5 mL Eppendorf tube that was filled with 1.0 mL of 4% paraformaldehyde in 0.1 M PB. The tubes were then placed on a nutating rocker for 21 hrs at 4° C. For the subsequent cryoprotection, each muscle was submerged in a 1.5 mL Eppendorf tube filled with 1.0 mL of 15% sucrose in 0.1 M PB and placed back on a nutating rocker for 6 hrs at 4° C, followed by immersion in 45% sucrose in 0.1M PB for 18 hrs at 4° C. Each muscle was then rapidly immersed in OCT (Tissue-Tek), frozen in liquid nitrogen-chilled isopentane, and stored at -80° C [261].

Collection and Processing of Human Skeletal Muscle Biopsies

Human biopsy samples were collected in conjunction with a recently published study by the Roberts and Kavazis laboratories [262]. Briefly, healthy (BMI: 25.2 +/- 5 kg/m^2) young (23 +/- 4 years) male participants who had not performed organized resistance training over the previous three years were selected. Participants performed resistance exercise twice a week for 7 weeks, which included leg press, bench press, leg extension, cable pull-down, and leg curls. Both

the training volume and load were progressively increased throughout the 7-week training program. Muscle biopsies were collected at the mid-belly of the vastus lateralis muscle before and 72 hrs after completion of the seven weeks of resistance training. Biopsies were fixed in 4% paraformaldehyde in 0.1M PB for 24 hrs, incubated in a 15% sucrose in 0.1M PB solution for 6 hrs, incubated in a 30% sucrose in 0.1M PB solution for 18 hrs at 4° C, immersed in OCT, and then frozen in liquid nitrogen-chilled isopentane, and stored at -80° C. For more details about participant selection and the resistance training regimen please refer to Mesquita et al. (2023) [262].

Immunohistochemistry

Unless otherwise noted, mid-belly (mouse) and biopsy (human) cross-sections (5 μm thick) from muscles frozen in OCT were taken with a cryostat chilled to -30° C and collected on Superfrost Plus™ microscope slides (Fisher Scientific). Immediately upon collection, the sections were transferred to diH_2O water for 15 min to hydrate the samples. While ensuring that the sections remained hydrated, the area on the slide surrounding the section was dried with a Kimwipe, and then a hydrophobic circle was drawn around the section using an Aqua Hold 2 pen (Scientific Device Laboratory). Slides were then placed into a humidified box for all subsequent washing and incubation steps, which were all performed at room temperature on a rotating rocker set to 50 RPM.

Primary Antibody Labeling: Sections were washed with PBS for 5 min and then incubated for 30 min in blocking solution (0.5% Triton X-100, 0.5% bovine serum albumin (BSA) dissolved in PBS). For mouse samples, sections were incubated overnight in blocking solution containing mouse IgG1 anti-SERCA1 (1:100, VE121G9, Santa Cruz #SC-58287) and rabbit anti-dystrophin

(1:100, ThermoFisher #PA1-21011). For human biopsy samples, sections were incubated overnight in blocking solution containing mouse IgG1 anti-SERCA1 or mouse IgG1 anti-SERCA2 (1:200, Santa Cruz #SC-53010) and rabbit anti-dystrophin. Following the overnight incubation, sections were washed three times for 10 min with PBS, followed by three more washes for 30 min with PBS.

Secondary Antibody Labeling: All sections labeled with primary antibodies were incubated overnight in blocking solution containing AlexaFluor® 594 conjugated goat anti-mouse IgG, Fcγ Subclass 1 specific (1:2000, Jackson Immunoresearch #3115-585-205) and AlexaFluor® 488 conjugated goat anti-rabbit IgG (1:5000, Invitrogen #A11008). Following the overnight incubation, sections were washed three times for 10 min with PBS, followed by three more times for 30 min with PBS.

Labeling with Phalloidin: In some instances, after the secondary antibody labeling step, sections were incubated in blocking solution containing Phallodin-CF680R (1:50, Biotium #00048) for 20 min. Following the incubation, the sections were washed three times for 10 min with PBS, followed by three more times for 30 min with PBS.

Mounting: Washed sections were mounted with 30 µL of ProLong™ Gold Antifade Mountant (ThermoFisher #P36930) and covered with a 22 x 22 mm No.1 glass slip (Globe Scientific #1404-10). All sections were allowed to cure in the mountant for at least 24 hrs while being protected from light before imaging.

Assessment of Muscle Fiber Size

The cross-sections that had been labeled for dystrophin and SERCA1/2 were imaged with a Keyence automated BZX700 inverted epifluorescence microscope via a 10x objective lens. For

each fluorescent channel (FITC and TxRED filter), a 3 x 3 (mouse samples) or 5 x 5 (human samples) field was captured and stitched together using the Keyence Analyzer Software. The mean cross-sectional area of all qualified muscle fibers within the stitched images was then measured with our previously published CellProfiler pipeline [263].

Fluorescence Imaging of Myofibrils and Image Deconvolution (FIM-ID)

Randomly selected regions of interest (ROIs) from the cross-sections that had been labeled for dystrophin and SERCA1/2 were imaged with an HC PL APO 63x/1.40 oil immersion objective on a THUNDER Imager Tissue 3D microscope (Leica). Images for dystrophin were captured through a GFP filter (EX:470/40, EM: 525/50), SERCA1/2 through a TXR filter (EX: 560/40, EM: 630/76), and autofluorescence was captured through a 405 filter (EX: 405/60, EM: 470/40). Z-stacks with a step size of 0.22 μm were captured through the entire thickness of the sample. Deconvolution was then applied to all images in the Z-stack for each channel using Leica's Small Volume Computational Clearing (SVCC) algorithm with the refractive index set to 1.47, strength set to 80-100%, and regularization set to 0.05. The deconvoluted images were then opened in ImageJ and the Z-plane with the most in-focus image for SERCA1/2 was chosen. When appropriate, the autofluorescence signal from the same plane was merged with the image for SERCA1. This was done in ImageJ with the Z-Project function set to "Sum Slices" and the merged image was saved as a single grayscale TIFF image. The single or merged images were then converted to a 16-bit TIFF file format and the pixel density was adjusted to 6144 x 6144 by using the ImageJ resize function with the following settings: "Constrain aspect ratio", "Average when downsizing", and "Bilinear" interpolation.

Total Protein Labeling and Scoring for Sectioning Artifacts.

Longitudinal sections of the EDL muscle (3 μm thick) were collected on a cryostat that was chilled at -15 to -30° C and collected on Superfrost Plus™ microscope slides. The sections were stained for total protein with a No-Stain™ kit (Invitrogen #A44449). Specifically, 25 μL of the 20X No-Stain Labeling Buffer stock solution was diluted into 475 μL diH_2O to create a working 1X solution. Next, 1 μL of the No-Stain Activator was added to the 500 μL 1X solution and vortexed. Then, 1 μL of the No-Stain Derivatizer was added to the 1X solution and vortexed. Labeling was then performed by adding 50 μL of the prepared No-Stain solution to the sections, which were then incubated for 30 min at room temperature with rocking at 50 RPM. Labeled sections were then washed three times for 5 min with diH_2O. After washing, the diH_2O was removed, and 4 μL of Prolong Diamond mounting medium (Life Technologies #P36965) was added to the sections before covering with a 12 mm No. 1 glass slip (Neuvitro #GG1215H). After curing for 48 hrs, randomly selected ROIs were imaged with a THUNDER Imager with a Y3 filter (Ex: 545/26, EM: 605/70) and subjected to deconvolution as described for FIM-ID. The images were then examined by a blinded investigator and each fiber within a given ROI was scored for the presence of artifacts on the surface of the section (a score of 1 indicates no artifacts and a score of 10 indicates extensive distortions).

Automated Measurements of Myofibril Size and Number with FIM-ID

Assessment of Myofibril Size and Number in Muscles from Mice: Within each image from FIM-ID, individual fibers were randomly selected by a blinded investigator and manually traced in ImageJ to record the fiber CSA. Then, the traced fiber was isolated for automated analysis by choosing the 'Clear Outside' option. The resulting image was then cropped so that it only contained

the isolated fiber. The cropped image was then saved as a .tiff file. For the studies in Figures 2-4 and 2-5, preliminary analyses were performed on 24 fibers per sample with an approximately equal number of autofluorescent and non-autofluorescent fibers. Additional ROIs / fibers were then randomly selected for analysis until the average CSA of the selected fibers fell within ± 10% of the mean fiber CSA that was observed for the entire muscle during the Keyence-based analyses. For automated measurements of myofibril size, each single fiber image was imported and processed with our custom pipeline "Myofibril CSA Analysis" in CellProfiler Version 4.2.1, which measures the mean myofibril CSA for each fiber [264]. To calculate the number of myofibrils per fiber, the total CSA of the fiber that was occupied by myofibrils had to be determined. To obtain this value, each single fiber image that contained the merged signal for autofluorescence and SERCA1 was imported and processed with our custom pipeline "Intermyofibrillar Area" in CellProfiler (Figure 2-4 – Figure Supplement 3). This pipeline performs automated measurements of the area occupied by the merged autofluorescence and SERCA1 signal for each fiber (i.e., the area occupied by the intermyofibrillar components such as the sarcoplasmic reticulum, mitochondria, etc.). This value was then subtracted from the fiber CSA to obtain the total area occupied by the myofibrils for each fiber. Finally, the number of myofibrils per fiber was determined by dividing the total area occupied by the myofibrils by the mean myofibril CSA. Note: the "Myofibril CSA Analysis" and "Intermyofibrillar Area" pipelines as well as user instructions and test images have all been included as supplemental material.

Assessment of Myofibril Size and Number in Muscles from Humans: The same general methods that were used in mice were applied to the analysis of human samples. Exceptions to this included that the analyses were performed on images of SERCA1 or SERCA2. Furthermore, preliminary analyses were performed on 16 fibers (8 SERCA1, 8 SERCA2 fibers), and additional

ROIs / fibers were selected for analysis until the average CSA of the selected fibers fell within ± 4% of the mean fiber CSA that was observed with for the entire muscle section during the Keyence-based analyses.

Processing of Mouse Skeletal Muscle for Electron Microscopy

The hindlimbs of mice were removed and secured to an aluminum wire mesh as described in the section entitled 'collection and processing of the mouse skeletal muscles'. The hindlimbs were then submerged in a 100 mL glass beaker filled with 20 mL of Karnovsky fixative [265] ((2.5% EM-grade glutaraldehyde (Electron Microscopy Sciences #16019) plus 2.0% EM-grade paraformaldehyde (Electron Microscopy Sciences #15714-S) in 0.1M PB)) for 3 hrs at room temperature on a tabletop rocker set to 50 RPM. Each plantaris muscle was then extracted from the hindlimb and submerged in a 1.5 mL Eppendorf tube containing 1.0 mL of 2.5% EM-grade glutaraldehyde plus 2.0% EM-grade paraformaldehyde in 0.1M PB solution and placed on a nutating rocker for 21 hrs at 4° C. The fixed plantaris muscles were then transversely cut at the mid-belly and further transversely cut into 1 mm thick slices on either side of the midline.

Unless otherwise noted, the following steps were performed at room temperature in approximately 10 mL of solution in 20 mL scintillation vials on a rotator set at 10 RPM. Tissue slices were first washed three times for 15 min with 0.1M PB solution, followed by overnight incubation in 1% osmium tetroxide (Electron Microscopy Sciences #19170) in 0.1M PB solution at room temperature. The samples were then washed four times for 5 min in 0.1M PB solution, followed by graded dehydration in ethanol with 5 min incubation steps (2 x 35%, 2 x 50%, 2 x 70%, 2 x 80%, 2 x 90%, 2 x 95%, 4 x 100%). Samples were then incubated in 100% anhydrous acetone for 2 x 5 min and 2 x 10 min. Epon resin was prepared by mixing 6.25 grams Epon 812,

3.25 grams DDSA, 3.0 grams NMA, and 8 drops of DMP 30 (Electron Microscopy Sciences #14120) before incubating the samples in a 3:1 acetone:epon solution overnight at room temperature. Samples were then incubated in a 1:1 acetone/epon solution for 2 hrs, followed by a 1:3 acetone/epon solution for 2 hrs, before being placed in 100% epon overnight in a vacuum at room temperature. Samples were then added to fresh 100% epon for 3 x 30 min at 60° C before being placed into molds with fresh 100% epon to cure at 60° C overnight.

The resin-embedded samples were sectioned on a Leica EM UC6 ultramicrotome at 500 nm to generate semi-thin sections using a Histo Diamond Knife (DiATOME) and stained with Toluidine blue to confirm proper orientation (i.e., the cross-sections of the muscle fibers were oriented perpendicular to the length of the fibers). After confirming the correct orientation of the block, the samples were sectioned at 100 nm and collected on carbon formvar-coated copper grids (Electron Microscopy Sciences #S2010NOT). Sections were then contrast-stained with 8% uranyl acetate (Electron Microscopy Sciences #22400) in 50% ethanol for 10 min at room temperature, followed by lead citrate (Electron Microscopy Sciences #22410) for 10 min at room temperature with 4 x 30 sec washes in diH_2O water after each contrast stain. The sections were viewed at 80kV on a Philips CM120 transmission electron microscope equipped with AMT BioSprint12 digital camera.

Manual Measurements of Myofibril Size and Number with Electron Microscopy

For each muscle processed for EM, 20 oxidative and 20 non-oxidative fibers were randomly selected for imaging. For each fiber, one low-magnification image (1250x) and one randomly chosen high-magnification region (5600x) within the fiber were captured. The low-magnification images were used to measure the fiber CSA and the high-magnification images were

used to measure the myofibril CSA as well as the percentage of the fiber CSA that was occupied by myofibrils. Specifically, for each high-magnification image, ~30 randomly selected myofibrils were manually traced and used to determine the mean myofibril CSA for that fiber. To estimate the percentage of the fiber CSA that was occupied by myofibrils, an ROI from the high-magnification image that had an equal representation of the A- and I-band regions of the myofibrils was selected. Then, within that ROI, all areas containing myofibrils were manually traced and the total area occupied by the myofibrils was recorded. The total CSA of the myofibrils in the ROI was then divided by the total area of the ROI to obtain the percentage of the fiber CSA that was occupied by the myofibrils. This value was then used to calculate the total CSA of fiber that was occupied by myofibrils. Finally, the number of myofibrils per fiber was determined by dividing the total CSA of the fiber that was occupied by myofibrils by its mean myofibril CSA. See Figure 2-4 – Figure Supplement 2 for an example of the process for manual measurements.

Statistical Analysis

Statistical significance was determined by using Student's t-tests, paired t-tests, Wilcoxon-matched paired t-tests, 2-way ANOVA with Bonferroni post hoc comparisons, or repeated measures 2-way ANOVA with Bonferroni post hoc comparisons, as indicated in the figure legends. Samples that deviated more than three times from the mean within a given group were excluded as outliers. Differences between groups were considered significant when $P < 0.05$. All statistical analyses were performed with GraphPad Prism version 10.0.0 for Windows (Dotmatics).

Ethics

The current study was reviewed and approved by the Institutional Review Board at Auburn University (Protocol # 21-390 FB) and conformed to the standards of the Declaration of Helsinki, except that it was not registered as a clinical trial. All participants were informed of the procedures and risks of the current study before providing written consent. The Institutional Animal Care and Use Committee (IACUC) at the University of Wisconsin-Madison approved all the methods used in this study under protocol #V005375.

Data Availability

The "Myofibril CSA Analysis" and "Intermyofibrillar Area" CellProfiler pipelines as well as user instructions and test images have all been included as source data within the fully published article. Furthermore, all data used to generate the figures are also included in the fully published article as source data files.

ID: PMC10928493; https://doi.org/10.7554/eLife.92674.3

Acknowledgments

The research reported in this publication was supported by the National Institute of Arthritis and Musculoskeletal and Skin Diseases of the National Institutes of Health (NIH) under Awards AR074932 and AR082816 to T.A.H, the National Institute of General Medical Sciences of the NIH under Award GM141739 to M.C.M., and a National Strength and Conditioning Foundation Doctoral Student Award to P.H.C.M. The authors would like to thank Benjamin August and Randy Massey for their assistance with the electron microscopy, Nathaniel Steinert, Wenyuan Zhu, and Philip Flejsierowicz for their contributions to the validation of the CellProfiler pipeline, as well as, Breanna Mueller, Casey Sexton, and Cleiton Libardi for their contributions to the human study.

Figure 2-1

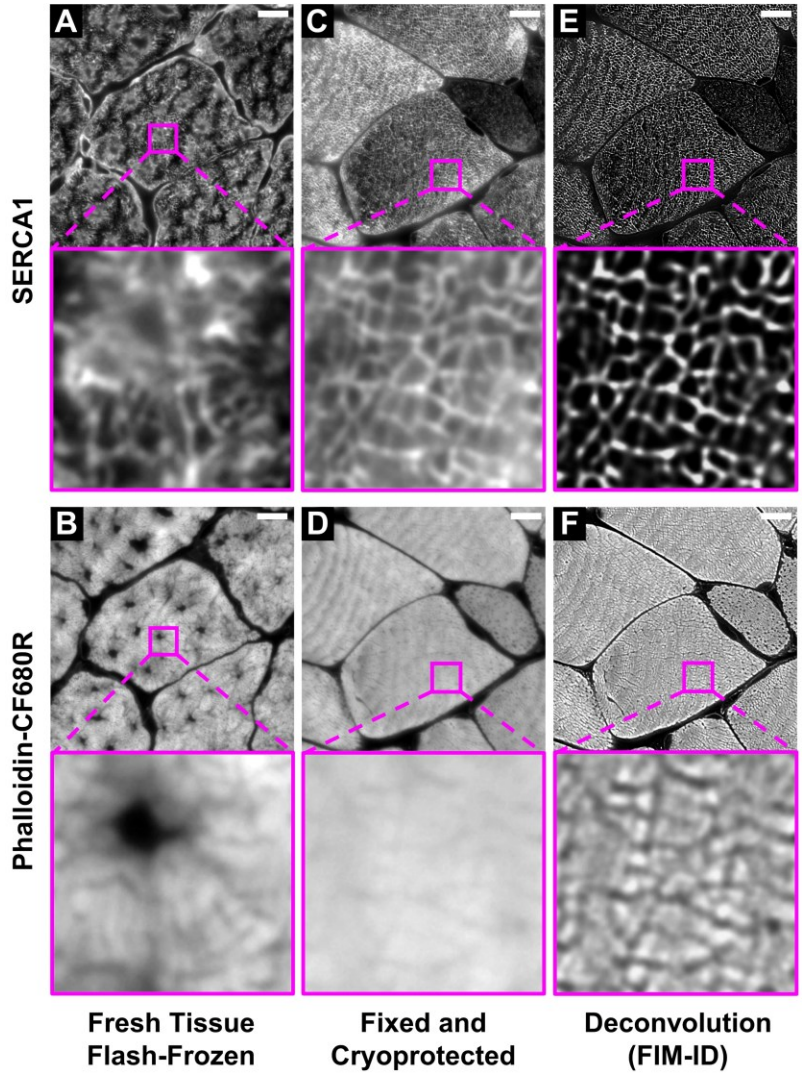

Figure 2-1. Optimization of the fixation, cryoprotection, and sectioning conditions for Fluorescence Imaging of Myofibrils with Image Deconvolution (FIM-ID). Plantaris muscles from mice were collected and either (**A-B**) immediately flash-frozen and sectioned at -20º C, or (**C-D**) subjected to optimized fixation, cryoprotection, and sectioning conditions. Cross-sections of the muscles were stained with phalloidin-CF680R to identify f-actin and SERCA1 was immunolabeled with Alexa 594 to identify the periphery of the myofibrils. Images of SERCA1 (top) and f-actin (bottom) were captured from identical regions with a widefield fluorescence microscope. (**E-F**) The images in C-D were subjected to deconvolution. Scale bar in all images = 10 μm.

Figure 2-1 - Figure Supplement 1

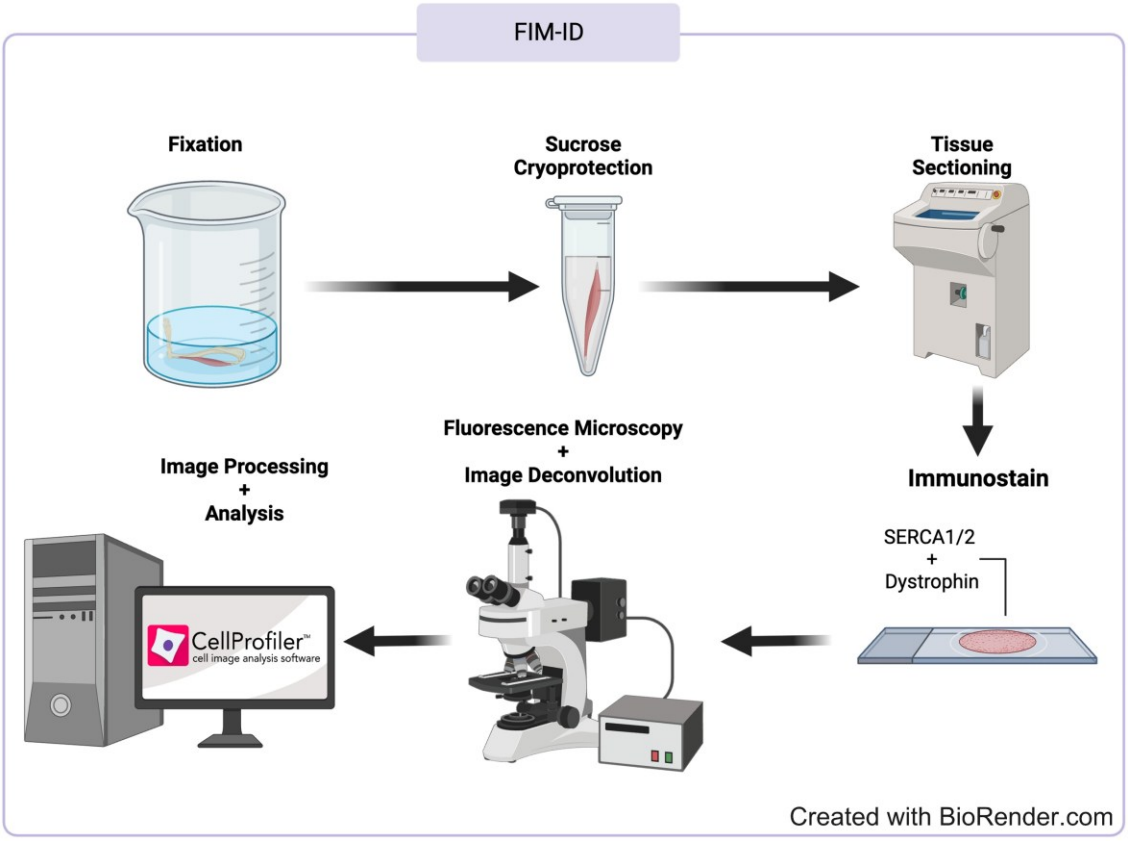

Figure 2-1 – Figure Supplement 1. Overview of the FIM-ID Workflow.

Figure 2-2

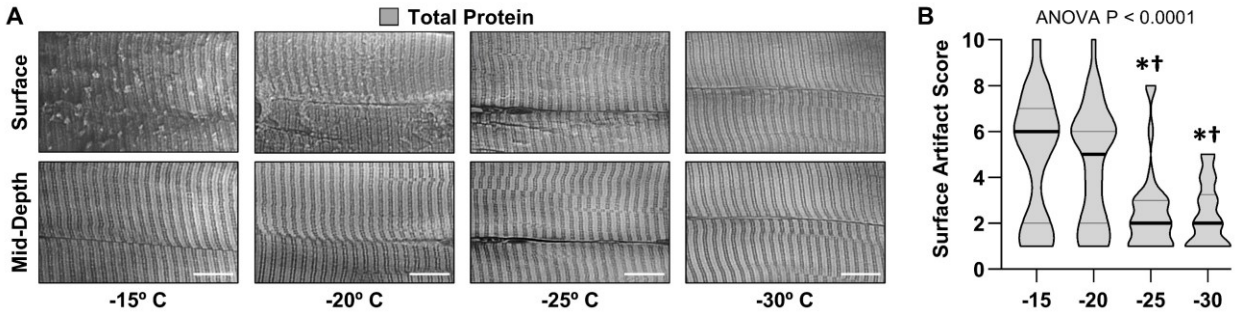

Figure 2-2. The effect of sectioning temperature on surface artifacts. An EDL muscle from a mouse was fixed with 4% paraformaldehyde, cryoprotected with 45% sucrose, and longitudinally sectioned at -15, -20, -25, or -30º C. The sections were stained for total protein and then five randomly selected regions of interest (ROI) were imaged. Each fiber within the ROIs was scored for the presence of artifacts on the surface (a score of 1 indicates no artifacts and a score of 10 indicates extensive distortions). (**A**) Representative images from the surface and mid-depth of the sections. Scale bars = 10 μm. (**B**) Violin plot of the surface scores for the fibers at each of the different sectioning temperatures. Thick bars represent the median and thin bars represent the quartiles, n = 28-39 fibers / group. Data was analyzed with one-way ANOVA. Significantly different from, * -15º, † -20º C. Scale bar in all images = 10 μm. Data used to generate Figure 2-2B is available within the fully published article as Figure 2 – Source Data (https://doi.org/10.7554/eLife.92674.3).

Figure 2-3

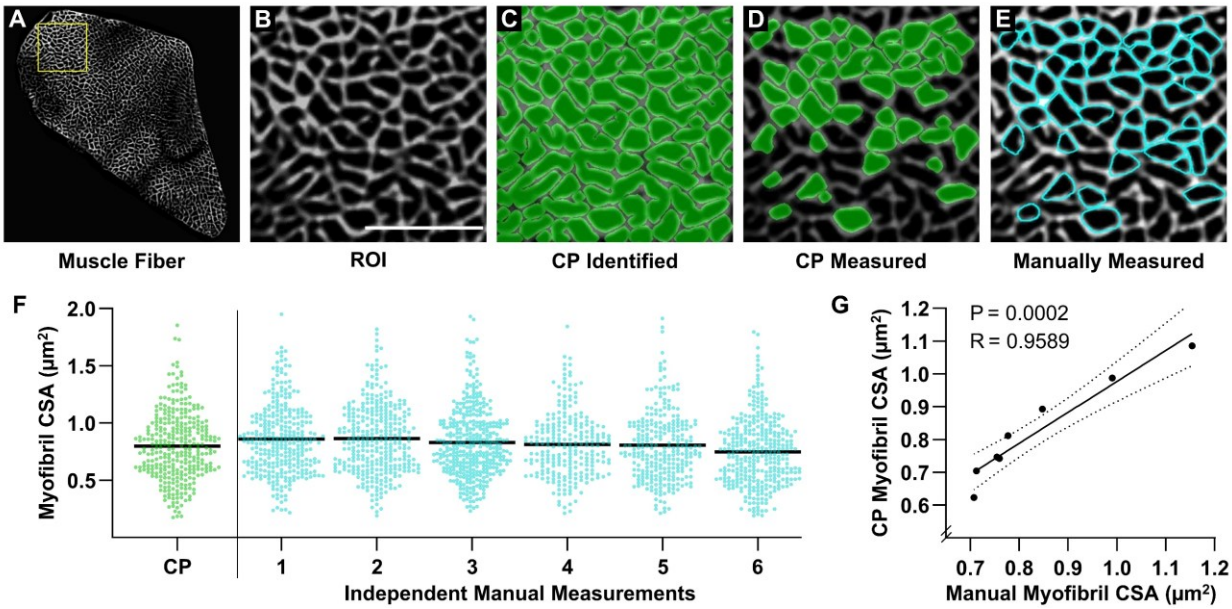

Figure 2-3. Validation of an automated pipeline for measuring myofibril size with FIM-ID. A cross-section from a mouse plantaris muscle was subjected to FIM-ID, and then eight regions of interest (ROI) from a fiber (**A**) were subjected to automated and manual measurements of myofibril size. (**B**) Representation of an ROI from the fiber in A, scale bar = 5 µm. (**C**) Example of how the automated CellProfiler (CP) pipeline identifies the myofibrils (green). (**D**) Illustration of the myofibrils in CP that met the morphological criteria for subsequent measurements of cross-sectional area (CSA). (**E**) Example of the same ROI in B-D that was manually assessed for myofibrils that met the morphological criteria for subsequent measurements of CSA (cyan). (**F**) Scatter plot of the CSA of all myofibrils that were automatically measured by CP, or manually measured by independent investigators (n = 6 investigators). The black bars represent the mean for each group. (**G**) For each ROI, the mean myofibril CSA as determined by CP was compared with the mean myofibril CSA from all of the manual measurements. The solid line represents the best fit from linear regression, the dashed lines represent the 95% confidence intervals, R indicates Pearson's correlation coefficient, and P indicates the likelihood that the relationship is significantly different from zero. Data used to generate Figures 2-3F-G is available within the fully published article as Figure 3 – Source Data (https://doi.org/10.7554/eLife.92674.3).

Figure 2-4

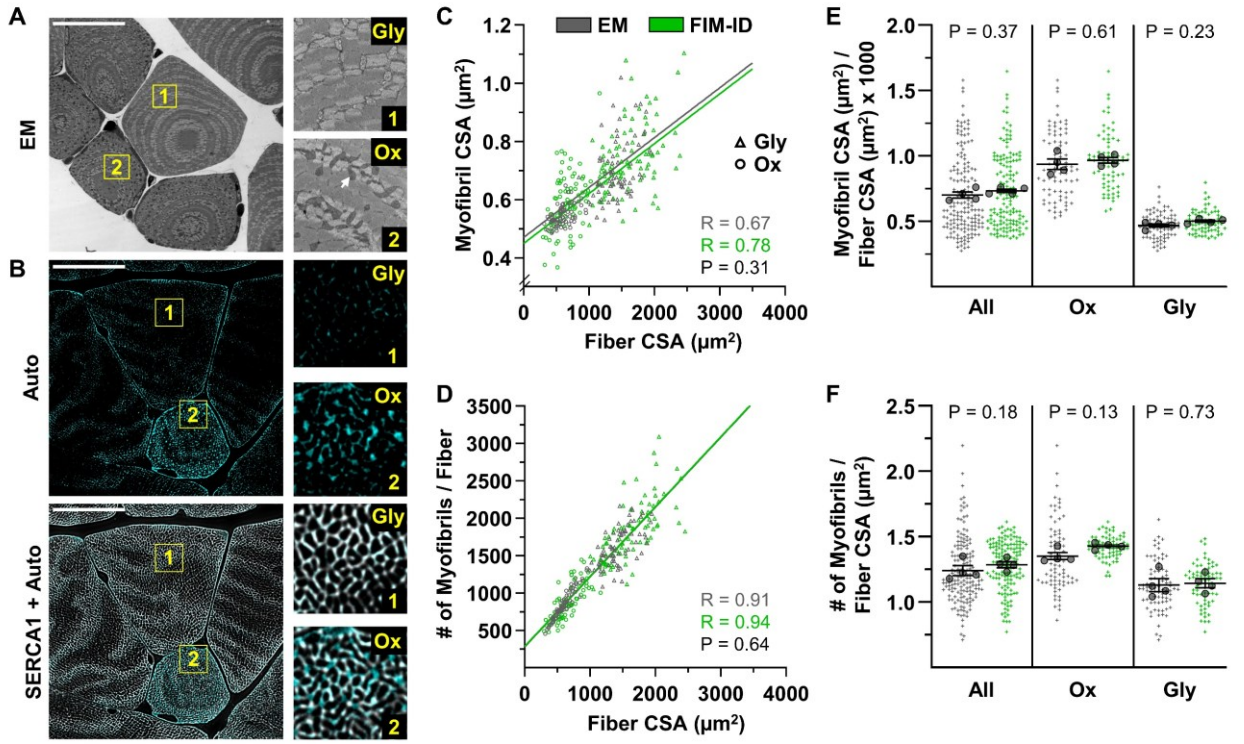

Figure 2-4. Automated measurements of myofibril size and number with FIM-ID versus manual measurements with electron microscopy. For each mouse, one plantaris muscle was (**A**) processed for imaging with electron microscopy (EM), and the contralateral plantaris was (**B**) processed for FIM-ID, n = 4 mice. In the EM images, glycolytic fibers (Gly) and oxidative fibers (Ox) fibers were distinguished by the presence of extensive intermyofibrillar mitochondria (arrow). In FIM-ID, the autofluorescence signal (Auto) was used to distinguish the Gly vs. Ox fibers. The 'Auto' signal was also merged with the signal from SERCA1 to provide a comprehensive decoration of the periphery of the myofibrils. (**C-D**) Scatter plots that illustrate the relationships between (C) myofibril cross-sectional area (CSA) vs. fiber CSA, and (D) the number of myofibrils per fiber vs. fiber CSA. The automated measurements from the FIM-ID samples are shown in green and the manual measurements from the EM samples are shown in gray. Individual values are presented as triangles for the Gly fibers and circles for the Ox fibers, n = 144-160 fibers / condition (36-40 fibers per muscle). The solid lines represent the best fit from linear regression for each condition, R indicates Pearson's correlation coefficient, and P indicates the likelihood of a significant difference between the automated FIM-ID and the manual EM measurements. (**E-F**) The data in C-D was used to compare ratios of (E) the myofibril CSA to fiber CSA, and (F) the myofibril number to fiber CSA. The data is provided for all of the analyzed fibers and also separated according to fiber type. The large dots indicate the mean for each muscle. The data in C and D were analyzed with extra-sums-of-squares F-tests and the data in E and F were analyzed with paired t-tests or a Wilcoxon-matched paired t-test when the test for normality failed (i.e., the EM measurements of oxidative fibers in F). Data used to generate Figure 2-4C-F is available within the fully published article as Figure 4 – Source Data (https://doi.org/10.7554/eLife.92674.3).

Figure 2-4 - Figure Supplement 1

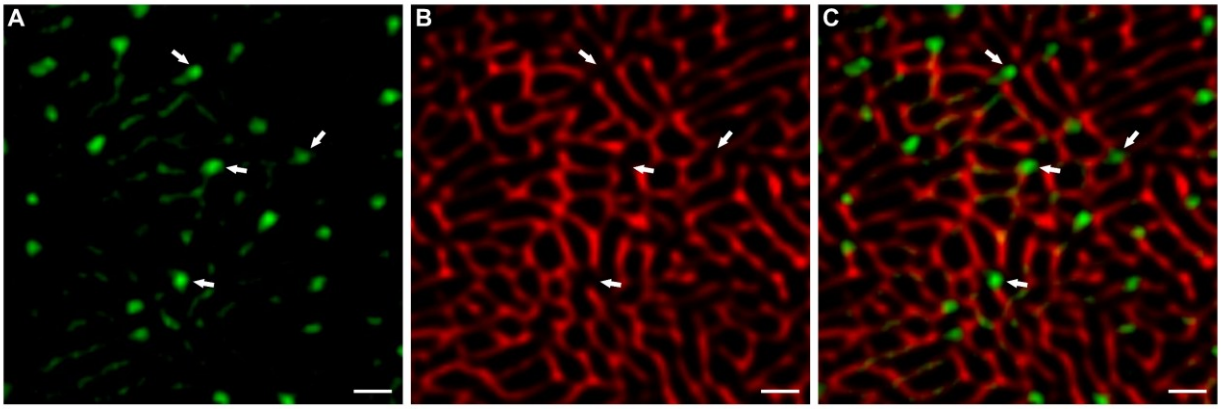

Figure 2-4 – Figure Supplement 1. Punctate sites of autofluorescence align with gaps in the signal for SERCA1. Representative images from a plantaris muscles that was processed for FIM-ID as described in Figure 4. The representative images are from an oxidative (Ox) fiber. The signal for autofluorescence is shown in (**A**) and the signal for SERCA1 is shown in (**B**). The merge of these signals (**C**) reveals that the intense autofluorescent puncta which are frequently observed in Ox fibers are positioned at points in which there is a gap in the signal for SERCA1.

Figure 2-4 - Figure Supplement 2

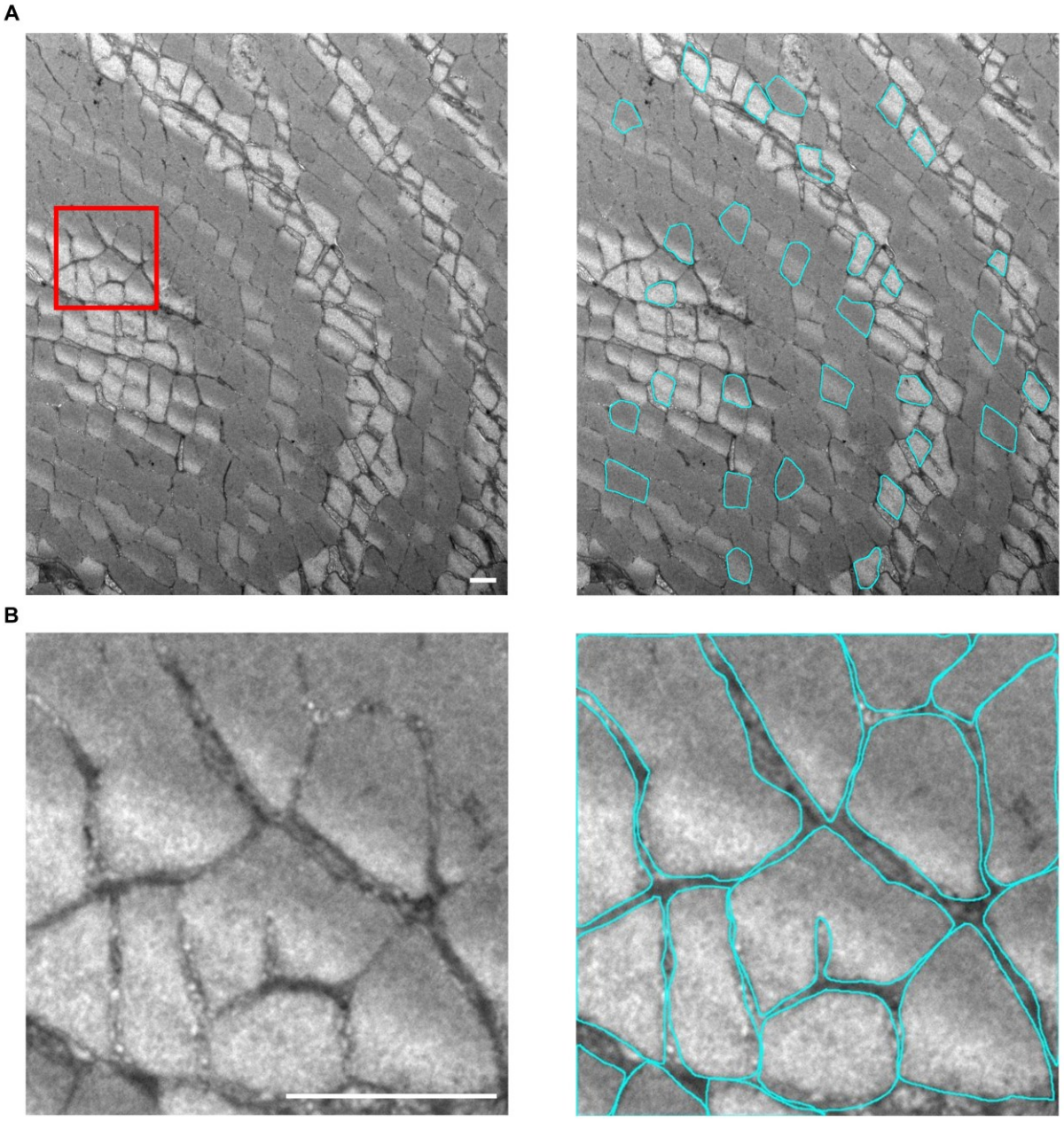

Figure 2-4 – Figure Supplement 2. Manual tracing of myofibrils from images acquired using electron microscopy. (**A**) Representative images show the manual tracing (cyan) of 30 randomly selected myofibrils for measurements of the average myofibril CSA. (**B**) Myofibrils within the red-boxed region of interest (ROI) were manually traced to obtain the CSA occupied by myofibrils within the ROI. The percentage of the fiber CSA occupied by myofibrils was calculated by dividing the CSA occupied by myofibrils within the ROI by the total area of the ROI and then multiplying by the fiber CSA. The number of myofibrils for the fiber was calculated by dividing the percentage of the fiber CSA occupied by myofibrils by the average myofibril CSA for that fiber (Scale bar = 1 μm).

Figure 2-4 - Figure Supplement 3

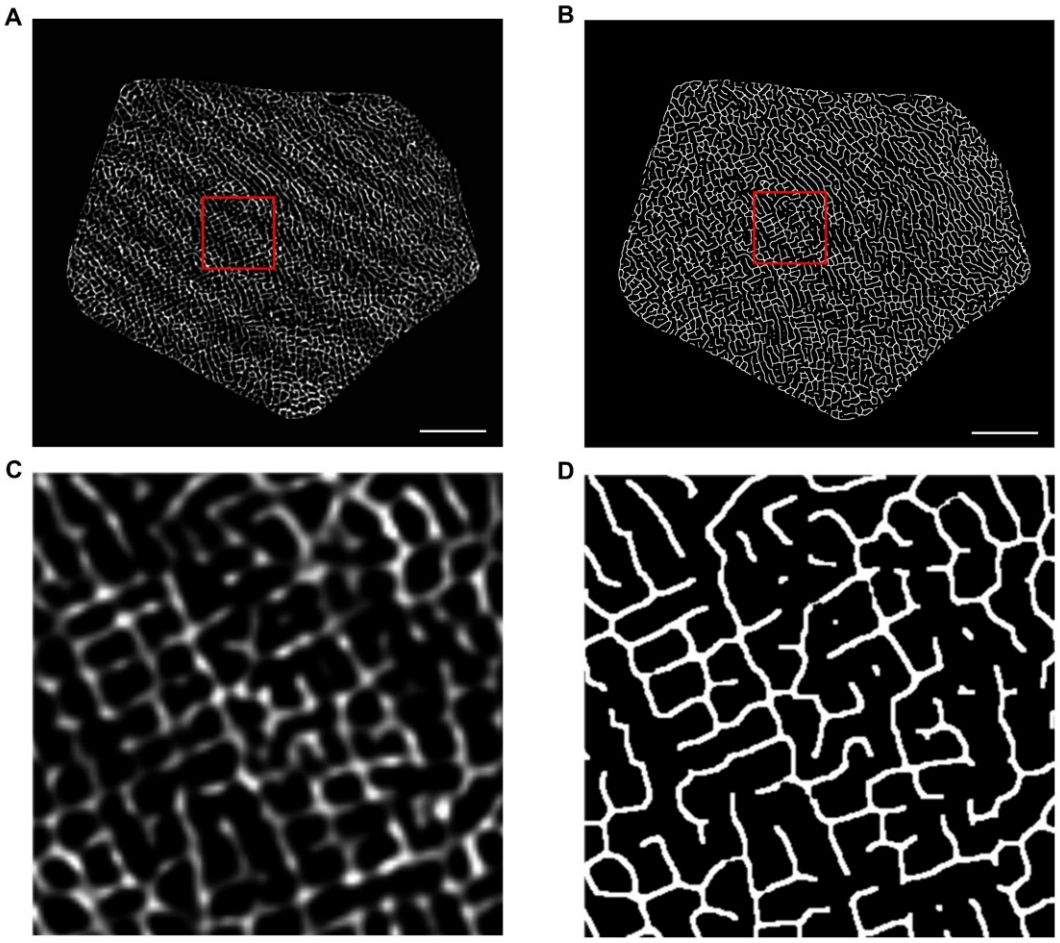

Figure 2-4 – Figure Supplement 3. Using CellProfiler to determine the area occupied by the intermyofibrillar components. (**A**) A representative image of an isolated muscle fiber before processing in CellProfiler. (**B**) Binary version of the image from A that was created by the custom "Intermyofibrillar Area" CellProfiler pipeline. The area occupied by the intermyofibrillar components is calculated from the area that is occupied by the white pixels in the binary image. (**C-D**) Zoomed-in images of the red-boxed regions in A and B. Scale bar = 10 μm

Figure 2-5

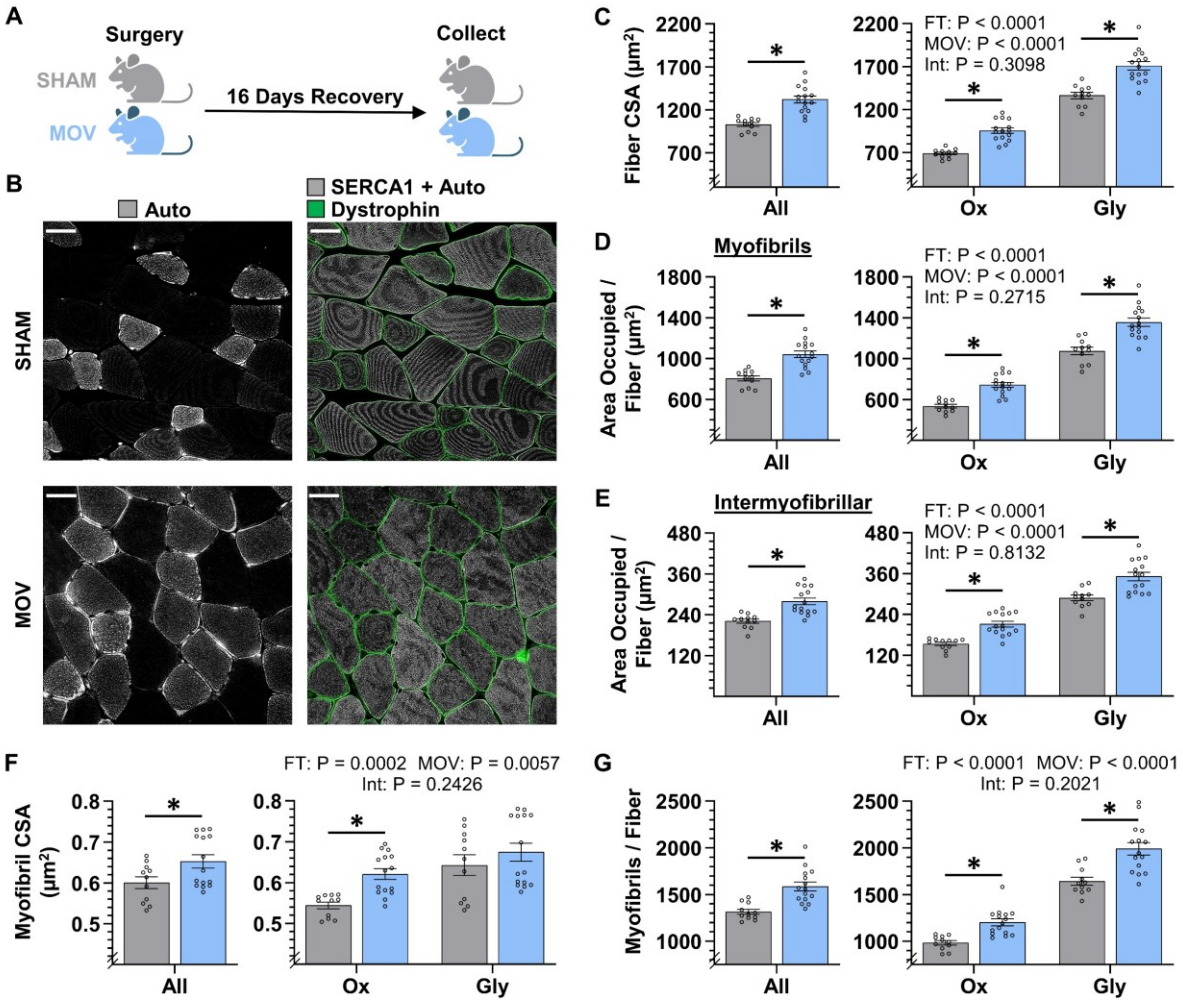

Figure 2-5. The radial growth of fibers that occurs in response to chronic mechanical overload is largely mediated by myofibrillogenesis. (**A**) The plantaris muscles of mice were subjected to a chronic mechanical overload (MOV) or sham surgery, allowed to recover for 16 days, and then mid-belly cross-sections were subjected to FIM-ID. (**B**) Immunolabeling for dystrophin was used to identify the periphery of muscle fibers, autofluorescence (Auto) was used to distinguish glycolytic fibers (Gly) from highly oxidative fibers (Ox), and the signal from SERCA1 plus Auto was merged and used to identify the periphery of the myofibrils, scale bar = 25 μm. (**C-G**) Graphs contain the results from all of the fibers that were analyzed, as well as the same data after it was separated according to fiber type. (C) fiber CSA, (D) the area per fiber occupied by myofibrils, (E) the area per fiber occupied by intermyofibrillar components, (F) myofibril CSA, and (G) the number of myofibrils per fiber. The data are presented as the mean ± SEM, n = 11-15 muscles / group (All = 24-54 fibers / muscle, Ox and Gly = 10-24 fibers / muscle, Gly = 10-24 fibers / muscle, and an average of 356 ± 17 myofibrils / fiber). Student's t-tests were used to analyze the data in the 'All' graphs and two-way ANOVA was used to analyze the data in the fiber type graphs. Insets show the P values for the main effects of MOV, fiber type (FT), and the interaction (Int). * Significant effect of MOV, $P < 0.05$. Graphic illustration in (A) was created with BioRender.com. Data used to generate Figures 2-5C-G is available within the fully published article as Figure 5 – Source Data (https://doi.org/10.7554/eLife.92674.3).

Figure 2-5 - Figure Supplement 1

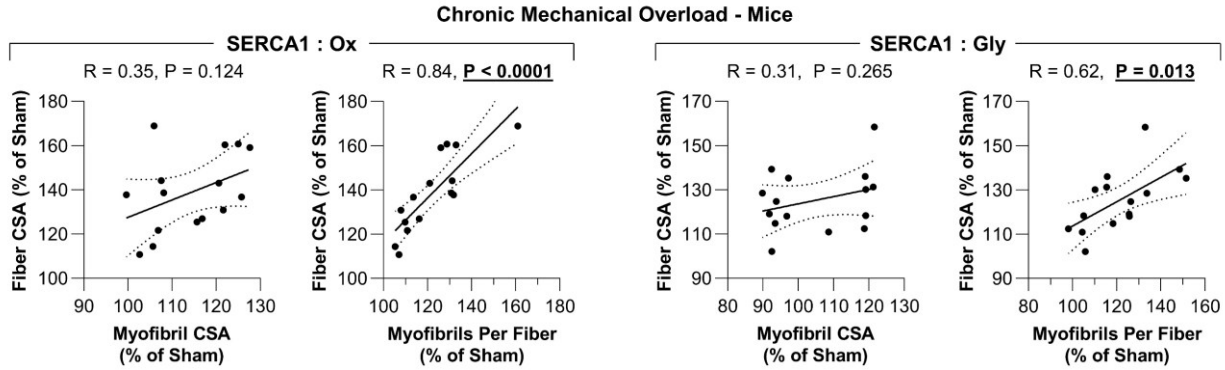

Figure 2-5 – Figure Supplement 1. The radial growth of fibers that occurs in response to an increase in mechanical loading is correlated with the induction of myofibrillogenesis. The plantaris muscles of mice were subjected to a chronic mechanical overload (MOV) or sham surgery and then collected after 16 days of recovery. Each sample was subjected to FIM-ID and then individual fiber types were analyzed for the mean fiber cross-sectional area (CSA), mean myofibril CSA, and the mean number of myofibril per fiber as reported in Figure 2-5. Data for the mouse MOV samples were expressed relative to the mean of the sham samples (% of Sham). The resulting data were used to create scatter plots that illustrate the relationship between the changes in fiber CSA and myofibril CSA for each sample, or the relationship between the changes in fiber CSA and the number of myofibrils per fiber (i.e., myofibrillogenesis) for each sample. Solid lines represent the best fit from linear regression, the dashed lines represent the 95% confidence intervals, R indicates Pearson's correlation coefficient, and P indicates the likelihood that the relationship is significantly different from zero. Data used to generate Figure 2-5 – Figure Supplement 1 is available within the fully published article as Figure 5 – Source Data (https://doi.org/10.7554/eLife.92674.3).

Figure 2-6

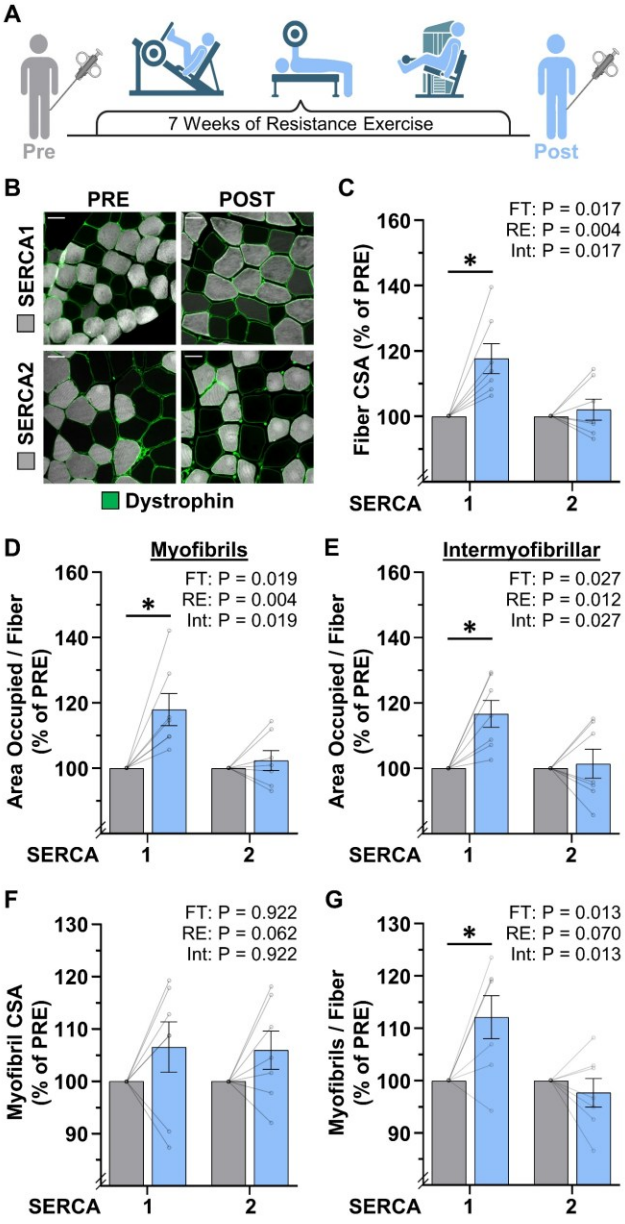

Figure 2-6. The radial growth of fibers that occurs in response to resistance exercise is largely mediated by myofibrillogenesis. (**A**) Biopsies of the vastus lateralis were collected before (PRE) and after (POST) participants performed 7 weeks of progressive resistance exercise (RE). (**B**) Cross-sections were immunolabeled for dystrophin (to identify the periphery of muscle fibers), SERCA1 (to identify the periphery of the myofibrils in Type II fibers), or SERCA2 (to identify the periphery of the myofibrils in Type I fibers), and subjected to FIM-ID, scale bar = 50 μm. (**C-G**) Graphs contain the values for each subject expressed relative to their PRE sample. (C) fiber CSA, (D) the area per fiber occupied by myofibrils, (E) the area per fiber occupied by intermyofibrillar components, (F) myofibril CSA, and (G) the number of myofibrils per fiber. The data are presented as the mean ± SEM, n = 7 participants (SERCA1 15-33 fibers / participant, SERCA2 8-38 fibers / participant, and an average of 1101 ± 60 myofibrils / fiber). Significance was determined by repeated measures two-way ANOVA. Insets show the P values for the main effects of RE, fiber type (FT), and the interaction (Int). * Significant effect of RE, $P < 0.05$. Graphic illustration in (A) was created with BioRender.com. Data used to generate Figures 2-6C-G is available within the fully published article as Figure 6 – Source Data (https://doi.org/10.7554/eLife.92674.3).

Figure 2-6 - Figure Supplement 1

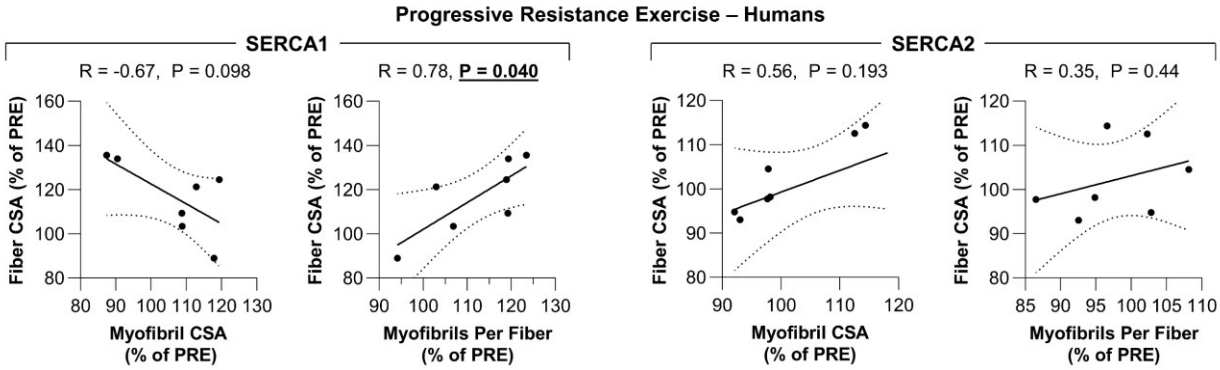

Figure 2-6 – Figure Supplement 1. The radial growth of fibers that occurs in response to an increase in mechanical loading is correlated with the induction of myofibrillogenesis. Biopsies of the vastus lateralis muscle were collected before (PRE) and after (POST) human participants performed 7 weeks of progressive resistance exercise. Each sample was subjected to FIM-ID and then individual fiber types were analyzed for the mean fiber cross-sectional area (CSA), mean myofibril CSA, and the mean number of myofibril per fiber as reported in Figure 2-6. Data for each human POST sample was expressed relative to its respective PRE sample (% of PRE). The resulting data were used to create scatter plots that illustrate the relationship between the changes in fiber CSA and myofibril CSA for each sample, or the relationship between the changes in fiber CSA and the number of myofibrils per fiber (i.e., myofibrillogenesis) for each sample. Solid lines represent the best fit from linear regression, the dashed lines represent the 95% confidence intervals, R indicates Pearson's correlation coefficient, and P indicates the likelihood that the relationship is significantly different from zero. Data used to generate Figure 2-6 – Figure Supplement 1 is available within the fully published article as Figure 6 – Source Data (https://doi.org/10.7554/eLife.92674.3).

Chapter Three: Extended Discussion and Future Directions

The preservation of skeletal muscle mass is essential for maintaining overall health and well-being. Mechanical loading, such as resistance exercise, plays a critical role in regulating muscle mass. Although extensive research has explored both macroscopic and microscopic changes due to increased mechanical load, the specific ultrastructural adaptations that drive skeletal muscle growth remain poorly understood. The overarching goal of this project, therefore, was to identify the ultrastructural adaptations in response to mechanical load and how these changes ultimately contribute to muscle mass growth.

To pinpoint the adaptations that drive the radial growth of skeletal muscle, we developed a novel method to visualize changes in myofibril cross-sectional area and myofibril count using fluorescence microscopy with image deconvolution (FIM-ID) [266]. Our study revealed that the primary driver of muscle fiber radial growth in response to mechanical loading is an increase in the number of myofibrils per cross-section, a process known as myofibrillogenesis. While the increase in myofibril count was the dominant factor in both mouse and human samples, there was a slight trend suggesting an increase in myofibril cross-sectional area in response to mechanical loading. This trend supports our hypothesis that mechanical loading may initially cause an increase in myofibril cross-sectional area, leading to myofibril splitting once the area reaches a critical size, which then results in an overall increase in myofibril number [221]. However, this phenomenon was not directly addressed in our studies, warranting further investigation to confirm its occurrence.

Additionally, our lab is investigating the ultrastructural adaptations underlying the longitudinal growth of muscle fibers in response to mechanical loading. Previous studies suggest

that mechanical loads can lead to an increase in muscle fiber length. Given that sarcomere length within myofibrils remains conserved, it is plausible to hypothesize that an increase in muscle fiber length would require the addition of sarcomeres in-series within the muscle fibers [221]. Notably, unpublished data from our lab suggest that mechanical loading leads still leads to increased rates of protein synthesis and an increase in the number of muscle fibers observed in cross-sections at the muscle mid-belly even when muscle fiber hypertrophy is blocked through inhibition of mTORC1. This observation led us to hypothesize that a unique growth adaptation, separate from muscle fiber hypertrophy, occurs in response to mechanical loading.

We further speculated that this unique adaptation might involve an increase in muscle fiber length. By applying geometric models and formulas outlined by Maxwell [75], we calculated that even small increases in muscle fiber length within the plantaris muscle could lead to significant increases in overall muscle cross-sectional area and the number of muscle fibers observed in mid-belly cross-sections [221]. This led us to hypothesize that the increase in the number of muscle fibers in response to mechanical loading, even when muscle fiber hypertrophy is inhibited, is driven by muscle fiber lengthening via a mTORC1-independent mechanism.

To test this hypothesis, we sought to replicate our preliminary data to determine whether muscle fiber lengthening occurs in response to mechanical loading, even when hypertrophy is blocked by inhibiting signaling through mTORC1. Our experiments again demonstrated an increase in the number of muscle fibers observed in tissue cross-sections following mechanical loading, even when hypertrophy was inhibited. Furthermore, additional data showed that mechanical load-induced muscle fiber lengthening persists despite mTORC1 inhibition. However, the mechanism underlying this mTORC1-independent increase in muscle fiber length remains undefined.

As previously theorized [221], the mechanical load-induced increase in muscle fiber length could be driven by the addition of new sarcomeres in-series at specialized sites along the muscle fiber, called sphenodes. To gain further insight into this mechanism, we aim to visualize the prevalence of sphenodes in response to mechanical loading, both with and without mTORC1 inhibition. To this end, we are using a method known as Bio-Orthogonal Non-Canonical Amino acid Tagging (BONCAT) to visualize newly synthesized proteins in longitudinal sections of skeletal muscle [267, 268]. We hypothesize that mechanical loading promotes muscle fiber lengthening by adding sarcomeres at sphenodes, and these sites should be enriched with newly synthesized proteins. Furthermore, we predict that the prevalence of sphenodes and the deposition of newly synthesized proteins at these sites will be unaffected by mTORC1 inhibition, suggesting these regions are actively involved in sarcomere addition. We have already collected substantial data supporting this hypothesis, and a manuscript is currently being prepared to present our findings.

In conclusion, although the growth of skeletal muscle in response to mechanical loading has been studied for centuries, the fundamental ultrastructural adaptations driving this growth are not yet fully understood. Advances in microscopy and protein-labeling technologies, such as those presented here, are poised to provide critical insights into these adaptations, forming the basis for future studies in skeletal muscle physiology.

References

1. McLeod, M., et al., *Live strong and prosper: the importance of skeletal muscle strength for healthy ageing*. Biogerontology, 2016. **17**(3): p. 497-510.
2. Doherty, T.J., *Invited Review: Aging and sarcopenia*. Journal of Applied Physiology, 2003. **95**(4): p. 1717-1727.
3. Mitchell, W.K., et al., *Sarcopenia, dynapenia, and the impact of advancing age on human skeletal muscle size and strength; a quantitative review*. Frontiers in physiology, 2012. **3**: p. 260-260.
4. Kalyani, R.R., M. Corriere, and L. Ferrucci, *Age-related and disease-related muscle loss: the effect of diabetes, obesity, and other diseases*. Lancet Diabetes Endocrinol, 2014. **2**(10): p. 819-29.
5. Shou, J., P.-J. Chen, and W.-H. Xiao, *Mechanism of increased risk of insulin resistance in aging skeletal muscle*. Diabetology & metabolic syndrome, 2020. **12**: p. 14-14.
6. Beaudart, C., et al., *Health Outcomes of Sarcopenia: A Systematic Review and Meta-Analysis*. PloS one, 2017. **12**(1): p. e0169548-e0169548.
7. Chen, H., et al., *The association between sarcopenia and fracture in middle-aged and elderly people: A systematic review and meta-analysis of cohort studies*. Injury, 2020. **51**(4): p. 804-811.
8. Janssen, I., et al., *The Healthcare Costs of Sarcopenia in the United States*. Journal of the American Geriatrics Society, 2004. **52**(1): p. 80-85.
9. Nations, U., *World Population Prospects 2019: Highlights. ST/ESA/SER.A/423*. Department of Economic and Social Affairs, Population Division (2019), 2019
10. Todd, J., *From Milo to Milo: A History of Barbells, Dumbells, and Indian Clubs*. Iron Game History, 1995. **3**(6): p. 4-16.
11. Abe, T., et al., *Whole body muscle hypertrophy from resistance training: distribution and total mass*. Br J Sports Med, 2003. **37**(6): p. 543-5.
12. Trappe, T.A., et al., *Influence of acetaminophen and ibuprofen on skeletal muscle adaptations to resistance exercise in older adults*. Am J Physiol Regul Integr Comp Physiol, 2011. **300**(3): p. R655-62.
13. Franchi, M.V., et al., *Architectural, functional and molecular responses to concentric and eccentric loading in human skeletal muscle*. Acta Physiol (Oxf), 2014. **210**(3): p. 642-54.
14. Mandić, M., et al., *Automated assessment of regional muscle volume and hypertrophy using MRI*. Scientific Reports, 2020. **10**(1): p. 2239.
15. Mitchell, C.J., et al., *Acute post-exercise myofibrillar protein synthesis is not correlated with resistance training-induced muscle hypertrophy in young men*. PLoS One, 2014. **9**(2): p. e89431.
16. Aagaard, P., et al., *A mechanism for increased contractile strength of human pennate muscle in response to strength training: changes in muscle architecture*. J Physiol, 2001. **534**(Pt. 2): p. 613-23.
17. Mitchell, C.J., et al., *Resistance exercise load does not determine training-mediated hypertrophic gains in young men*. J Appl Physiol (1985), 2012. **113**(1): p. 71-7.
18. Hornberger, T.A., Jr. and R.P. Farrar, *Physiological hypertrophy of the FHL muscle following 8 weeks of progressive resistance exercise in the rat*. Can J Appl Physiol, 2004. **29**(1): p. 16-31.
19. Wong, T.S. and F.W. Booth, *Skeletal muscle enlargement with weight-lifting exercise by rats*. J Appl Physiol, 1988. **65**(2): p. 950-4.

20. Ogasawara, R., et al., *The role of mTOR signalling in the regulation of skeletal muscle mass in a rodent model of resistance exercise.* Sci Rep, 2016. **6**: p. 31142.
21. Lowe, D.A. and S.E. Alway, *Animal models for inducing muscle hypertrophy: are they relevant for clinical applications in humans?* J Orthop Sports Phys Ther, 2002. **32**(2): p. 36-43.
22. Goodman, C.A., et al., *The role of skeletal muscle mTOR in the regulation of mechanical load-induced growth*. J Physiol, 2011. **589**(Pt 22): p. 5485-501.
23. Holly, R.G., et al., *Stretch-induced growth in chicken wing muscles: a new model of stretch hypertrophy*. Am J Physiol, 1980. **238**(1): p. C62-71.
24. Frontera, W.R. and J. Ochala, *Skeletal Muscle: A Brief Review of Structure and Function.* Calcified Tissue International, 2015. **96**(3): p. 183-195.
25. Lieber, R.L., *Skeletal muscle adaptability. I: Review of basic properties.* Dev Med Child Neurol, 1986. **28**(3): p. 390-7.
26. Henderson, C.A., et al., *Overview of the Muscle Cytoskeleton.* Compr Physiol, 2017. **7**(3): p. 891-944.
27. Narici, M., M. Franchi, and C. Maganaris, *Muscle structural assembly and functional consequences*. The Journal of Experimental Biology, 2016. **219**(2): p. 276-284.
28. Biferali, B., et al., *Fibro-Adipogenic Progenitors Cross-Talk in Skeletal Muscle: The Social Network.* Front Physiol, 2019. **10**: p. 1074.
29. Tedesco, F.S., L.A. Moyle, and E. Perdiguero, *Muscle Interstitial Cells: A Brief Field Guide to Non-satellite Cell Populations in Skeletal Muscle.* Methods Mol Biol, 2017. **1556**: p. 129-147.
30. Murach, K.A., et al., *Starring or Supporting Role? Satellite Cells and Skeletal Muscle Fiber Size Regulation.* Physiology (Bethesda), 2018. **33**(1): p. 26-38.
31. MacDougall, J.D., et al., *Muscle ultrastructural characteristics of elite powerlifters and bodybuilders*. Eur J Appl Physiol Occup Physiol, 1982. **48**(1): p. 117-26.
32. Seiden, D., *Quantitative analysis of muscle cell changes in compensatory hypertrophy and work-induced hypertrophy.* Am J Anat, 1976. **145**(4): p. 459-65.
33. Luthi, J.M., et al., *Structural changes in skeletal muscle tissue with heavy-resistance exercise.* Int J Sports Med, 1986. **7**(3): p. 123-7.
34. Goldspink, G. and K.F. Howells, *Work-induced hypertrophy in exercised normal muscles of different ages and the reversibility of hypertrophy after cessation of exercise.* J Physiol, 1974. **239**(1): p. 179-93.
35. Toth, M.J., et al., *Resistance training alters skeletal muscle structure and function in human heart failure: effects at the tissue, cellular and molecular levels.* J Physiol, 2012. **590**(5): p. 1243-59.
36. Lavorato, M., et al., *Elongated mitochondrial constrictions and fission in muscle fatigue.* J Cell Sci, 2018. **131**(23).
37. Dirksen, R.T., *Sarcoplasmic reticulum-mitochondrial through-space coupling in skeletal muscle*. Appl Physiol Nutr Metab, 2009. **34**(3): p. 389-95.
38. Gordon, A.M., E. Homsher, and M. Regnier, *Regulation of contraction in striated muscle.* Physiol Rev, 2000. **80**(2): p. 853-924.
39. Billeter, R. and H. Hoppeler, *Muscular Basis of Strength. Strength and Power in Sport*. 2003: Blackwell Science Ltd.
40. Edman, K.A., *The velocity of unloaded shortening and its relation to sarcomere length and isometric force in vertebrate muscle fibres.* J Physiol, 1979. **291**: p. 143-59.
41. Gordon, A.M., A.F. Huxley, and F.J. Julian, *The variation in isometric tension with sarcomere length in vertebrate muscle fibres.* J Physiol, 1966. **184**(1): p. 170-92.

42. Burkholder, T.J. and R.L. Lieber, *Sarcomere length operating range of vertebrate muscles during movement*. J Exp Biol, 2001. **204**(Pt 9): p. 1529-36.
43. Fry, A.C., *The role of resistance exercise intensity on muscle fibre adaptations*. Sports Med, 2004. **34**(10): p. 663-79.
44. Fry, A.C., *The Role of Resistance Exercise Intensity on Muscle Fibre Adaptations*. Sports Medicine, 2004. **34**(10): p. 663-679.
45. Scott, W., J. Stevens, and S.A. Binder–Macleod, *Human Skeletal Muscle Fiber Type Classifications*. Physical Therapy, 2001. **81**(11): p. 1810-1816.
46. Hilber, K., et al., *Kinetic properties of myosin heavy chain isoforms in single fibers from human skeletal muscle*. FEBS Letters, 1999. **455**(3): p. 267-270.
47. Smerdu, V., et al., *Type IIx myosin heavy chain transcripts are expressed in type IIb fibers of human skeletal muscle*. American Journal of Physiology-Cell Physiology, 1994. **267**(6): p. C1723-C1728.
48. Ennion, S., et al., *Characterization of human skeletal muscle fibres according to the myosin heavy chains they express*. J Muscle Res Cell Motil, 1995. **16**(1): p. 35-43.
49. Pette, D., H. Peuker, and R.S. Staron, *The impact of biochemical methods for single muscle fibre analysis*. Acta Physiol Scand, 1999. **166**(4): p. 261-77.
50. Goldspink, G., *Increase in Length of Skeletal Muscle during Normal Growth*. Nature, 1964. **204**: p. 1095-6.
51. Williams, P.E. and G. Goldspink, *Longitudinal growth of striated muscle fibres*. J Cell Sci, 1971. **9**(3): p. 751-67.
52. Beaucage, K.L., et al., *Quantitative in vivo micro-computed tomography for assessment of age-dependent changes in murine whole-body composition*. Bone Rep, 2016. **5**: p. 70-80.
53. Zöllner, A.M., et al., *Stretching skeletal muscle: chronic muscle lengthening through sarcomerogenesis*. PloS one, 2012. **7**(10): p. e45661-e45661.
54. Aoki, M.S., et al., *Expression of genes related to myostatin signaling during rat skeletal muscle longitudinal growth*. Muscle Nerve, 2009. **40**(6): p. 992-9.
55. Simpson, A.H., et al., *The response of muscle to leg lengthening*. J Bone Joint Surg Br, 1995. **77**(4): p. 630-6.
56. Caiozzo, V.J., et al., *Effects of distraction on muscle length: mechanisms involved in sarcomerogenesis*. Clin Orthop Relat Res, 2002(403 Suppl): p. S133-45.
57. Roy, R.R. and V.R. Edgerton, *Response of mouse plantaris muscle to functional overload: comparison with rat and cat*. Comp Biochem Physiol A Physiol, 1995. **111**(4): p. 569-75.
58. Terena, S.M., et al., *Systematic review of the synergist muscle ablation model for compensatory hypertrophy*. Rev Assoc Med Bras (1992), 2017. **63**(2): p. 164-172.
59. Kawakami, Y., et al., *Training-induced changes in muscle architecture and specific tension*. Eur J Appl Physiol Occup Physiol, 1995. **72**(1-2): p. 37-43.
60. Roman, W.J., et al., *Adaptations in the elbow flexors of elderly males after heavy-resistance training*. J Appl Physiol (1985), 1993. **74**(2): p. 750-4.
61. Welle, S., S. Totterman, and C. Thornton, *Effect of age on muscle hypertrophy induced by resistance training*. J Gerontol A Biol Sci Med Sci, 1996. **51**(6): p. M270-5.
62. Angleri, V., C. Ugrinowitsch, and C.A. Libardi, *Crescent pyramid and drop-set systems do not promote greater strength gains, muscle hypertrophy, and changes on muscle architecture compared with traditional resistance training in well-trained men*. Eur J Appl Physiol, 2017. **117**(2): p. 359-369.
63. Damas, F., C.A. Libardi, and C. Ugrinowitsch, *The development of skeletal muscle hypertrophy through resistance training: the role of muscle damage and muscle protein synthesis*. Eur J Appl Physiol, 2018. **118**(3): p. 485-500.

64. Housh, D.J., et al., *Hypertrophic response to unilateral concentric isokinetic resistance training.* J Appl Physiol (1985), 1992. **73**(1): p. 65-70.
65. McMahon, G.E., et al., *Impact of range of motion during ecologically valid resistance training protocols on muscle size, subcutaneous fat, and strength.* J Strength Cond Res, 2014. **28**(1): p. 245-55.
66. Bellamy, L.M., et al., *The acute satellite cell response and skeletal muscle hypertrophy following resistance training.* PLoS One, 2014. **9**(10): p. e109739.
67. Blazevich, A.J., et al., *Influence of concentric and eccentric resistance training on architectural adaptation in human quadriceps muscles.* J Appl Physiol (1985), 2007. **103**(5): p. 1565-75.
68. Narici, M.V., et al., *Human quadriceps cross-sectional area, torque and neural activation during 6 months strength training.* Acta Physiol Scand, 1996. **157**(2): p. 175-86.
69. Sakuma, K., A. Yamaguchi, and S. Katsuta, *Are region-specific changes in fibre types attributable to nonuniform muscle hypertrophy by overloading?* Eur J Appl Physiol Occup Physiol, 1995. **71**(6): p. 499-504.
70. Gardiner, P.F., B.J. Jasmin, and P. Corriveau, *Rostrocaudal pattern of fiber-type changes in an overloaded rat ankle extensor.* J Appl Physiol (1985), 1991. **71**(2): p. 558-64.
71. Antonio, J., *Nonuniform Response of Skeletal Muscle to Heavy Resistance Training: Can Bodybuilders Induce Regional Muscle Hypertrophy?* The Journal of Strength & Conditioning Research, 2000. **14**(1): p. 102-113.
72. Alway, S.E., et al., *Regionalized adaptations and muscle fiber proliferation in stretch-induced enlargement.* J Appl Physiol (1985), 1989. **66**(2): p. 771-81.
73. Counts, B.R., et al., *Muscle growth: To infinity and beyond?* Muscle Nerve, 2017. **56**(6): p. 1022-1030.
74. Damas, F., et al., *Early resistance training-induced increases in muscle cross-sectional area are concomitant with edema-induced muscle swelling.* Eur J Appl Physiol, 2016. **116**(1): p. 49-56.
75. Maxwell, L.C., J.A. Faulkner, and G.J. Hyatt, *Estimation of number of fibers in guinea pig skeletal muscles.* J Appl Physiol, 1974. **37**(2): p. 259-64.
76. Jorgenson, K.W. and T.A. Hornberger, *The Overlooked Role of Fiber Length in Mechanical Load-Induced Growth of Skeletal Muscle.* Exerc Sport Sci Rev, 2019. **47**(4): p. 258-259.
77. O'Brien, T.D., et al., *Muscle-tendon structure and dimensions in adults and children.* J Anat, 2010. **216**(5): p. 631-42.
78. Timmins, R.G., et al., *Architectural Changes of the Biceps Femoris Long Head after Concentric or Eccentric Training.* Med Sci Sports Exerc, 2016. **48**(3): p. 499-508.
79. Sharifnezhad, A., R. Marzilger, and A. Arampatzis, *Effects of load magnitude, muscle length and velocity during eccentric chronic loading on the longitudinal growth of the vastus lateralis muscle.* J Exp Biol, 2014. **217**(Pt 15): p. 2726-33.
80. Reeves, N.D., et al., *Differential adaptations to eccentric versus conventional resistance training in older humans.* Exp Physiol, 2009. **94**(7): p. 825-33.
81. Baroni, B.M., et al., *Muscle architecture adaptations to knee extensor eccentric training: rectus femoris vs. vastus lateralis.* Muscle Nerve, 2013. **48**(4): p. 498-506.
82. Ullrich, B., et al., *Neuromuscular Responses to 14 Weeks of Traditional and Daily Undulating Resistance Training.* Int J Sports Med, 2015. **36**(7): p. 554-62.
83. Ema, R., et al., *Inhomogeneous architectural changes of the quadriceps femoris induced by resistance training.* Eur J Appl Physiol, 2013. **113**(11): p. 2691-703.
84. Erskine, R.M., et al., *Inter-individual variability in the adaptation of human muscle specific tension to progressive resistance training.* Eur J Appl Physiol, 2010. **110**(6): p. 1117-25.

85. Alegre, L.M., et al., *Effects of isometric training on the knee extensor moment-angle relationship and vastus lateralis muscle architecture*. Eur J Appl Physiol, 2014. **114**(11): p. 2437-46.
86. Ema, R., et al., *Training-induced changes in architecture of human skeletal muscles: current evidence and unresolved issues*. The Journal of Physical Fitness and Sports Medicine, 2016. **5**(1): p. 37-46.
87. Franchi, M.V., et al., *Fascicle length does increase in response to longitudinal resistance training and in a contraction-mode specific manner*. Springerplus, 2016. **5**: p. 94.
88. Timmins, R.G., et al., *Architectural adaptations of muscle to training and injury: a narrative review outlining the contributions by fascicle length, pennation angle and muscle thickness*. Br J Sports Med, 2016. **50**(23): p. 1467-1472.
89. Franchi, M.V., N.D. Reeves, and M.V. Narici, *Skeletal Muscle Remodeling in Response to Eccentric vs. Concentric Loading: Morphological, Molecular, and Metabolic Adaptations*. Front Physiol, 2017. **8**: p. 447.
90. Young, M., et al., *Examination of intrafascicular muscle fiber terminations: implications for tension delivery in series-fibered muscles*. J Morphol, 2000. **245**(2): p. 130-45.
91. Paul, A.C. and N. Rosenthal, *Different modes of hypertrophy in skeletal muscle fibers*. J Cell Biol, 2002. **156**(4): p. 751-60.
92. Swatland, H.J. and R.G. Cassens, *Muscle growth: the problem of muscle fibers with an intrafascicular termination*. J Anim Sci, 1972. **35**(2): p. 336-44.
93. Alway, S.E., W.J. Gonyea, and M.E. Davis, *Muscle fiber formation and fiber hypertrophy during the onset of stretch-overload*. Am J Physiol, 1990. **259**(1 Pt 1): p. C92-102.
94. Roy, R.R., et al., *Functional significance of compensatory overloaded rat fast muscle*. J Appl Physiol Respir Environ Exerc Physiol, 1982. **52**(2): p. 473-8.
95. Lindsey, C.A., et al., *The effect of the amount of limb lengthening on skeletal muscle.* Clin Orthop Relat Res, 2002(402): p. 278-87.
96. Butterfield, T.A., T.R. Leonard, and W. Herzog, *Differential serial sarcomere number adaptations in knee extensor muscles of rats is contraction type dependent*. J Appl Physiol (1985), 2005. **99**(4): p. 1352-8.
97. Lynn, R. and D.L. Morgan, *Decline running produces more sarcomeres in rat vastus intermedius muscle fibers than does incline running*. J Appl Physiol (1985), 1994. **77**(3): p. 1439-44.
98. You, J.S., et al., *The role of raptor in the mechanical load-induced regulation of mTOR signaling, protein synthesis, and skeletal muscle hypertrophy.* FASEB J, 2019. **33**(3): p. 4021-4034.
99. Goh, Q., et al., *Myonuclear accretion is a determinant of exercise-induced remodeling in skeletal muscle.* Elife, 2019. **8**.
100. Morpurgo, B., *Eine experimentelle Studie*. Archiv für pathologische Anatomie und Physiologie und für klinische Medicin, 1897. **150**(3): p. 522-554.
101. Haun, C.T., et al., *A Critical Evaluation of the Biological Construct Skeletal Muscle Hypertrophy: Size Matters but So Does the Measurement.* Front Physiol, 2019. **10**: p. 247.
102. Gonyea, W.J. and G.C. Ericson, *An experimental model for the study of exercise-induced skeletal muscle hypertrophy.* Journal of Applied Physiology, 1976. **40**(4): p. 630-633.
103. Goldspink, G., *The Combined Effects of Exercise and Reduced Food Intake on Skeletal Muscle Fibers*. J Cell Comp Physiol, 1964. **63**: p. 209-16.
104. Schiaffino, S., S. Pierobon Bormioli, and M. Aloisi, *Cell proliferation in rat skeletal muscle during early stages of compensatory hypertrophy*. Virchows Archiv B, 1972. **11**(1): p. 268-273.

105. Sola, O.M., D.L. Christensen, and A.W. Martin, *Hypertrophy and hyperplasia of adult chicken anterior latissimus dorsi muscles following stretch with and without denervation*. Exp Neurol, 1973. **41**(1): p. 76-100.
106. Conceicao, M.S., et al., *Muscle Fiber Hypertrophy and Myonuclei Addition: A Systematic Review and Meta-analysis*. Med Sci Sports Exerc, 2018. **50**(7): p. 1385-1393.
107. Kosek, D.J., et al., *Efficacy of 3 days/wk resistance training on myofiber hypertrophy and myogenic mechanisms in young vs. older adults*. J Appl Physiol (1985), 2006. **101**(2): p. 531-44.
108. Campos, G.E., et al., *Muscular adaptations in response to three different resistance-training regimens: specificity of repetition maximum training zones*. Eur J Appl Physiol, 2002. **88**(1-2): p. 50-60.
109. Antonio, J. and W.J. Gonyea, *Progressive stretch overload of skeletal muscle results in hypertrophy before hyperplasia*. J Appl Physiol (1985), 1993. **75**(3): p. 1263-71.
110. Murach, K.A., et al., *Muscle Fiber Splitting Is a Physiological Response to Extreme Loading in Animals*. Exerc Sport Sci Rev, 2019. **47**(2): p. 108-115.
111. Schwartz, M.S., M. Sargeant, and M. Swash, *Longitudinal fibre splitting in neurogenic muscular disorders--its relation to the pathogenesis of "myopathic" change*. Brain, 1976. **99**(4): p. 617-36.
112. Pichavant, C. and G.K. Pavlath, *Incidence and severity of myofiber branching with regeneration and aging*. Skeletal Muscle, 2014. **4**(1): p. 9.
113. Antonio, J. and W.J. Gonyea, *Muscle fiber splitting in stretch-enlarged avian muscle*. Med Sci Sports Exerc, 1994. **26**(8): p. 973-7.
114. Tamaki, T., et al., *Characteristics of compensatory hypertrophied muscle in the rat: I. Electron microscopic and immunohistochemical studies*. Anat Rec, 1996. **246**(3): p. 325-34.
115. Eriksson, A., et al., *Hypertrophic muscle fibers with fissures in power-lifters; fiber splitting or defect regeneration?* Histochemistry and Cell Biology, 2006. **126**(4): p. 409-417.
116. Ho, K.W., et al., *Skeletal muscle fiber splitting with weight-lifting exercise in rats*. Am J Anat, 1980. **157**(4): p. 433-40.
117. Gonyea, W., G.C. Ericson, and F. Bonde-Petersen, *Skeletal muscle fiber splitting induced by weight-lifting exercise in cats*. Acta Physiol Scand, 1977. **99**(1): p. 105-9.
118. Vaughan, H.S. and G. Goldspink, *Fibre number and fibre size in a surgically overloaded muscle*. J Anat, 1979. **129**(Pt 2): p. 293-303.
119. Gollnick, P.D., et al., *Muscular enlargement and number of fibers in skeletal muscles of rats*. J Appl Physiol Respir Environ Exerc Physiol, 1981. **50**(5): p. 936-43.
120. Gollnick, P.D., et al., *Fiber number and size in overloaded chicken anterior latissimus dorsi muscle*. J Appl Physiol Respir Environ Exerc Physiol, 1983. **54**(5): p. 1292-7.
121. Timson, B.F., et al., *Fiber number, area, and composition of mouse soleus muscle following enlargement*. J Appl Physiol (1985), 1985. **58**(2): p. 619-24.
122. Gonyea, W.J., et al., *Exercise induced increases in muscle fiber number*. Eur J Appl Physiol Occup Physiol, 1986. **55**(2): p. 137-41.
123. Li, M., et al., *Not all the number of skeletal muscle fibers is determined prenatally*. BMC Dev Biol, 2015. **15**: p. 42.
124. Timson, B.F. and G.A. Dudenhoeffer, *Skeletal muscle fibre number in the rat from youth to adulthood*. J Anat, 1990. **173**: p. 33-6.
125. Rehfeldt, C., et al., *Environmental and Genetic Factors as Sources of Variation in Skeletal Muscle Fibre Number*. Basic Appl. Myol., 1999. **9** (5): p. 235-253.

126. Kelley, G., *Mechanical overload and skeletal muscle fiber hyperplasia: a meta-analysis*. J Appl Physiol (1985), 1996. **81**(4): p. 1584-8.
127. Taylor, N.A. and J.G. Wilkinson, *Exercise-induced skeletal muscle growth. Hypertrophy or hyperplasia?* Sports Med, 1986. **3**(3): p. 190-200.
128. Gonyea, W.J., *Role of exercise in inducing increases in skeletal muscle fiber number.* J Appl Physiol Respir Environ Exerc Physiol, 1980. **48**(3): p. 421-6.
129. Alway, S.E., *Stretch induces non-uniform isomyosin expression in the quail anterior latissimus dorsi muscle*. Anat Rec, 1993. **237**(1): p. 1-7.
130. Abruzzo, P.M., et al., *Moderate exercise training induces ROS-related adaptations to skeletal muscles*. Int J Sports Med, 2013. **34**(8): p. 676-87.
131. Alway, S.E., *Perpetuation of muscle fibers after removal of stretch in the Japanese quail.* Am J Physiol, 1991. **260**(3 Pt 1): p. C400-8.
132. Antonio, J. and W.J. Gonyea, *Skeletal muscle fiber hyperplasia.* Med Sci Sports Exerc, 1993. **25**(12): p. 1333-45.
133. Brown, L.E. and T. Incledon, *Skeletal Muscle Fiber Hyperplasia: Why It Can or Cannot Occur in Humans*. Strength & Conditioning Journal, 2000. **22**(2): p. 28.
134. Tamaki, T., S. Uchiyama, and S. Nakano, *A weight-lifting exercise model for inducing hypertrophy in the hindlimb muscles of rats.* Med Sci Sports Exerc, 1992. **24**(8): p. 881-6.
135. Williams, P.E. and G. Goldspink, *The effect of immobilization on the longitudinal growth of striated muscle fibres.* J Anat, 1973. **116**(1): p. 45-55.
136. Barnett, J.G., R.G. Holly, and C.R. Ashmore, *Stretch-induced growth in chicken wing muscles: biochemical and morphological characterization.* Am J Physiol, 1980. **239**(1): p. C39-46.
137. Koh, T.J., *Do adaptations in serial sarcomere number occur with strength training?* Human Movement Science, 1995. **14**(1): p. 61-77.
138. Zollner, A.M., et al., *Stretching skeletal muscle: chronic muscle lengthening through sarcomerogenesis*. PLoS One, 2012. **7**(10): p. e45661.
139. Matano, T., K. Tamai, and T. Kurokawa, *Adaptation of skeletal muscle in limb lengthening: a light diffraction study on the sarcomere length in situ.* J Orthop Res, 1994. **12**(2): p. 193-6.
140. Kinney, M.C., et al., *Reduced skeletal muscle satellite cell number alters muscle morphology after chronic stretch but allows limited serial sarcomere addition.* Muscle Nerve, 2017. **55**(3): p. 384-392.
141. Goldspink, G., *Alterations in myofibril size and structure during growth, exercise and change in environmental temperature.* , in *In Handbook of Physiology*. 1983, American Physiological Society, Bethesda MD. p. 539–554.
142. Griffin, G.E., P.E. Williams, and G. Goldspink, *Region of longitudinal growth in striated muscle fibres*. Nat New Biol, 1971. **232**(27): p. 28-9.
143. Jahromi, S.S. and M.P. Charlton, *Transverse sarcomere splitting. A possible means of longitudinal growth in crab muscles*. J Cell Biol, 1979. **80**(3): p. 736-42.
144. Crawford, G.N., *An experimental study of muscle growth in the rabbit*. J Bone Joint Surg Br, 1954. **36-B**(2): p. 294-303.
145. Mackay, B. and T.J. Harrop, *An experimental study of the longitudinal growth of skeletal muscle in the rat*. Acta Anat (Basel), 1969. **72**(1): p. 38-49.
146. Bennett, M.R., H. Fernandez, and N.A. Lavidis, *Development of the mature distribution of synapses on fibres in the frog sartorius muscle.* J Neurocytol, 1985. **14**(6): p. 981-95.
147. Yu, J.G., L. Carlsson, and L.E. Thornell, *Evidence for myofibril remodeling as opposed to myofibril damage in human muscles with DOMS: an ultrastructural and immunoelectron microscopic study*. Histochem Cell Biol, 2004. **121**(3): p. 219-27.

148. Yu, J.G., D.O. Furst, and L.E. Thornell, *The mode of myofibril remodelling in human skeletal muscle affected by DOMS induced by eccentric contractions.* Histochem Cell Biol, 2003. **119**(5): p. 383-93.
149. Yu, J.G. and L.E. Thornell, *Desmin and actin alterations in human muscles affected by delayed onset muscle soreness: a high resolution immunocytochemical study.* Histochem Cell Biol, 2002. **118**(2): p. 171-9.
150. Carlsson, L., et al., *Myotilin: a prominent marker of myofibrillar remodelling.* Neuromuscul Disord, 2007. **17**(1): p. 61-8.
151. Friden, J., *Changes in human skeletal muscle induced by long-term eccentric exercise.* Cell Tissue Res, 1984. **236**(2): p. 365-72.
152. Orfanos, Z., et al., *Breaking sarcomeres by in vitro exercise.* Sci Rep, 2016. **6**: p. 19614.
153. Friden, J., M. Sjostrom, and B. Ekblom, *Myofibrillar damage following intense eccentric exercise in man.* Int J Sports Med, 1983. **4**(3): p. 170-6.
154. Gibala, M.J., et al., *Changes in human skeletal muscle ultrastructure and force production after acute resistance exercise.* J Appl Physiol (1985), 1995. **78**(2): p. 702-8.
155. Clarkson, P.M. and M.J. Hubal, *Exercise-induced muscle damage in humans.* Am J Phys Med Rehabil, 2002. **81**(11 Suppl): p. S52-69.
156. Heidenhain, M., *Uber die Noniusfelder der Muskelfaser.* Anatomische Hefte, 1919. **Bd. 56**: p. 321-402.
157. Close, R.I., *Dynamic properties of mammalian skeletal muscles.* Physiol Rev, 1972. **52**(1): p. 129-97.
158. Fitts, R.H., K.S. McDonald, and J.M. Schluter, *The determinants of skeletal muscle force and power: their adaptability with changes in activity pattern.* J Biomech, 1991. **24 Suppl 1**: p. 111-22.
159. Erskine, R.M., et al., *What causes in vivo muscle specific tension to increase following resistance training?* Exp Physiol, 2011. **96**(2): p. 145-55.
160. Trappe, S., et al., *Effect of resistance training on single muscle fiber contractile function in older men.* J Appl Physiol (1985), 2000. **89**(1): p. 143-52.
161. Trappe, S., et al., *Resistance training improves single muscle fiber contractile function in older women.* Am J Physiol Cell Physiol, 2001. **281**(2): p. C398-406.
162. Widrick, J.J., et al., *Functional properties of human muscle fibers after short-term resistance exercise training.* Am J Physiol Regul Integr Comp Physiol, 2002. **283**(2): p. R408-16.
163. D'Antona, G., et al., *Skeletal muscle hypertrophy and structure and function of skeletal muscle fibres in male body builders.* J Physiol, 2006. **570**(Pt 3): p. 611-27.
164. Paoli, A., et al., *Protein Supplementation Does Not Further Increase Latissimus Dorsi Muscle Fiber Hypertrophy after Eight Weeks of Resistance Training in Novice Subjects, but Partially Counteracts the Fast-to-Slow Muscle Fiber Transition.* Nutrients, 2016. **8**(6).
165. Claflin, D.R., et al., *Effects of high- and low-velocity resistance training on the contractile properties of skeletal muscle fibers from young and older humans.* J Appl Physiol (1985), 2011. **111**(4): p. 1021-30.
166. Pansarasa, O., et al., *Resistance training of long duration modulates force and unloaded shortening velocity of single muscle fibres of young women.* J Electromyogr Kinesiol, 2009. **19**(5): p. e290-300.
167. Dankel, S.J., et al., *Resistance training induced changes in strength and specific force at the fiber and whole muscle level: a meta-analysis.* Eur J Appl Physiol, 2019. **119**(1): p. 265-278.

168. Mendias, C.L., et al., *Changes in muscle fiber contractility and extracellular matrix production during skeletal muscle hypertrophy*. J Appl Physiol (1985), 2017. **122**(3): p. 571-579.
169. Vann, C.G., et al., *Skeletal Muscle Myofibrillar Protein Abundance Is Higher in Resistance-Trained Men, and Aging in the Absence of Training May Have an Opposite Effect*. Sports (Basel), 2020. **8**(1).
170. Aguiar, A.F., et al., *Creatine does not promote hypertrophy in skeletal muscle in supplemented compared with nonsupplemented rats subjected to a similar workload*. Nutr Res, 2011. **31**(8): p. 652-7.
171. Penman, K.A., *Ultrastructural changes in human striated muscle using three methods of training*. Res Q, 1969. **40**(4): p. 764-72.
172. Meijer, J.P., et al., *Single muscle fibre contractile properties differ between body-builders, power athletes and control subjects*. Exp Physiol, 2015. **100**(11): p. 1331-41.
173. Haun, C.T., et al., *Muscle fiber hypertrophy in response to 6 weeks of high-volume resistance training in trained young men is largely attributed to sarcoplasmic hypertrophy*. PLoS One, 2019. **14**(6): p. e0215267.
174. Roberts, M.D., et al., *Skeletal muscle mitochondrial volume and myozenin-1 protein differences exist between high versus low anabolic responders to resistance training*. PeerJ, 2018. **6**: p. e5338.
175. Kadi, F., et al., *Effects of anabolic steroids on the muscle cells of strength-trained athletes*. Med Sci Sports Exerc, 1999. **31**(11): p. 1528-34.
176. Eriksson, A., et al., *Skeletal muscle morphology in power-lifters with and without anabolic steroids*. Histochem Cell Biol, 2005. **124**(2): p. 167-75.
177. Kesmodel, U.S., *Cross-sectional studies - what are they good for?* Acta Obstet Gynecol Scand, 2018. **97**(4): p. 388-393.
178. Setia, M.S., *Methodology Series Module 3: Cross-sectional Studies*. Indian J Dermatol, 2016. **61**(3): p. 261-4.
179. Mann, C.J., *Observational research methods. Research design II: cohort, cross sectional, and case-control studies*. Emerg Med J, 2003. **20**(1): p. 54-60.
180. Haun, C.T., et al., *Effects of Graded Whey Supplementation During Extreme-Volume Resistance Training*. Front Nutr, 2018. **5**: p. 84.
181. Huxley, H.E., *Electron microscope studies of the organisation of the filaments in striated muscle*. Biochim Biophys Acta, 1953. **12**(3): p. 387-94.
182. Millman, B.M., *The filament lattice of striated muscle*. Physiol Rev, 1998. **78**(2): p. 359-91.
183. Luther, P.K. and J.M. Squire, *The intriguing dual lattices of the Myosin filaments in vertebrate striated muscles: evolution and advantage*. Biology (Basel), 2014. **3**(4): p. 846-65.
184. Ashmore, C.R. and P.J. Summers, *Stretch-induced growth in chicken wing muscles: myofibrillar proliferation*. Am J Physiol, 1981. **241**(3): p. C93-7.
185. Goldspink, G., *The proliferation of myofibrils during muscle fibre growth*. J Cell Sci, 1970. **6**(2): p. 593-603.
186. Goldspink, G., *Changes in striated muscle fibres during contraction and growth with particular reference to myofibril splitting*. J Cell Sci, 1971. **9**(1): p. 123-37.
187. Patterson, S. and G. Goldspink, *Mechanism of myofibril growth and proliferation in fish muscle*. J Cell Sci, 1976. **22**(3): p. 607-16.
188. MacIntosh BR, G.P., McComas AJ. , *Skeletal Muscle: Form and Function*. 2006: Human Kinetics.
189. Komi, P.V., *Strength and Power in Sport*. 2008: John Wiley & Sons.
190. Bourne, G.H., *The Structure and Function of Muscle*. 2013: Elsevier.

191. McComas, A.J., *Neuromuscular Function and Disorders*. 2013: Butterworth-Heinemann.
192. Morkin, E., *Postnatal muscle fiber assembly: localization of newly synthesized myofibrillar proteins*. Science, 1970. **167**(3924): p. 1499-501.
193. Galavazi, G. and J.A. Szirmai, *The influence of age and testosterone on the ribosomal population in the m. levator ani and a thigh muscle of the rat.* Z Zellforsch Mikrosk Anat, 1971. **121**(4): p. 548-60.
194. Galavazi, G., *Identification of helical polyribosomes in sections of mature skeletal muscle fibers*. Z Zellforsch Mikrosk Anat, 1971. **121**(4): p. 531-47.
195. Salpeter, M.M., L. Bachmann, and E.E. Salpeter, *Resolution in electron microscope radioautography*. J Cell Biol, 1969. **41**(1): p. 1-32.
196. Caro, L.G., *High-resolution autoradiogaphy. II. The problem of resolution*. J Cell Biol, 1962. **15**: p. 189-99.
197. Goodman, C.A., et al., *Novel insights into the regulation of skeletal muscle protein synthesis as revealed by a new nonradioactive in vivo technique.* FASEB J, 2011. **25**(3): p. 1028-39.
198. Tom Dieck, S., et al., *Metabolic labeling with noncanonical amino acids and visualization by chemoselective fluorescent tagging*. Curr Protoc Cell Biol, 2012. **Chapter 7**: p. Unit7 11.
199. Hermann, R., P. Walther, and M. Muller, *Immunogold labeling in scanning electron microscopy*. Histochem Cell Biol, 1996. **106**(1): p. 31-9.
200. Huang, B., H. Babcock, and X. Zhuang, *Breaking the diffraction barrier: super-resolution imaging of cells.* Cell, 2010. **143**(7): p. 1047-58.
201. Raulf, A., et al., *Click chemistry facilitates direct labelling and super-resolution imaging of nucleic acids and proteinsdaggerElectronic supplementary information (ESI) available. See DOI: 10.1039/c4ra01027bClick here for additional data file*. RSC Adv, 2014. **4**(57): p. 30462-30466.
202. Mobius, W. and G. Posthuma, *Sugar and ice: Immunoelectron microscopy using cryosections according to the Tokuyasu method*. Tissue Cell, 2019. **57**: p. 90-102.
203. Holmes, R. and P.J. Rasch, *Effect of exercise on number of myofibrils per fiber in sartorius muscle of the rat*. Am J Physiol, 1958. **195**(1): p. 50-2.
204. Toffolo, R.L. and C.D. Ianuzzo, *Myofibrillar adaptations during cardiac hypertrophy.* Mol Cell Biochem, 1994. **131**(2): p. 141-9.
205. Richter, G.W. and A. Kellner, *Hypertrophy of the human heart at the level of fine structure. An analysis and two postulates*. J Cell Biol, 1963. **18**: p. 195-206.
206. Anversa, P., et al., *Stereological measurement of cellular and subcellular hypertrophy and hyperplasia in the papillary muscle of adult rat.* J Mol Cell Cardiol, 1980. **12**(8): p. 781-95.
207. Betts G.J., Y.K.A., Wise J.A., Johnson E, Poe B, Kruse D.H., Korol O, Johnson J.E., Womble M, DeSaix P, *Anatomy and Physiology*. 2013: OpenStax.
208. Burkholder, T.J., et al., *Relationship between muscle fiber types and sizes and muscle architectural properties in the mouse hindlimb*. J Morphol, 1994. **221**(2): p. 177-90.
209. Klein, J.S., et al., *Examination of the contributions of size and avidity to the neutralization mechanisms of the anti-HIV antibodies b12 and 4E10*. Proc Natl Acad Sci U S A, 2009. **106**(18): p. 7385-90.
210. Izumiya, Y., et al., *Fast/Glycolytic muscle fiber growth reduces fat mass and improves metabolic parameters in obese mice.* Cell Metab, 2008. **7**(2): p. 159-72.
211. Srikanthan, P. and A.S. Karlamangla, *Relative muscle mass is inversely associated with insulin resistance and prediabetes. Findings from the third National Health and Nutrition Examination Survey*. J Clin Endocrinol Metab, 2011. **96**(9): p. 2898-903.

212. Seguin, R. and M.E. Nelson, *The benefits of strength training for older adults*. Am J Prev Med, 2003. **25**(3 Suppl 2): p. 141-9.
213. Janssen, I., et al., *The healthcare costs of sarcopenia in the United States*. J Am Geriatr Soc, 2004. **52**(1): p. 80-5.
214. Proctor, D.N., P. Balagopal, and K.S. Nair, *Age-related sarcopenia in humans is associated with reduced synthetic rates of specific muscle proteins*. J Nutr, 1998. **128**(2 Suppl): p. 351S-355S.
215. Pahor, M. and S. Kritchevsky, *Research hypotheses on muscle wasting, aging, loss of function and disability*. J Nutr Health Aging, 1998. **2**(2): p. 97-100.
216. Goates, S., et al., *Economic Impact of Hospitalizations in US Adults with Sarcopenia*. J Frailty Aging, 2019. **8**(2): p. 93-99.
217. Bodine, S.C., *Disuse-induced muscle wasting*. Int J Biochem Cell Biol, 2013. **45**(10): p. 2200-8.
218. Adams, G.R. and M.M. Bamman, *Characterization and regulation of mechanical loading-induced compensatory muscle hypertrophy*. Compr Physiol, 2012. **2**(4): p. 2829-70.
219. Goldberg, A.L., et al., *Mechanism of work-induced hypertrophy of skeletal muscle.* Med Sci Sports, 1975. **7**(3): p. 185-98.
220. Roberts, M.D., et al., *Mechanisms of mechanical overload-induced skeletal muscle hypertrophy: current understanding and future directions*. Physiol Rev, 2023. **103**(4): p. 2679-2757.
221. Jorgenson, K.W., S.M. Phillips, and T.A. Hornberger, *Identifying the Structural Adaptations that Drive the Mechanical Load-Induced Growth of Skeletal Muscle: A Scoping Review*. Cells, 2020. **9**(7).
222. Roberts, M.D., et al., *Sarcoplasmic Hypertrophy in Skeletal Muscle: A Scientific "Unicorn" or Resistance Training Adaptation?* Front Physiol, 2020. **11**: p. 816.
223. Wang, N., et al., *Muscle fiber types of women after resistance training--quantitative ultrastructure and enzyme activity*. Pflugers Arch, 1993. **424**(5-6): p. 494-502.
224. Goldspink, G., *Alterations in myofibril size and structure during growth, exercise and change in environmental temperature*. Handbook of Physiology, 1983. **10** p. 539–554.
225. D'Amico, F., E. Skarmoutsou, and F. Stivala, *State of the art in antigen retrieval for immunohistochemistry*. Journal of Immunological Methods, 2009. **341**(1): p. 1-18.
226. Cochran, W.G., *Sampling Techniques, 3rd Edition*. 1977: John Wiley and Sons.
227. Jorgensen, A.O., et al., *Ultrastructural localization of the Ca2+ + Mg2+-dependent ATPase of sarcoplasmic reticulum in rat skeletal muscle by immunoferritin labeling of ultrathin frozen sections*. J Cell Biol, 1982. **92**(2): p. 409-16.
228. Rossi, A.E. and R.T. Dirksen, *Sarcoplasmic reticulum: the dynamic calcium governor of muscle*. Muscle Nerve, 2006. **33**(6): p. 715-31.
229. Brandl, C.J., et al., *Adult forms of the Ca2+ATPase of sarcoplasmic reticulum. Expression in developing skeletal muscle*. Journal of Biological Chemistry, 1987. **262**(8): p. 3768-3774.
230. Braun, J.L., et al., *Heterozygous SOD2 deletion selectively impairs SERCA function in the soleus of female mice*. Physiol Rep, 2022. **10**(10): p. e15285.
231. Johansson, C., et al., *Isometric force and endurance in skeletal muscle of mice devoid of all known thyroid hormone receptors*. J Physiol, 2003. **547**(Pt 3): p. 789-96.
232. Majerczak, J., J. Karasinski, and J.A. Zoladz, *Training induced decrease in oxygen cost of cycling is accompanied by down-regulation of SERCA expression in human vastus lateralis muscle*. J Physiol Pharmacol, 2008. **59**(3): p. 589-602.
233. Periasamy, M. and A. Kalyanasundaram, *SERCA pump isoforms: their role in calcium transport and disease*. Muscle Nerve, 2007. **35**(4): p. 430-42.

234. Nguyen, T., et al., *Effect of chronic obstructive pulmonary disease on calcium pump ATPase expression in human diaphragm.* J Appl Physiol (1985), 2005. **98**(6): p. 2004-10.
235. Rudolf, R., P.J. Magalhaes, and T. Pozzan, *Direct in vivo monitoring of sarcoplasmic reticulum Ca2+ and cytosolic cAMP dynamics in mouse skeletal muscle.* J Cell Biol, 2006. **173**(2): p. 187-93.
236. Toral-Ojeda, I., et al., *Calpain 3 deficiency affects SERCA expression and function in the skeletal muscle.* Expert Rev Mol Med, 2016. **18**: p. e7.
237. Meng, H., et al., *Tissue triage and freezing for models of skeletal muscle disease.* J Vis Exp, 2014(89).
238. Nix, J.S. and S.A. Moore, *What Every Neuropathologist Needs to Know: The Muscle Biopsy.* J Neuropathol Exp Neurol, 2020. **79**(7): p. 719-733.
239. Gaspar, B.L., R.K. Vasishta, and B.D. Radotra, *Commonly Encountered Artifacts in Muscle Biopsy*, in *Myopathology: A Practical Clinico-pathological Approach to Skeletal Muscle Biopsies*. 2019, Springer Singapore: Singapore. p. 57-66.
240. Tokuyasu, K.T., *A technique for ultracryotomy of cell suspensions and tissues.* J Cell Biol, 1973. **57**(2): p. 551-65.
241. Stemmer, A., M. Beck, and R. Fiolka, *Widefield fluorescence microscopy with extended resolution.* Histochemistry and Cell Biology, 2008. **130**(5): p. 807-817.
242. Shaw, P.J., *Comparison of Widefield/Deconvolution and Confocal Microscopy for Three-Dimensional Imaging*, in *Handbook Of Biological Confocal Microscopy*, J.B. Pawley, Editor. 2006, Springer US: Boston, MA. p. 453-467.
243. Schumacher, J. and L. Bertrand, *THUNDER imagers: how do they really work.* THUNDER Imager Technical Note, 2019.
244. Carpenter, A.E., et al., *CellProfiler: image analysis software for identifying and quantifying cell phenotypes.* Genome Biol, 2006. **7**(10): p. R100.
245. Kruger, P. and P.G. Gunther, *[Fibers with fibrillar structure and fibers with field structure in striated musculature of mammals and man; opposing reply].* Z Anat Entwicklungsgesch, 1955. **118**(4): p. 312-23.
246. Shear, C.R. and G. Goldspink, *Structural and physiological changes associated with the growth of avian fast and slow muscle.* J Morphol, 1971. **135**(3): p. 351-72.
247. Cheng, K. and G.M. Breinin, *Fine structure of nerve endings in extraocular muscle.* Arch Ophthalmol, 1965. **74**(6): p. 822-34.
248. Durston, J.H., *Histochemistry of primate extraocular muscles and the changes of denervation.* Br J Ophthalmol, 1974. **58**(3): p. 193-216.
249. Gooz, M. and E.N. Maldonado, *Fluorescence microscopy imaging of mitochondrial metabolism in cancer cells.* Front Oncol, 2023. **13**: p. 1152553.
250. Schaefer, P.M., et al., *NADH Autofluorescence-A Marker on its Way to Boost Bioenergetic Research.* Cytometry A, 2019. **95**(1): p. 34-46.
251. Kolenc, O.I. and K.P. Quinn, *Evaluating Cell Metabolism Through Autofluorescence Imaging of NAD(P)H and FAD.* Antioxid Redox Signal, 2019. **30**(6): p. 875-889.
252. Shadiow, J., et al., *Exercise-induced changes to the fiber type-specific redox state in human skeletal muscle are associated with aerobic capacity.* J Appl Physiol (1985), 2023. **135**(3): p. 508-518.
253. Lam, F., et al., *Super-resolution for everybody: An image processing workflow to obtain high-resolution images with a standard confocal microscope.* Methods, 2017. **115**: p. 17-27.

254. Makarkin, M. and D. Bratashov, *State-of-the-Art Approaches for Image Deconvolution Problems, including Modern Deep Learning Architectures*. Micromachines (Basel), 2021. **12**(12).
255. Katoh, K., *Software-Based Three-Dimensional Deconvolution Microscopy of Cytoskeletal Proteins in Cultured Fibroblast Using Open-Source Software and Open Hardware*. J Imaging, 2019. **5**(12).
256. Su, C., et al., *AutoDeconJ: a GPU-accelerated ImageJ plugin for 3D light-field deconvolution with optimal iteration numbers predicting*. Bioinformatics, 2023. **39**(1).
257. Wang, J., et al., *STED analysis reveals the organization of nonmuscle muscle II, muscle myosin II, and F-actin in nascent myofibrils*. Cytoskeleton (Hoboken), 2022. **79**(12): p. 122-132.
258. Fenix, A.M., et al., *Muscle-specific stress fibers give rise to sarcomeres in cardiomyocytes*. Elife, 2018. **7**.
259. Rhee, D., J.M. Sanger, and J.W. Sanger, *The premyofibril: evidence for its role in myofibrillogenesis*. Cell Motil Cytoskeleton, 1994. **28**(1): p. 1-24.
260. Sanger, J.W., et al., *Myofibrillogenesis in skeletal muscle cells*. Clin Orthop Relat Res, 2002(403 Suppl): p. S153-62.
261. Hibbert, J.E., et al., *Protocol for quantifying the in vivo rate of protein degradation in mice using a pulse-chase technique*. STAR Protoc, 2023. **4**(4): p. 102574.
262. Mesquita, P.H.C., et al., *Resistance training diminishes mitochondrial adaptations to subsequent endurance training in healthy untrained men*. J Physiol, 2023. **601**(17): p. 3825-3846.
263. Zhu, W.G., et al., *Weight Pulling: A Novel Mouse Model of Human Progressive Resistance Exercise*. Cells, 2021. **10**(9).
264. Stirling, D.R., et al., *CellProfiler 4: improvements in speed, utility and usability*. BMC Bioinformatics, 2021. **22**(1): p. 433.
265. Karnovsky, M.J., et al., *A formaldehyde-glutaraldehyde fixative of high osmolality for use in electron-microscopy*. Journal of Cell Biology, 1965. **27**: p. 137.
266. Jorgenson, K.W., et al., *A novel imaging method (FIM-ID) reveals that myofibrillogenesis plays a major role in the mechanically induced growth of skeletal muscle*. Elife, 2024. **12**.
267. Liu, Y., et al., *Author Correction: Application of bio-orthogonal proteome labeling to cell transplantation and heterochronic parabiosis*. Nat Commun, 2020. **11**(1): p. 3550.
268. Liu, Y., et al., *Application of bio-orthogonal proteome labeling to cell transplantation and heterochronic parabiosis*. Nat Commun, 2017. **8**(1): p. 643.